INFORMATION TO USERS

This material was produced from a microfilm copy of the original document. While the most advanced technological means to photograph and reproduce this document have been used, the quality is heavily dependent upon the quality of the original submitted.

The following explanation of techniques is provided to help you understand markings or patterns which may appear on this reproduction.

1. The sign or "target" for pages apparently lacking from the document photographed is "Missing Page(s)". If it was possible to obtain the missing page(s) or section, they are spliced into the film along with adjacent pages. This may have necessitated cutting thru an image and duplicating adjacent pages to insure you complete continuity.

2. When an image on the film is obliterated with a large round black mark, it is an indication that the photographer suspected that the copy may have moved during exposure and thus cause a blurred image. You will find a good image of the page in the adjacent frame.

3. When a map, drawing or chart, etc., was part of the material being photographed the photographer followed a definite method in "sectioning" the material. It is customary to begin photoing at the upper left hand corner of a large sheet and to continue photoing from left to right in equal sections with a small overlap. If necessary, sectioning is continued again — beginning below the first row and continuing on until complete.

4. The majority of users indicate that the textual content is of greatest value, however, a somewhat higher quality reproduction could be made from "photographs" if essential to the understanding of the dissertation. Silver prints of "photographs" may be ordered at additional charge by writing the Order Department, giving the catalog number, title, author and specific pages you wish reproduced.

5. PLEASE NOTE: Some pages may have indistinct print. Filmed as received.

University Microfilms International
300 North Zeeb Road
Ann Arbor, Michigan 48106 USA
St. John's Road, Tyler's Green
High Wycombe, Bucks, England HP10 8HR

Analysis of falling film reactors

by

Siu-Ming Yih

A Dissertation Submitted to the

Graduate Faculty in Partial Fulfillment of

The Requirements for the Degree of

DOCTOR OF PHILOSOPHY

Department: Chemical Engineering and
Nuclear Engineering
Major: Chemical Engineering

Approved:

Signature was redacted for privacy.

In Charge of Major Work

Signature was redacted for privacy.

For the Major Department

Signature was redacted for privacy.

For the Graduate College

Iowa State University
Ames, Iowa

1977

TABLE OF CONTENTS

NOMENCLATURE

a	displacement of liquid surface
a'	$\frac{0.4v_0}{\bar{\lambda}}$
a_n	series solution coefficients
A, B	integration constants defined by Equations 241 and 242
A^*, A_a, B^*	constants defined by Equations A4; A1; A3
$\bar{A}$, $\bar{B}$, $\bar{C}$, $\bar{D}$	integration constants in Equation 178 or 207
A', B', C', D'	constants defined by Equations 208; 209; 210; 211
b	$\frac{1}{4} - \sqrt{\frac{1}{16} + \frac{k_1^*}{4\beta^*}}$
b_2, b_3	constants defined by Equations 216; 217
B_1, B_2	$\frac{1-\beta}{(1+\alpha-e^{\alpha})z_1}$; $\frac{\beta}{(e^{\alpha}-1)z_1}$
$\hat{c}$, c, c_r, c_i	wave velocity; dimensionless; real; imaginary
c_0, c_1	first approximation of wave velocity; second approximation
c_0'	$c_0 - \bar{U}(1)$
C, C^+, C^*, C^+_{bulk}	concentration of absorbed gas; $\frac{C}{C_s}$; $1 - C^+$; bulk
C_i	series expansion coefficients
C_S, C_{As}	gas solubility; of component A
C_0, C_{B0}	initial concentration of absorbed gas; of liquid component B
D, D_0, D_A, D_B	molecular diffusivity; at T_0; of component A; of component B
D_{turb}	turbulent diffusivity
$\hat{E}$, E_a	activation energy for chemical reaction; for viscosity

E	$\dfrac{\bar{U}''\|_{\eta=1}}{c_0-\bar{U}(1)}$
f, $\hat{F}$	variables in stream function for pressure and temperature defined by Equations 143 and 144
F	Froude number, $\dfrac{<U>}{(g\Delta)^{\frac{1}{2}}}$
${}_2F_1$	generalized hypergeometric series
g	gravitational acceleration constant
G, H	$\dfrac{\rho_1<U>^2\Sigma}{\Delta}$; $\dfrac{\rho_1<U>^2\Pi}{\Delta}$
h	$\dfrac{H_s}{R_g E_a}$, dimensionless
H_S	heat of solution
$\bar{k}$, k	wave number; dimensionless
$\hat{k}$, k_0, k_1	reaction rate constant; for zero-order; for first-order
k_{00}, k_{10}	rate constant for zero-order reaction at T_0, for first-order reaction at T_0
k_0^*, k_1^*, k_n^*	$\dfrac{k_{00}\Delta^2}{D_0 C_S(T_1)}$, dimensionless; $\dfrac{k_{10}\Delta^2}{D_0}$, Damkohler Group II; dimensionless pseudo-n-th order rate constant
k', k_L	mass transfer coefficient
m	$-\rho_1 g \sin\theta$
m_1, m_2	$\dfrac{-\alpha \pm \sqrt{\alpha^2+4k_1^*}}{2}$
n	integer
$N_A\|_{\eta=1}$	mass flux through interface
N	eigenfunction

p	$\frac{\hat{E}}{E_a R_g}$, dimensionless
$\hat{p}$, p_1, p', $\overline{P}$	pressure; $\hat{p}/\rho_l\langle U\rangle^2$; fluctuations; mean
Pe	Peclet number, $\frac{\langle U\rangle\Delta}{\alpha_t}$
Q	flow rate per unit width
Q_0	amount of gas absorbed in time θ_c
R, Re, R_{cr}, Re_{cr}	Reynolds number, $\frac{\Delta\langle U\rangle\rho_l}{\mu_0}$; $4\frac{\Delta\langle U\rangle\rho_l}{\mu_0}$; critical values
s	exponent in Frobenius series solution
S	dimensionless surface tension, $\frac{\sigma}{\rho_l\langle U\rangle^2\Delta}$
Sh', Sh, Sh'_∞	Sherwood number defined with respect to (C_s-C_{bulk}); defined with respect to (C_s-C_0); limiting Sh'
t	time
T, T_0, T_1	temperature; at the wall (also the reference temperature for isothermal condition); at the gas-liquid interface
$\hat{T}$, $\overline{T}$, T'	$\frac{T-T_1}{T_0-T_1}$, dimensionless temperature; mean; fluctuations
u	"transient part" of solution
$\hat{u}$, u_1, u'	X-component velocity; $\hat{u}/\langle U\rangle$; fluctuations
U, U_1, $\langle U\rangle$, U^*, $\overline{U}$	X-component velocity of primary flow; at gas-liquid interface; average; $\frac{U}{U_1}$; $\frac{U}{\langle U\rangle}$
v	"steady part" of solution
$\hat{v}$, v_1, v'	Y-component velocity; $\hat{v}/\langle U\rangle$; fluctuations
v_0	friction velocity of eddies

V	$N'e^{\alpha\eta}$
W_A, $\tilde{W}_A$, $\tilde{W}_{A_{sat}}$	total absorption rate per unit width; $\frac{W_A}{C_s(T_1)}$; at saturation
x	$\frac{X}{\Delta}$, dimensionless
X, X^*	axial distance or exposed film length; $\frac{XD_0}{\Delta^2 U_1}$, dimensionless
Y, $\bar{Y}$	normal distance from the wall; from the interface
z	number of moles
z'	$-\beta^*(1-\eta)^2$
z_1	constant defined by Equation 135

Greek Symbols

α	$E_a(T_1-T_0)/T_0^2$, dimensionless
α_1, α_2, α_3, α_4	constants
α_t	thermal diffusivity
β	$\frac{\tau_1\Delta}{\mu_0 U_1}\frac{e^{\alpha}-1}{\alpha}$, dimensionless
β^*	$\frac{a'\Delta^2}{D}$, dimensionless
γ'	transcendental variable defined by Equation 130
Δ	average film thickness
η, $\bar{\eta}$	dimensionless Y-distance from the wall; from the interface
θ	angle of inclination
θ_c	gas-liquid contact time
λ	eigenvalue

$\bar{\lambda}$	thickness of the zone of damped turbulence
μ, μ_0, μ_1, $\tilde{\mu}$	liquid viscosity; at T_0; at T_1; $\frac{\mu}{\mu_0}$, dimensionless
ν	kinematic viscosity of liquid
ξ	$\frac{\partial N}{\partial \lambda}$
Π	$\frac{\tau_t}{\rho_l <U>^2}$, dimensionless
ρ	$\frac{\partial V}{\partial \lambda}$
ρ_l	liquid density
σ, σ_{equiv}	surface tension; surface tension + gravitational pressure
Σ	$\frac{\tau_t}{\rho_l <U>^2}$, dimensionless
τ	dimensionless time
τ_1	constant interfacial stress
τ_n, τ_t	normal perturbation stress; tangential
ϕ	variable in the stream function defined by Equation 142
Φ, Φ_I, Φ_N	enhancement factor; isothermal; nonisothermal
ψ	stream function

INTRODUCTION

The flow of thin liquid films, as a special case of two-phase flow, occurs frequently in the natural environment as in the case of rainfall flowing on solid surfaces or in drain pipes. In recent years, extensive research efforts have been conducted on falling film flow because it has found wide applications in modern process industries dealing with heat and mass transfer. These include film condensation, water desalination, gas-liquid contacting, solid dissolution, withdrawal and coating processes. Common process equipment utilizing film flow include heat exchangers, vertical condensers, film evaportors, distillation columns, packed and wetted-wall columns, trickling-type cooling or absorption towers, and annular two-phase flow in pipelines or boiler tubes. In addition, flowing films have also been used to protect metal surfaces from contamination by hot gases. Wetted-wall columns and wetted spheres are common laboratory devices for measuring molecular diffusion coefficients and obtaining kinetic rate data. The large interfacial area encountered in film flow makes it a favorable device for a number of gas-liquid contacting processes.

The characteristics of film flow are widely different from those of confined flows. This is mainly because of the mobile free surface where ripples usually appear at relatively low flow rates. Surface tension and gravity forces thus play a dominant role. Another reason is related to the geometry of the falling film with its small thickness and large interfacial area. The motion of the interface governs to a large extent the transport processes through the interface.

Film flow is often classified, in a broad sense, into three regimes in the order of increasing Reynolds number: laminar without rippling, wavy laminar, and turbulent. More concrete hydrodynamic and mass transfer results have been obtained for the smooth laminar flow regime inasmuch as it is more amenable to detailed analytical study. Film thicknesses, velocity profiles and mass transfer coefficients that are measured in this regime usually agree with the theory based on smooth laminar flow. Short wetted-wall columns have been used in the past to simulate the penetration model for flow through packed columns (83). Long wetted-wall columns are often used for gas absorption studies with surface active agents (SAA) added to suppress the formation of ripples. Molecular diffusion coefficients and kinetic rate constants are also measured quite accurately by the wetted-wall sphere technique (21,67).

The appearance of finite amplitude waves on the free surface at small flow rates, however, greatly complicates the hydrodynamic and transfer processes. Experiments show that the waves bring about large increases in the pressure drop and the mass transfer coefficient in the gas phase. While the waves apparently increase the heat transfer rate in a liquid film by only 20-30%, studies have shown (26) that the mass transfer rate may increase by 200-300%. The slight increase in the interfacial area cannot explain this large discrepancy, and it is thought that the waves modify the velocity distribution in the film and induce additional mixing through eddy circulation (63). Due to the fact that a spectrum of wave frequencies exists and the shape of the wave profile cannot be uniquely represented by just one or two components of a Fourier series, modeling of the wave structure is only partially successful, as pointed out by Dukler

(24). In essence, a variety of waves are found to exist on the free surface, depending on the flow rate. They may be capillary waves, gravity waves, roll waves, or a combination of these. The mechanism by which these waves enhance the transfer processes is yet unknown. All these complications tend to make the hydrodynamic and transport analysis in wavy films extremely difficult, if not impossible. Existing experimental studies (76,80) have been mainly confined to measurements in the region near wave inception where regular waves can be found. A number of theoretical works (6,19,87) are engaged in using small disturbance theory to predict the instability of the flow, that is, conditions under which the waves will appear and grow to finite amplitude when infinitesimal disturbances are imposed on the mean flow.

As the Reynolds number based on the film thickness exceeds approximately 1100-2000, the falling film becomes turbulent. Experimental measurements (62) have shown that the universal velocity profile concept is quite useful in predicting the film thickness. Past experience seems to suggest that the well-developed analogies of turbulent momentum, heat, and mass transfer for fixed interfaces may be equally applicable to film flow. While the analogies may hold for the solid-liquid interface in a film, they fail to apply at the mobile gas-liquid interface where the velocity gradient vanishes in the absence of gas shear. For mass transfer through the gas-liquid interface, the liquid-side resistance resides mainly in a region very near the interface because of the large Schmidt number commonly found in liquids. In general there are two approaches for analyzing the mass transfer rate at a turbulent interface. The first is to integrate the convective-diffusion equation using an empirical eddy

diffusivity expression. The second is to develop hypothetical models and deduce the mass transfer coefficient from parameters that characterize the turbulent structure. Preliminary attempts to describe heat and mass transfer using statistical film flow hydrodynamics have also been recently made (10,11).

Levich (48), using purely physical intuition, derives an eddy diffusivity expression on the basis that the eddy motion will be damped at the interface by surface tension. The concept is used and refined in most of the later work of Davies (22). King (43) generalized it into a surface-renewal-damped-eddy diffusivity model. Lamourelle and Sandall (45) experimentally correlated an eddy diffusivity expression for gas absorption into a turbulent falling film of water. Sandall and co-workers (41,53,54) later used the expression to study mass transfer with first-order and instantaneous reactions. Good agreement was found between experimental absorption rates and the numerical solution. However, their numerical calculations show that a very finely-spaced grid has to be used in the finite difference solution in order to attain convergence and accuracy. This is mainly due to the steep concentration gradient near the interface. Moreover, to study the effect of variable flow conditions and reaction rates on mass transfer by using a numerical method would require exhaustive calculations over a range of operating variables and is practically very inefficient and time-consuming. An analytical solution is therefore highly desirable. The use of hypothetical models, as proposed by a number of researchers (4,66), also suffers from the disadvantage that one or more empirical parameters in the model have to be adjusted from experimental evaluation. None of the above methods have been

entirely satisfactory. However, the use of an eddy diffusivity concept seems to be a more convenient tool for studying chemical reactions in a turbulent falling film than any of the other approaches presently available.

Objectives of the Present Study

Although an enormous quantity of research has been carried out for film flow under isothermal conditions, much less is known about the hydrodynamic and mass transfer behavior when significant temperature gradients exist in the liquid film. This occurs, for example, in the process of sulfonating and sulfating an organic acid in a wetted-wall column where the reaction between the organic acid with sulfur trioxide is highly exothermic (82). The color of the product, which is very sensitive to temperature, has to be controlled carefully by cooling through the walls. Other physical or chemical absorption studies (15,18) have also stressed the importance of considering these heat effects. To avoid complication, previous analyses on processes such as film condensation or film cooling have usually assumed that the physical properties are either independent of temperature or can be represented by a mean value. Since the film thickness is small and the liquid viscosity is a strong function of temperature, the velocity distribution in the film will change considerably when there is a large temperature gradient. Moreover, the molecular diffusion coefficient, kinetic rate constant and gas solubility are all functions of temperature and their effects on mass transfer must be considered when a significant temperature gradient exists. Another important parameter is the cocurrent or countercurrent gas shear which

modifies not only the velocity distribution and transfer rates, but also has a dominant influence on the stability of the flow.

The objectives of the present study are mainly threefold. First, mass transfer into a laminar finite falling film is analyzed under different conditions of interfacial shear and heat transfer. The analysis is then extended to include chemical reactions with linear reaction kinetics. The problem is solved for a linear temperature drop across the liquid film and a constant cocurrent shear stress at the gas-liquid interface. Assumptions are made such that the viscosity varies exponentially with temperature, the molecular diffusion coefficient varies according to the Stokes-Einstein relation, and the kinetic rate constant obeys the Arrhenius expression. The variation of the gas solubility with temperature is also explicitly taken into account. Mass transfer coefficients are predicted by an exact solution of the governing equations and compared with the isothermal, zero interfacial shear case. Effects of change in film thickness and flow rate on the absorption rate are scrutinized. Hypotheses and computations by Jennis (37) are compared with this work whenever possible. Then, first-order and zero-order reactions are included to examine the interactions between the hydrodynamic and reaction parameters. Pertinent quantities such as the chemical absorption rate are compared with those obtained for physical absorption. Average isothermal and nonisothermal enhancement factors are then examined to determine the effects of heat transfer.

Another important aspect of the problem is concerned with the influence of heat transfer and interfacial shear on the hydrodynamic stability of a liquid film. In some processes such as withdrawal or coating,

the appearance of ripples may contribute to product nonuniformity and cause undesirable effects. In other cases such as film cooling, film condensation and gas absorption, it is important to assess the critical conditions under which waves will appear, since these waves enhance momentum, heat and mass transfer rates considerably. Process design and predictions based on the laminar flow theory may well underestimate the transfer rates if the stability conditions are unknown in the presence of heat transfer and interfacial shear. Although a few investigations have been performed on the influence of heat transfer on shear wave instability of plane Poiseuille flow (65) and boundary-layer flow (84), hardly any are available for studying the influence of heat transfer on surface wave instability in falling liquid films. The only exceptions found are that of Marschall and Lee (49) who analyzed the stability of condensate flow, and Bankoff (5) who studied the evaporation effects on film instability. Both have assumed constant physical properties independent of temperature. However, the assumption that the liquid viscosity is constant can hardly be justified if a significant temperature gradient exists in the liquid film.

The second objective is, therefore, to establish stability criteria for liquid films that are flowing down an inclined plane and are influenced by heat transfer and interfacial shear. Specifically, the effect of variation of viscosity with temperature is taken into account, the importance of which has already been demonstrated by the above studies on shear wave instability. Stability criteria are developed by a successive

perturbation analysis. The similarities and differences in which heat transfer influence shear wave and surface wave instability are discussed.

Lastly, the laminar flow analysis and solution technique are applied to mass transfer in isothermal turbulent film flow using an eddy diffusivity concept. The procedure is extended to include chemical reactions with linear reaction kinetics. The exact solutions are compared with previous numerical solutions and experimental data for a first-order reaction. New solutions are presented for a zero-order reaction and then generalized to pseudo-n-th order reactions. The exact solution thus provides a coherent description on the effect of variables on mass transfer in turbulent falling films and can be conveniently extended to other operating conditions and chemical reactions. It is hoped that, through the present analysis, more information can be extracted and applied to the experimental testing and design of industrial equipment employing film flow.

LITERATURE REVIEW

Due to the extensive amount of research involved in falling film flow, it is not feasible to review all of the pertinent work published in the past fifty years. A short summary of the major research efforts as related to the present work is shown in Table 1. More detailed review is given in the following.

Falling Film Hydrodynamics

The hydrodynamics of film flow have been intensively studied. A comprehensive survey of the literature has been given by Fulford (28). The characteristics of film flow are generally dependent on various dimensionless groups such as the Reynolds, Weber and Froude numbers, and on the interfacial drag exerted by the adjoining gas flow. The gas/liquid flow is usually cocurrent to avoid flooding, and vertical film flow tends to be unstable in most circumstances.

It is useful to classify film flow into three categories in the order of increasing Reynolds number: smooth laminar, wavy laminar and turbulent. In general, as Fulford (28) has pointed out, smooth laminar flow occurs only at small Reynolds numbers on the order of ten. Gravity waves appear at a moderate Reynolds number and at a Froude number of about one to two. Capillary waves are present mainly at larger flow rates and at a Weber number of approximately one. Roll waves occur frequently above a Reynolds number of a few hundred. The wave structure changes gradually from stationary to nonstationary as the flow rate increases, and finally changes to a stochastic and random nature when turbulent flow begins.

Table 1. General research efforts on falling film flow (both experimental and theoretical)

Hydrodynamics (Effects of physical properties, τ_l, θ, SAA on film thickness and velocity profile)	Laminar	Wavy, pseudo-laminar	Turbulent
	$Re \lesssim 10$	Linear stability theory, predict neutral stability conditions and wave properties; Integral solution of boundary-layer equations of momentum, predict Re_{cr} and wave properties	$Re > 1100 \sim 2000$
	Entrance region flow; Steady uniform flow	only valid for small Re or long waves	Von Karman's UVP
Heat, mass transfer with chemical reaction	Film condensation, evaporation, cooling, heating, gas absorption or desorption		
	Measurement of molecular diffusivities and kinetic rate constants, solid dissolution, withdrawal, coating	Mostly experimental work and empirical correlations, complex nature of wave makes theoretical prediction very difficult	Surface renewal and eddy diffusivity models

Transition to turbulent flow usually occurs in the Reynolds number range of 1100-2000. Even in turbulent flow, a large part of the total film thickness may still be occupied by the laminar sublayer. Film flow is therefore a complicated function of the physical properties of the liquid, the flow rate, and the slope of the wall.

For smooth laminar flow, the velocity distribution and film thickness for a viscous Newtonian liquid flowing down an inclined plane with no interfacial drag was first developed by Nusselt and has been regarded as a basis for almost all the later studies on film flow. Entrance region film flow has been studied by Cerro and Whitaker (13), and Stucheli and Ozisik (79). It is found that for mobile liquids or for moderately long columns, inertia effects are usually negligible. Measurements of velocity profile in the entrance region, in the steady laminar and wavy laminar regimes, have been made by Wilkes and Nedderman (86). They found that the rate of acceleration to steady state was governed mainly by surface tension. When waves were suppressed by the addition of SAA, the velocity fluctuations were damped and the velocity profile returned to the semi-parabolic form as predicted by Nusselt.

As the flow rate exceeds a certain initial value, waves begin to appear on the free surface. Dukler (24) has reviewed the different approaches of modeling the wave structure of vertical falling films. The more common approach is either to use a linear stability theory where small perturbation expansions for the stream function are performed to solve the momentum equation, or to search for a periodic solution to the boundary-layer momentum equations employing integral methods. The first comprehensive study on the hydrodynamics of wave formation on thin liquid

films was made by Kapitza (40). An approximate steady periodic solution for the film thickness and velocity profile was obtained by an integral solution of the boundary-layer momentum equations. Experimental results for the critical Reynolds number, film thickness, wave amplitude, wavelength and phase velocity were partially verified by theory. The influence of gas flow was also analyzed and the heat transfer rate was predicted to be 21% higher than that of smooth laminar flow. Kapitza's theory, however, is restricted only to long waves and to low flow rates where regular sinusoidal wave motion exists. Later experimental findings for higher flow rates (38,76,80) show that Kapitza's theory is inadequate. In particular, experimental data show that the equilibrium amplitude and the ratio of the wave celerity to average velocity varies with the flow rate and the liquid physical properties while Kapitza's theory predicts them to be constants. Kapitza also predicts that the wavelength will vary with the flow rate but experiments show that it is practically constant and independent of flow rate. Shkadov (74) resolved the same problem to a higher order of accuracy than Kapitza's by considering the flow as a nonlinear problem.

Experimental data on measured average wavelength for different falling liquid films were reported by Tailby and Portalski (80) for Reynolds number ranging from R = 40 to 850. Theoretical predictions based on the Kapitza theory, however, fell substantially below the data. They pointed out that since the wave motion lost its regularity at some distance below the line of wave inception, the only proper location for measuring meaningful wavelength data should be in the immediate vicinity

of the line of wave inception. Wave properties were also measured by Stainthorp and Allen (76) and Jones and Whitaker (38). Extensive film thickness data for a variety of liquids were taken by Portalski (62). A more detailed review on experimental measurements can be found in Fulford's article (28).

As the Reynolds number exceeds approximately 1100-2000, the falling film becomes turbulent. The transition to turbulence, however, is a gradual process so that reported values of the transition Reynolds number vary in the literature. The Nusselt and Kapitza predictions of film thickness and velocity profile are not applicable in this regime. Dukler and Bergelin (25) have extended the universal velocity profile (UVP) concept, originally developed for pipe flow, to smooth turbulent film flow with interfacial shear taken into account. The film thickness predicted in this way agree well with the experimental findings of Portalski (62) in the turbulent as well as in the wavy laminar regime. At high flow rates, e.g., Re>4000, the UVP predicts film thickness data that are lower than experimental values. In this case, empirical equations are then preferred. The accuracy of the film thickness prediction will depend largely on the form of the UVP selected. Also, the presence of large turbulent waves usually preclude an accurate measurement of the average film thickness and this may explain the deviation between the theory and experiment at large Reynolds number. Statistical film flow hydrodynamics has recently evolved (24), but the procedure is quite limited and too complicated for practical use.

Hydrodynamic Stability

Since surface waves appear on the falling film throughout almost the entire range of practical flow situations except at low flow rates, it is important to predict the onset and growth of these waves under different flow conditions. Kapitza's study (40) shows that a critical Reynolds number, R_{Cr}, exists which depends on the kinematic surface tension, the viscosity of the liquid and the angle of inclination. Rigorous formulation and solution for the linear stability of a liquid film flowing down an inclined plane under the influence of gravity and surface tension were first treated in detail by Benjamin (6) and Yih (87). Benjamin uses a power series expansion which is accurate to the sixth-order in wave number k and to the third order in kR. His results for long waves are in more accord with experimental observations. He has argued that even if the Reynolds number is extremely small, there can be unstable waves formed which may grow to appreciable size far downstream, so that a critical Reynolds number in the usual sense does not exist for a vertical film. Yih resolves the stability problem by using successive perturbation expansions and gives additional results for the cases of small Reynolds number and of large wave number. His low wave number theory is accurate to the second-order in wave number. It is found that only two perturbations are accurate enough to define the conditions of instability as presented by Benjamin. A number of approximate analytical and numerical solutions for the same problem have also appeared in the literature (1,85). The majority of the experimental data on wave properties have been taken under room conditions where the most highly amplified waves

appear. Krantz and Goren (44) measured wavelengths, wave celerities and growth rates of two-dimensional waves under imposed disturbances of controlled amplitude and frequency for low Reynolds number film flow. Their results seem to confirm, at least semi-quantitatively, that the linear stability and momentum integral theories are valid for small amplitude long waves on falling films flowing at small Reynolds number. Craik (19) studied the stability of a horizontal liquid film under the influence of air flow. It was found that the tangential stress perturbation component was a dominant destabilizing factor in very thin films. Smith (75) investigated the influence of wind stress and surface active agents on three-dimensional film flow down an inclined plane. Surface contamination was found to be a stabilizing factor in agreement with other previous investigations.

A limited number of studies have been performed on the influence of heat transfer on shear wave instability. The stability of laminar boundary-layer flow with heat transfer was studied by Wazzan et al. (84). The equation that governs the stability of the flow to shear wave (Tollmein-Schlichting wave) disturbances is a modified Orr-Sommerfeld (O-S) equation including the effect of temperature variation on viscosity. Numerical calculations for water show that for cooling of the boundary-layer, the critical Reynolds number is reduced; while for heating, the critical Reynolds number increases until it reaches a maximum and then decreases with further heating. It was concluded that the velocity profile had a great influence on the flow stability and the viscosity derivative terms in the modified Orr-Sommerfeld equation had a destabilizing

effect. Potter and Graber (65) extended the above heat transfer analyses to plane Poiseuille flow. They showed that a temperature difference between the two walls was always a destabilizing factor with the critical Reynolds number reduced below that of isothermal conditions. They further showed that even when the viscosity gradient terms were small, their inclusion was extremely important for liquids.

Relatively few studies have appeared in the literature on the stability of falling films undergoing heat transfer. Marschall and Lee (49) have analyzed the two-dimensional instability of a condensate film flowing down a vertical wall by assuming that the mean temperature profile is linear and the mean velocity profile is semi-parabolic. The Orr-Sommerfeld equation remains unchanged while the normal stress boundary condition is modified to include a balance between the vapor velocity and the heat flux at the interface. It was shown that the condensation mass transfer had a stabilizing effect on the film for a constant temperature drop while no stabilizing effect could be found for the case of constant heat flux. Bankoff (5) considered the evaporative flux as influencing only the pressure boundary condition at the interface and carried out an analysis similar to Yih's (87). He showed that evaporation had a destabilizing effect on the film. Both of the investigations above have neglected the variation of physical properties with temperature. Since in evaporation or condensation processes, large temperature gradients exist in the film, the assumption of constant property flow can hardly be justified, especially when the liquid viscosity is a strong function of temperature.

Mass Transfer With or Without Chemical Reaction

Theoretical mass transfer coefficients in falling liquid films have been determined generally by two approaches: (1) a direct integration of the species mass balance equation using a velocity profile predicted from hydrodynamic analysis; and (2) use of hypothetical models which involve unknown or adjustable parameters. The first approach is more accurate and desirable because no empirical parameters are needed. However, the velocity profile in a falling film is not always predictable and the second approach may then be useful.

Laminar flow

The classical Graetz-Nusselt formulation which neglects axial diffusion has been commonly used to describe physical absorption into a finite falling film. For short contact times, Higbie's penetration theory gives nearly identical results. Vivian and Peaceman (83) have used short wetted-wall columns to simulate the flow conditions in a packed bed. The purposes of using short columns are to simulate the size of the packing and to avoid the development of ripples. The liquid film is visualized as flowing over a piece of packing for a short period of time, and as being completely mixed at the discontinuities before flowing to the next piece of packing. Absorption therefore occurs in a sequence of short contacts in which Higbie's penetration theory is closely followed. By properly designing the column using downflow and upflow slots, Vivian and Peaceman showed that the entrance and exit effects could be minimized. For longer columns, SAA is usually added to suppress ripple formation. Although the SAA can affect the rate of absorption by introducing an

interfacial resistance, the influence is of minor importance as compared to the effect of waves. Goodridge and Gartside (29,30) used a nearly horizontal channel of less than one degree slope to measure transient absorption rates and liquid diffusivities. Long exposure times of up to 90 seconds were possible because of the absence of rippling for Reynolds number (Re) as high as 900. The velocity profile was found to be semi-parabolic but the mean film thickness did not agree with Nusselt's formula for very small angles of inclination (less than 10 minutes). Good agreement was obtained with literature values for measured liquid diffusivities and absorption rates. Entrance and exit effects were accounted for in a simple fashion.

A wetted-wall sphere has the advantage that the entrance and exit effects are much smaller than in a wetted-wall column. Davidson and Cullen (21) have successfully measured diffusion coefficients in Newtonian liquids using such a device. Ratcliff and Holdcroft (67) extended the method to measure both the diffusion coefficient and the first-order kinetic rate constant for fast reactions. Olbrich and Wild (59) generalized Davidson and Cullen's approach and solved the convective-diffusion equation for various flow geometries that have a certain degree of symmetry. The same kind of problem was treated by Tamir and Taitel (81) but they considered thermodynamic nonequilibrium at the gas-liquid interface by adding a constant interfacial resistance. Rotem and Neilson (68) analyzed low Peclet number film flow by including the axial diffusion term. Chavan and Mashelkar (14) and Mashelkar et al. (51) also solved the convective-diffusion equation for a non-Newtonian pseudoplastic liquid film. Similarly, an Ellis model was treated by Mohr and Williams (58).

Mashelkar and Soylu (50) subsequently measured diffusion coefficients in six different polymeric systems using the wetted-wall sphere technique. It was found that an increase in polymer concentration generally resulted in an increase in the diffusion coefficients, but in some polymer solutions, a maximum in the diffusivity was noted. A sensitive test of the shear rate dependence of the diffusion coefficient could not be made because of the absence of shear stress at the interface. Due to viscoelastic stretching, shear rate dependence of the diffusion coefficient, end effects and possible rippling, reported measurements of diffusion coefficient in laminar jets, wetted-wall columns, and spheres have been contradictory. The discrepancy lies mainly in the wide variation of the diffusion coefficient with the polymer concentration and the type of polymer tested. Perez and Sandall (61) have made molecular diffusivity measurements for carbon dioxide in aqueous Carbopol solutions using a long wetted-wall column with SAA added to eliminate ripples. A maximum is also found for increasing polymer concentration but a comparison with the data of Mashelkar and Soylu (50) on Carbopol solutions show that wide discrepancies still exist.

In analyzing dispersion in a falling film accompanied by heat transfer and interfacial shear, Shair (73) showed that the flow characteristics could be greatly affected by a change in the physical properties within the film and by the interfacial drag. Jennis (37) made a preliminary investigation on the mass transfer into a falling film by assuming a linear variation of viscosity and mass diffusion coefficient with temperature. The series solution obtained, however, was restricted only to small changes in the temperature gradient with relatively large inter-

facial shear. Obviously, solutions for the more important cases of high temperature gradient and low interfacial shear are needed.

Most of the gas/liquid contacting processes are often accompanied by chemical reactions which have the favorable property of enhancing the absorption rate. Detailed description of the subject can be found in the text by Astarita (2) and Danckwerts (20). Danckwerts has also provided many examples of processes of industrial importance where gas absorption occurs in the presence of chemical reaction. Ratcliff and Holdcroft (67) measured the absorption rates of CO_2 and 1,1-dimethoxyethane vapor into a spherical liquid film undergoing first-order chemical reactions. The kinetic rate constant obtained was in good agreement with other independent kinetic measurements. They suggested that the method might be useful for the measurement of the kinetics of fast reactions. Gottfredi et al. (31) presented both perturbation and numerical solutions for mass transfer with chemical reaction in a laminar falling film. A parabolic velocity profile was assumed which incorporated the effect of interfacial stress. Their solution compared well with the penetration theory for short contact times. However, the perturbation method failed to predict accurate results for long contact times. Important contributions were made by Jameson et al. (35) who numerically solved the problem of diffusion with a generalized chemical reaction in a finite falling film obeying Nusselt's relation. Absorption enhancement rates were presented for higher orders of reaction between the gas absorbed and the liquid reactant.

Wavy flow

The literature values on measured liquid-side mass transfer coefficients show substantial disagreement among various investigators as can be seen from Figure 1. This is mainly due to the presence of rippling in which the wave structure is continuously changing with increasing flow rate. A state-of-the-art review by Hobler and Kedzierski (33) has indicated that all the experimental work, with the semi-empirical and theoretical equations as proposed by different investigators using different assumptions, give widely different values of the mass transfer coefficient. A fundamental reason for these anomalies is that the mechanism in which the waves affect the hydrodynamic and transfer processes are not yet clear. Speculations have been made by Portalski (63) on examining the velocity distribution derived by Kapitza, that regions of reversed flow may exist under the troughs of a periodic traveling wave. The formation of circulating eddies in the flow thus promotes mixing and surface renewal. Massot et al. (52) have solved the two-dimensional linearized integral momentum equations using Kapitza's method and draw flow streamlines indicating the possibility of a reversed flow structure. Levich (48), and later, Ruckenstein and Berbente (69) have used the Kapitza type velocity distribution to integrate the species mass balance equation. The predicted enhancement is found to be only about 20% which is far below the experimentally measured 150-200% increase. They attribute this to the inaccuracy of Kapitza's velocity profile. Subsequently, Berbente and Ruckenstein (9) developed a solution of the boundary-layer momentum equations using a triple series expansion. The velocity was described by a

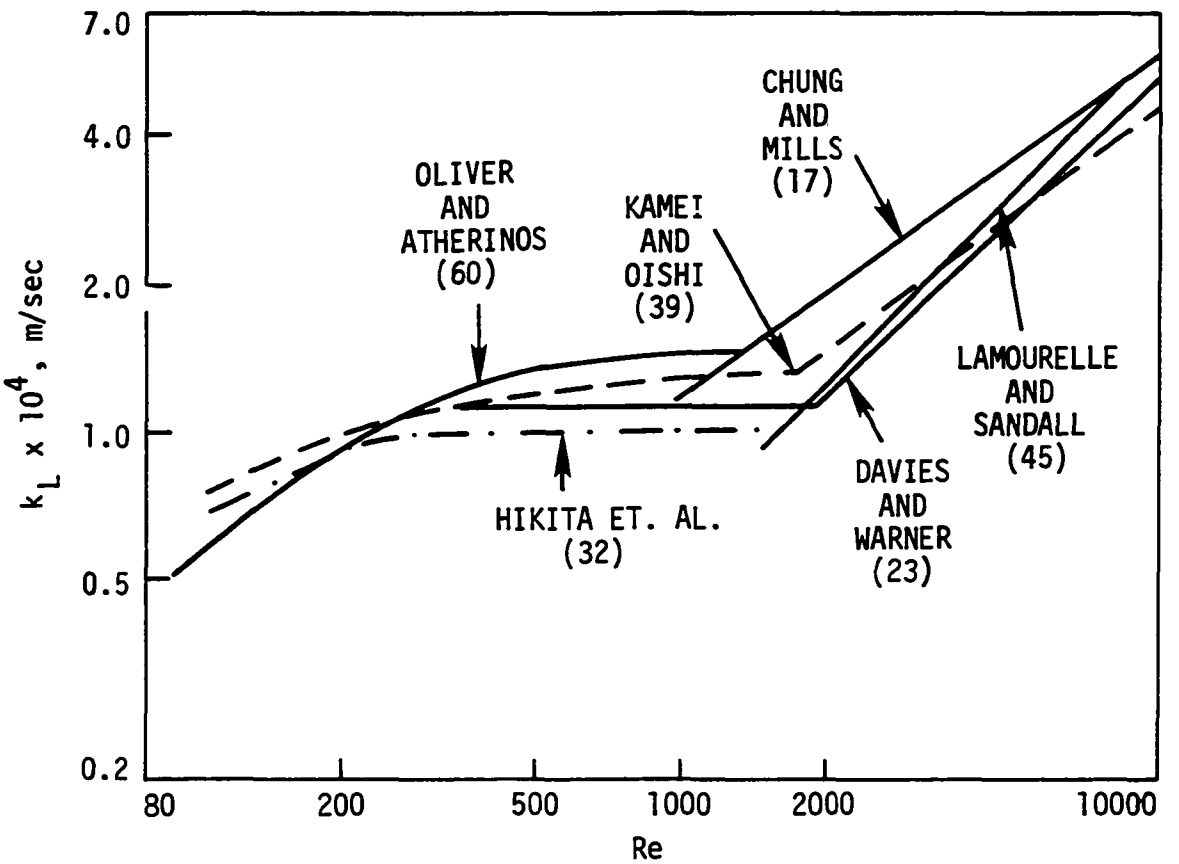

Figure 1. Experimental correlation of the mass transfer coefficient in wavy and turbulent falling films by different investigators

power series in normal distance up to the sixth degree. They found better agreement between the experimental and theoretical wave properties, and a better mass transfer prediction as well. However, the linearization procedure invoked in solving the momentum equations also restricts its validity to small flow rates.

Since the velocity profile in wavy flow cannot be predicted accurately from a hydrodynamic analysis, empirical approaches of determining the mass transfer coefficient become necessary. Banerjee et al. (3) have proposed an eddy flow model in which Harriott's random eddy modification of the penetration theory is used in conjunction with Levich's estimate of the distance of approach of an eddy towards the interface to evaluate the mass transfer coefficient semi-quantitatively. A more realistic model has been proposed by Javdani (36) in which the concentration fluctuations, induced by the fluctuating velocity field, are assumed to be a periodic quantity proportional to the mean concentration gradient. A periodic time average of the governing equation introduces an apparent diffusivity term. The solution for the concentration fluctuation is facilitated by employing the hydrodynamic stream function from linear stability theory. It was deduced that the apparent diffusivity due to waves was a function of the flow rate and wave properties such as the wave number, equilibrium amplitude and wave velocity. A simplified solution based on the penetration theory was presented and compared with a limited amount of experimental data obtained under controlled wave conditions. Although no conclusive evidence can be obtained because of insufficient experimental verification, the possibility of relating the enhancement in mass transfer

rate to wave properties is fully demonstrated. Studies of chemical reaction in a wavy film have not yet been attempted.

Turbulent flow

Predictions of mass transfer coefficients in turbulent film flow are based mainly on an empirical or semi-empirical approach. Nearly all treatments neglect the surface waves and assume the liquid film to be in smooth turbulent motion. The mass transfer coefficients measured in this regime are several fold higher than those in the wavy regime as shown in Figure 1. This means that a more vigorous mixing or renewal process is present in turbulent flow. Usually, eddy transport is assumed to occur in parallel with molecular transport, and the governing equation is integrated using an empirical eddy diffusivity expression (70). Another method is to relate the mass transfer coefficient to some measurable or predictable turbulent parameters in the film such as the rate of energy dissipation (4,66). A number of well-known models concerning mass transfer at a gas-liquid interface are available in the literature. Most of them hypothesize some type of surface renewal or eddy diffusion. A detailed review can be found in Bennett and Rathbun (8). Most of these models predict a dependence of the mass transfer coefficient on the square root of the molecular diffusivity, which agrees quite well with the experimental findings in turbulent film flow (32,45). In view of the fact that the liquid Schmidt numbers are large, the resistance to transport lies solely in a region very close to the interface where the concentration gradient is steep and it is necessary to know the transport coefficients accurately only in this region. Recent experimental visualization

studies (22) show that there are important eddy movements very close to the gas-liquid interface. This may help to explain why mass transfer in turbulent flow is much higher than that in the laminar or wavy flow regions.

Levich (48), and later Davies (22), have postulated that there is a zone of damped turbulence, $\overline{\lambda}$, near the interface where the normal fluctuating velocity component, v', decays towards the interface due to surface tension damping while the u' component remains constant. Beyond this zone, the turbulence is assumed normal. The eddy scale of motion and the velocity fluctuation, v', are assumed to vary linearly with the distance from the interface so that the eddy diffusivity is proportional to $\overline{Y}^2$. The thickness of the zone of damped turbulence is determined by a force balance between the dynamic pressure fluctuation of an eddy which causes deformation of the interface and the surface tension force which opposes the deformation. The mass transfer coefficient is obtained by considering steady state molecular diffusion through a diffusion sublayer:

$$k_L = 0.32\, D^{\frac{1}{2}}\, v_0^{\frac{3}{2}}\, \rho_l^{\frac{1}{2}}\, \sigma_{equiv}^{-\frac{1}{2}} \qquad (1)$$

where D = molecular diffusivity, v_0 = friction velocity of eddies, ρ_l = density of liquid, σ_{equiv} = surface tension + gravitational pressure. Since $v_0 = (g\, \Delta \sin \theta)^{\frac{1}{2}}$, then

$$k_L = 0.32\, D^{\frac{1}{2}}\, \Delta^{\frac{3}{4}} g^{\frac{3}{4}} (\sin \theta)^{\frac{3}{4}} \rho_l^{\frac{1}{2}}\, \sigma_{equiv}^{-\frac{1}{2}} \qquad (2)$$

where Δ = average film thickness, g = acceleration of gravity, θ = angle of inclination. More details of the above derivation can be found in the book by Davies (22). Equation 2, when compared with the experimental data

by Davies, was found to underestimate the mass transfer coefficient by about five times. This is mainly because Equation 2 predicts $k_L \propto Re^{0.4\sim0.5}$ while experiments show that $k_L \sim Re^{0.6\sim0.8}$. Another reason is that the assumption of $v' = v_0$ at $\bar{Y} = \bar{\lambda}$ used in deriving Equation 1 is quite questionable in film flow where the velocity gradients are large. To summarize, the Levich-Davies theory predicts that the eddy diffusivity varies as the square of the distance from the interface and is directly proportional to Reynolds number to some power and inversely proportional to surface tension. A number of experiments have been conducted to determine the above dependencies. Lamourelle and Sandall (45) absorbed four different gases into distilled water flowing down a long wetted-wall column at 25°C over the Reynolds number range of 1300-8300 and found by linear regression analysis that

$$k_L = 0.481\ Re^{0.837}\ D^{0.537}\ ft/hr \tag{3}$$

Since k_L is nearly proportional to $D^{0.5}$, it is in agreement with Danckwerts' surface renewal theory and the eddy diffusivity model. The surface renewal rate and eddy diffusivity were expressed respectively as:

$$s' = 0.115\ Re^{1.678}\ hr^{-1} \tag{4}$$

$$D_{turb} = 7.9 \times 10^{-5} Re^{1.678}\ \bar{Y}^2\ cm^2/sec \tag{5}$$

Mills and Chung (57) used the above eddy diffusivity expression for the interface region and the Van Driest eddy diffusivity profile for the wall region to correlate heat transfer coefficients for turbulent falling films. They found good agreement with the evaporation data by Chun and Seban (16). Kamei and Oishi's (39) experiment on CO_2 absorption in water at different temperatures in a long wetted-wall column showed that

$$k_L \propto D^{0.5} Re^{0.7} \quad (6)$$

Davies and Warner (23) absorbed three different gases into distilled water flowing over an inclined rough plate with the main purpose of studying the effect of roughness on mass transfer rate. They found that $k_L \propto D^{0.53}$. However, when different reported molecular diffusivity values from the literature were used, the dependency changed to $k_L \propto D^{0.6}$. This shows that the use of an accurate value of the molecular diffusivity is a critical factor in determining the experimental dependence of k_L on D. Recently, Chung and Mills (17) reported absorption of CO_2 into turbulent falling films of water and ethylene glycol-water mixtures. Effects of liquid viscosity and interfacial shear on k_L were investigated. They found that with cocurrent gas flow, the interfacial shear enhanced the transfer coefficient markedly while for countercurrent flow, the transfer coefficient decreased. For distilled water at 25°C, they correlated

$$k_L = 1.22 \times 10^{-6} Re^{0.67} \text{ m/sec} \quad (7)$$

Experimental curves of k_L versus Re as reported by the above investigators are replotted in Figure 1. By comparing Equation 7 with the correlations obtained by Lamourelle and Sandall (Equation 3), Kamei and Oishi (Equation 6), it is evident that $k_L \propto Re^{0.6 \sim 0.85}$ while Levich's equation predicts that $k_L \propto Re^{0.5}$ only. Nevertheless, Levich's deductions, by incorporating the effects of surface tension and the variation of k_L with the angle of inclination, provides a useful first order estimate of the mass transfer coefficient.

In several papers by Sandall and co-workers (41,53,54), the eddy diffusivity model was used to study gas absorption into a turbulent liquid

film with irreversible first-order reaction and instantaneous reaction. The species mass balance equation was integrated by numerical finite difference method using Equation 5 for the eddy diffusivity. The numerical results are in good agreement with experimental findings, and approximate empirical formulas are correlated by curve-fitting the numerical solution. The use of the numerical finite difference method for this situation, however, is practically inefficient because a very fine grid size is necessary to accommodate the steep concentration gradient and to insure numerical accuracy.

Recently, a statistical approach has been attempted. Brumfield et al. (11) employed the experimentally correlated statistical film flow hydrodynamic data as determined by Dukler and co-workers, together with a turbulence-based mass transfer model and an empirical estimate of the macroscale to correlate mass transfer data in turbulent falling films. Although the statistical approach is more rational, the correlated hydrodynamic data are based upon several weak assumptions such as an idealized wave and base film structure. The analyzed data were correlated at a certain Prandtl number and so may not be applicable to other operating conditions. The statistical approach is, on the whole, too complicated for practical engineering investigation on turbulent film flow.

MASS TRANSFER IN LAMINAR FALLING FILMS INVOLVING HEAT TRANSFER AND INTERFACIAL SHEAR

Statement of the Problem

A Newtonian liquid film of average thickness, Δ, is in steady, uniform laminar flow down an inclined plane under the action of gravity as shown in Figure 2. The gas flow is downward and cocurrent to avoid flooding. A chemical component which is uniformly distributed in the gas phase is diffusing from the gas into the liquid film. Initially, the liquid phase contains only pure liquid reactant. A small linear temperature drop is imposed across the film and the gas-liquid interface is sheared by a constant tangential stress, τ_1. The liquid phase concentration $C_s(T_1)$ at the gas-liquid interface is assumed to be in equilibrium with the gas phase. Other assumptions involved in the present treatment are:

1. The gas phase mass transfer resistance is negligible.
2. Volume change of the liquid phase due to absorption is negligible.
3. The liquid phase is nonvolatile.
4. Axial diffusion is neglected for high Peclet number film flow.
5. Entrance effects are not considered.
6. The viscosity of the liquid varies exponentially with temperature, the molecular diffusion coefficient follows the Stokes-Einstein relation, the kinetic rate constant obeys the Arrhenius law, and the solubility of the gas is a linear function of the surface temperature.

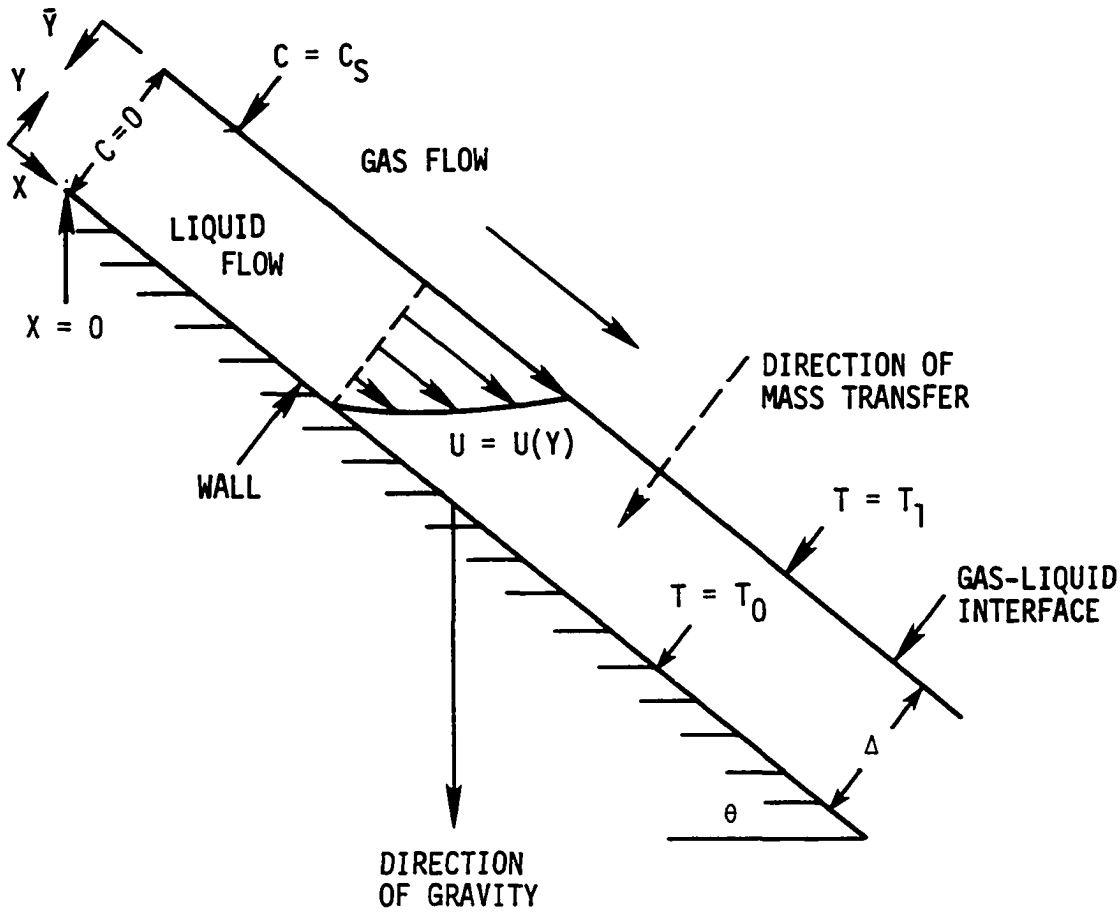

Figure 2. Gas absorption in a laminar falling film

Based on the physical model and the assumptions stated, the transport equations and boundary conditions may be expressed as in the following: For heat transfer the energy equation is reduced to

$$\frac{d^2T}{d\eta^2} = 0 \tag{8}$$

with the boundary conditions

$$T = T_0 \qquad \text{at} \qquad \eta = 0 \quad \text{(the wall)} \tag{9}$$

$$T = T_1 \qquad \text{at} \qquad \eta = 1 \quad \text{(the interface)} \tag{10}$$

where $\eta = \frac{Y}{\Delta}$. The solution is simply

$$T = T_0 + (T_1 - T_0)\eta \tag{11}$$

Since the temperature profile is known, the variation of viscosity and molecular diffusion coefficient with temperature can be determined. Employing the same assumptions as used by Shair (73), the viscosity-temperature dependence is of the form, for $(T_1 - T_0)/T_0 << 1$,

$$\mu = \mu_0 e^{-\alpha\eta} \tag{12}$$

where $\alpha = E_a(T_1 - T_0)/T_0^2$. μ_0 is the viscosity at the reference wall temperature T_0, and E_a represents a free energy of activation. Values of the parameter E_a have been determined experimentally by Iyer (34) who examined 87 different liquids of diverse chemical constitution. The exponential dependency was found to be quite adequate in describing the temperature variation on liquid viscosity for a variety of pure liquids. Increasing values of α therefore denotes increasing variation of viscosity with temperature across the film. Typical values of α lie between 0 and 1.

For many liquid binary systems, $D\mu/T$ is essentially a constant. Substitution of Equation 11 and 12 gives

$$D = D_0 e^{\alpha\eta} \tag{13}$$

for $(T_1 - T_0)/T_0 << 1$. Derivations for the above two expressions can be found in Appendix A.

By utilizing Equation 12, the dimensionless form of the momentum equation reduces to

$$\frac{d}{d\eta}\left(e^{-\alpha\eta}\frac{dU^*}{d\eta}\right) = \frac{m\Delta^2}{\mu_0 U_1} \tag{14}$$

with the boundary conditions

$$U^* = 0 \qquad \text{at} \qquad \eta = 0 \tag{15}$$

$$\frac{dU^*}{d\eta} = \frac{\tau_1 \Delta e^{\alpha}}{\mu_0 U_1} \qquad \text{at} \qquad \eta = 1 \tag{16}$$

where $U^* = U/U_1$, $m = -\rho_1 g \sin\theta$, and U_1 is the surface velocity. The solution has been given by Shair (73):

$$U^* = (1 - \beta)\left[\frac{\alpha\eta e^{\alpha\eta} - \alpha e^{\alpha\eta} - e^{\alpha\eta} + \alpha + 1}{1 + \alpha - e^{\alpha}}\right] + \beta\left[\frac{e^{\alpha\eta} - 1}{e^{\alpha} - 1}\right] \tag{17}$$

where $\beta = \frac{\tau_1 \Delta}{\mu_0 U_1}\left(\frac{e^{\alpha} - 1}{\alpha}\right)$. The value of $\beta = 0$ corresponds to the freely falling film case while $\beta = 1$ corresponds to a highly stressed film or plane Couette flow. When $\alpha = 0$, application of L'Hospital's rule to Equation 17 gives the expression for an isothermal film:

$$U^* = (\beta - 1)\eta^2 + (2 - \beta)\eta \tag{18}$$

The average velocity is

$$\frac{\langle U \rangle}{U_1} = (1 - \beta)\left[\frac{\alpha^2 + 2\alpha + 2 - 2e^{\alpha}}{\alpha^2 + \alpha - \alpha e^{\alpha}}\right] + \beta\left[\frac{e^{\alpha} - \alpha - 1}{\alpha e^{\alpha} - \alpha}\right] \tag{19}$$

When $\alpha = 0$, Equation 19 tends to

$$\frac{\langle U \rangle}{U_1} = \frac{4 - \beta}{6} \tag{20}$$

The volumetric flow rate per unit width can be shown to be

$$Q = \frac{m\Delta^3}{\mu_0\alpha^2}\left(\frac{\alpha^2+2\alpha+2-2e^{\alpha}}{\alpha}\right) + \frac{\tau_1\Delta^2}{\mu_0}\left(\frac{e^{\alpha}-\alpha-1}{\alpha^2}\right) \qquad \alpha \neq 0 \tag{21}$$

$$Q = -\frac{1}{3}\left[\frac{m\Delta^3}{\mu_0}\right] + \frac{\tau_1\Delta^2}{2\mu_0} \qquad \alpha = 0 \tag{22}$$

Since $\beta = \frac{\tau_1\Delta}{\mu_0 U_1}\left(\frac{e^{\alpha}-1}{\alpha}\right)$, or

$$\beta = \frac{\frac{\tau_1\Delta}{\mu_0}\left(\frac{e^{\alpha}-1}{\alpha}\right)}{\frac{m\Delta^2}{\mu_0\alpha^2}(1+\alpha-e^{\alpha}) + \frac{\tau_1\Delta}{\mu_0}\left(\frac{e^{\alpha}-1}{\alpha}\right)} \qquad \alpha \neq 0 \tag{23}$$

$$\beta = \frac{\frac{\tau_1\Delta}{\mu_0}}{-\frac{m\Delta^2}{2\mu_0} + \frac{\tau_1\Delta}{\mu_0}} \qquad \alpha = 0 \tag{24}$$

Equations 21 and 22 can be expressed in terms of β as

$$Q = \frac{m\Delta^3}{\mu_0}\left[\frac{\alpha^2+2\alpha+2-2e^{\alpha}}{\alpha^3} + \frac{\beta}{(1-\beta)}\cdot\frac{(1+\alpha-e^{\alpha})^2}{\alpha(1-e^{\alpha})}\right] \qquad \begin{matrix}\alpha \neq 0 \\ \beta \neq 1\end{matrix} \tag{25}$$

$$Q = \frac{-m\Delta^3}{\mu_0}\left[\frac{1}{3} + \frac{\beta}{4(1-\beta)}\right] \qquad \begin{matrix}\alpha = 0 \\ \beta \neq 1\end{matrix} \tag{26}$$

From the definition of β, it can be seen that for $\beta = 1$ and any α, $\frac{m}{\mu_0}$ will be zero. Therefore, the film thickness can be derived as in the following:

$$\Delta = \left[\frac{Q}{\frac{m}{\mu_0}\left[\frac{\alpha^2+2\alpha+2-2e^{\alpha}}{\alpha^3} + \frac{\beta}{(1-\beta)}\,\frac{(1+\alpha-e^{\alpha})^2}{\alpha(1-e^{\alpha})}\right]}\right]^{1/3} \qquad \begin{matrix}\alpha \neq 0 \\ \beta \neq 1\end{matrix} \tag{27}$$

$$\Delta = \left[\frac{Q}{\frac{-m}{\mu_0}\left[\frac{1}{3} + \frac{\beta}{4(1-\beta)}\right]} \right]^{1/3} \qquad \alpha = 0 \quad \beta \neq 1 \tag{28}$$

$$\Delta = \left[\frac{\alpha^2 Q}{\frac{\tau_1}{\mu_0}(e^{\alpha}-\alpha-1)} \right]^{1/2} \qquad \alpha \neq 0 \quad \beta = 1 \tag{29}$$

$$\Delta = \left[\frac{2Q}{(\tau_1/\mu_0)} \right]^{1/2} \qquad \alpha = 0 \quad \beta = 1 \tag{30}$$

Equations 27 and 28 show that for a given flow rate, Q, and angle of inclination, $\theta(m=-\rho_1 g \sin\theta)$, the film thickness depends on α and β(or τ_1). Increasing values of α and β, that is, increasing temperature gradient and cocurrent shear will both tend to decrease the film thickness. The film thickness is more sensitive to changes in interfacial shear than temperature gradient. In the limit of $\beta = 1$, the film thickness is determined solely by the interfacial shear instead of the gravity force.

Mass transfer begins at the axial distance X = 0. At steady state the concentration of the diffusing component satisfies the convective-diffusion equation:

$$U^* \frac{\partial C^+}{\partial X^*} = \frac{\partial}{\partial \eta}\left(e^{\alpha\eta} \frac{\partial C^+}{\partial \eta}\right) \tag{31}$$

with the boundary conditions

$$C^+ = 0 \qquad \text{at} \qquad X^* = 0 \tag{32}$$

$$\frac{\partial C^+}{\partial \eta} = 0 \qquad \text{at} \qquad \eta = 0 \tag{33}$$

$$C^+ = 1 \qquad \text{at} \qquad \eta = 1 \tag{34}$$

where C^+ and X^* are the dimensionless concentration and axial length defined respectively as $C^+ = \frac{C}{C_S(T_1)}$, and $X^* = \frac{XD_0}{\Delta^2 U_1}$. It should be noted

that the equilibrium surface concentration, C_s, is a function of the surface temperature T_1. Therefore, C_s will decrease when α increases, that is, when T_1 is increased while a reference temperature T_0 is maintained constant for all the cases considered. Following an analysis by Shah (71,72), C_s is assumed to be a linear function of the temperature change, or, for $(T_1 - T_0)/T_0 << 1$,

$$C_s(T_1) = C_s(T_0)\ (1 - h\alpha) \tag{35}$$

where $h = \frac{H_s}{R_g E_a}$ is a constant depending on the physical properties of the system considered. H_s is the heat of solution and R_g is the gas constant. The case of $h = 0$ represents an isothermal condition where $T_1 = T_0$. Typical values of h lie between 0.5 and 1.0. Derivations of Equation 35 can be found in Appendix A.

Method of Solution

Equation 31 is solved by the method of separation of variables. The nonhomogeneous boundary conditions are rendered homogeneous by letting $C^* = 1 - C^+$ and substituting into Equations 31-34. The analytical solution can thus be written as

$$C^+ = 1 - C^* = 1 - \sum_{i=1}^{\infty} C_i N_i(\eta) e^{-\lambda_i^2 X^*} \tag{36}$$

where λ_i and N_i are the eigenvalues and eigenfunctions, respectively, satisfying the following characteristic equation:

$$\frac{d}{d\eta}\left(e^{\alpha\eta}\frac{dN_i}{d\eta}\right) + \lambda_i^2 U^* N_i = 0 \tag{37}$$

with the boundary conditions

$$\frac{dN_i}{d\eta} = 0 \qquad \text{at} \qquad \eta = 0 \tag{38}$$

$$N_i = 0 \qquad \text{at} \qquad \eta = 1 \tag{39}$$

It can be seen that Equations 37-39 constitute a system of the Sturm-Liouville type for which there exists an infinite set of real, nonnegative eigenvalues and a corresponding set of real eigenfunctions. The expansion coefficients, C_i, may be obtained by applying the transformed boundary condition of Equation 32:

$$C^* = 1 \qquad \text{at} \qquad X^* = 0 \tag{40}$$

and the condition of orthogonality of eigenfunctions with respect to the weighting function, $U^*(\eta)$,

$$C_i = \frac{\int_0^1 U^* N_i \, d\eta}{\int_0^1 U^* N_i^2 \, d\eta} \tag{41}$$

$$= \frac{-\frac{1}{\lambda_i^2}\left(e^{\alpha}\frac{\partial N_i}{\partial \eta}\Big|_{\eta=1}\right)}{\frac{e^{\alpha}}{2\lambda_i}\left(\frac{\partial N_i}{\partial \eta}\frac{\partial N_i}{\partial \lambda_i}\right)_{\eta=1}} \tag{42}$$

$$= -\frac{2}{\lambda_i\left(\frac{\partial N_i}{\partial \lambda_i}\Big|_{\eta=1}\right)} \tag{43}$$

The proof of the orthogonality of eigenfunction and the derivation of Equation 43 can be found in Appendix A of Jennis (37).

Equation 37 with the associated boundary conditions Equations 38 and 39 are solved by two methods:

1. The method of Frobenius which assumes a series solution of the form:

$$N_i(\eta,\lambda_i) = \sum_{n=0}^{\infty} a_n \eta^{n+s} \tag{44}$$

2. Numerical integration using fourth-order Runge-Kutta-Gill method. Since the series solution will involve an approximation of the velocity profile for $\alpha \neq 0$ and only the lower eigenvalues can be computed, it is not an efficient method. However, the series solution is simple and easy to formulate, so it will be presented here as a supplement to the numerical solution.

Series solution

The solution is presented for different cases of α and β:

(a) $\alpha = 0$, $\beta = 0$, $U^* = 2\eta-\eta^2$. Equation 37 becomes

$$N_i'' + \lambda_i^2(2\eta-\eta^2)N_i = 0 \tag{45}$$

This case has been considered by Emmert and Pigford (26), and also by Tamir and Taitel (81) who used a boundary condition that took into account interfacial resistances, and by Rotem and Neilson (68) who analyzed low Peclet number film flow.

(b) $\alpha = 0$, $\beta \neq 0$, U^* = Equation 18. Equation 37 becomes

$$N_i'' + \lambda_i^2[(\beta-1)\eta^2 + (2-\beta)\eta]N_i = 0 \tag{46}$$

Substitution of Equation 46 into Equation 44 and application of the boundary conditions Equations 38 and 39 result in, for $s = 0$,

$$a_0 = 1,\ a_1 = 0,\ a_2 = 0,$$

$$a_3 = \frac{-\lambda_i^2(2-\beta)}{6},\quad a_4 = \frac{-\lambda_i^2(\beta-1)}{12} \tag{47}$$

The recurrence relation is

$$a_{n+5} = \frac{-a_{n+1}\lambda_i^2(\beta-1) - a_{n+2}\lambda_i^2(2-\beta)}{(n+5)(n+4)} \tag{48}$$

(c) $\alpha \neq 0$, $\beta \neq 0$, U^* = Equation 17. Equation 37 becomes, after dividing throughout by $e^{\alpha\eta}$,

$$N_i'' + \alpha N_i' + \lambda_i^2\left[(1-\beta)\left(\frac{\alpha\eta-\alpha-1+\alpha e^{-\alpha\eta}+e^{-\alpha\eta}}{1+\alpha-e^{\alpha}}\right) + \beta\left(\frac{1-e^{-\alpha\eta}}{e^{\alpha}-1}\right)\right]N_i = 0 \tag{49}$$

In order to obtain a series solution, the exponential terms must be expanded in a truncated Taylor series form:

$$e^{-\alpha\eta} = 1 - \alpha\eta + \frac{\alpha^2\eta^2}{2!} - \frac{\alpha^3\eta^3}{3!} + \frac{\alpha^4\eta^4}{4!} - \ldots \tag{50}$$

A five-term expansion will give a maximum error of only 0.8% and is considered sufficient for the present analysis. Equation 49 becomes, after substituting Equation 50 and rearranging,

$$N_i'' + \alpha N_i' + \lambda_i^2(\alpha_1\eta + \alpha_2\eta^2 + \alpha_3\eta^3 + \alpha_4\eta^4)N_i = 0 \tag{51}$$

where

$$\alpha_1 = \frac{\beta\alpha}{e^{\alpha}-1} - \frac{(1-\beta)\alpha^2}{1+\alpha-e^{\alpha}} \tag{52}$$

$$\alpha_2 = \frac{(1-\beta)\alpha^2(\alpha+1)}{2(1+\alpha-e^{\alpha})} - \frac{\beta\alpha^2}{2(e^{\alpha}-1)} \tag{53}$$

$$\alpha_3 = \frac{\beta\alpha^3}{6(e^{\alpha}-1)} - \frac{(1-\beta)\alpha^3(\alpha+1)}{6(1+\alpha-e^{\alpha})} \tag{54}$$

$$\alpha_4 = \frac{(1-\beta)\alpha^4(\alpha+1)}{24(1+\alpha-e^{\alpha})} - \frac{\beta\alpha^4}{24(e^{\alpha}-1)} \tag{55}$$

The coefficients can be obtained, for s = 0, as

$$a_0 = 1,\ a_1 = 0,\ a_2 = 0,\ a_3 = \frac{-\lambda_i^2\alpha_1}{6},$$

$$a_4 = \frac{-3\alpha a_3 - \lambda_i^2\alpha_2}{12},\ a_5 = \frac{-4\alpha a_4 - \lambda_i^2\alpha_3}{20} \tag{56}$$

The recurrence relation is

$$a_{n+6} = \frac{-\alpha a_{n+5}(n+5) - \lambda_i{}^2(\alpha_1 a_{n+3} + \alpha_2 a_{n+2} + \alpha_3 a_{n+1} + \alpha_4 a_n)}{(n+6)(n+5)} \tag{57}$$

The remaining unknowns left undetermined are the eigenvalues, λ_i, which are the roots of the equation:

$$N_i(1,\lambda_i) = 0 \tag{58}$$

The eigenvalues can be located by any standard root-finding procedure. Specifically, the chord method is used. Sufficient number of terms of a_n are computed until $a_n<10^{-8}$. Iteration under the formula

$$\lambda_i{}^{n+1} = \lambda_i{}^n - \frac{N_i(\lambda_i{}^n)(\lambda_i{}^n - \lambda_{i\ \text{fixed}})}{N_i(\lambda_i{}^n) - N_i(\lambda_{i\ \text{fixed}})} \tag{59}$$

is terminated when $|\lambda_i{}^{n+1} - \lambda_i{}^n| \le 10^{-6}$ or when $N_i(\lambda_i{}^{n+1}) \le 10^{-6}$. Some of the useful quantities are calculated by the following:

$$N_i|_{\eta=1} = \sum_{n=0}^{\infty} a_n \tag{60}$$

$$\frac{\partial N_i}{\partial \lambda_i}\Big|_{\eta=1} = \sum_{n=0}^{\infty} \frac{\partial a_n}{\partial \lambda_i} \tag{61}$$

$$\frac{\partial N_i}{\partial \eta}\Big|_{\eta=1} = \sum_{n=0}^{\infty} n a_n \tag{62}$$

Quasi-numerical solution

Since the eigenvalue problem Equations 37-39 constitute a proper Sturm-Liouville system of the two-point boundary value type, it can be transformed into an initial value problem (see Keller (42)) of two equivalent first-order differential equations and integrated numerically. Specifically the following equations are obtained:

$$N'(\eta) = Ve^{-\alpha\eta} \qquad N(0) = 1 \tag{63}$$

$$V'(\eta) = -\lambda^2 U^* N \qquad V(0) = 0 \tag{64}$$

$$\xi'(\eta) = \rho e^{-\alpha\eta} \qquad \xi(0) = 0 \tag{65}$$

$$\rho'(\eta) = -\lambda^2 U^* \xi - 2\lambda U^* N \qquad \rho(0) = 0 \tag{66}$$

The above set of equations with the associated boundary conditions must satisfy Equation 58. The eigenvalues are located by means of Newton's method. Equations 65 and 66 are used to calculate the derivative that is required in Newton's method where

$$\xi = \frac{\partial N}{\partial \lambda} \quad , \qquad \rho = \frac{\partial V}{\partial \lambda} \tag{67}$$

and the following relations have been used:

$$\frac{\partial}{\partial \lambda}\left(\frac{\partial N}{\partial \eta}\right) = \frac{\partial}{\partial \eta}\left(\frac{\partial N}{\partial \lambda}\right) = \xi' \tag{68}$$

$$\frac{\partial}{\partial \lambda}\left(\frac{\partial V}{\partial \eta}\right) = \frac{\partial}{\partial \eta}\left(\frac{\partial V}{\partial \lambda}\right) = \rho' \tag{69}$$

The set of coupled equations, Equations 63-66, are integrated by a fourth-order Runge-Kutta-Gill method with a step size of 0.005, the accuracy and stability of which has been well-documented. Newton's iteration is performed simultaneously with the integration where

$$\lambda_i^{n+1} = \lambda_i^n - \frac{N_i(1,\lambda_i^n)}{\xi(1,\lambda_i^n)} \tag{70}$$

The iteration is continued until $|\lambda_i^{n+1} - \lambda_i^n| \leq 10^{-6}$. The derivatives of N_i are evaluated by

$$\left.\frac{\partial N_i}{\partial \lambda_i}\right|_{\eta=1} = \xi(1,\lambda_i) \tag{71}$$

$$\frac{\partial N_i}{\partial \eta}\Big|_{\eta=1} = V(1,\lambda_i)e^{-\alpha} \tag{72}$$

If some derivative-free root-finding procedure is used other than Newton's method, Equations 65 and 66 are not needed.

Once the eigenvalues and their corresponding eigenfunctions are known, then the bulk concentration, Sherwood number and the absorption rate can be evaluated as in the following by using Equation 36:

$$C^+_{bulk} = \frac{\int_0^1 U^* C^+ d\eta}{\int_0^1 U^* d\eta} \tag{73}$$

$$= 1 - \frac{\sum_{i=1}^{\infty} C_i e^{-\lambda_i^2 X^*} \int_0^1 U^* N_i d\eta}{\langle U \rangle / U_1} \tag{74}$$

$$= 1 - \frac{\sum_{i=1}^{\infty} C_i e^{-\lambda_i^2 X^*} \left(-\frac{e^{\alpha}}{\lambda_i^2} \frac{\partial N_i}{\partial \eta}\Big|_{\eta=1}\right)}{\langle U \rangle / U_1} \tag{75}$$

The Sherwood number, Sh', is defined with respect to D_0 and the concentration difference $(C_s - C_{bulk})$:

$$Sh' = \frac{k'\Delta}{D_0} \tag{76}$$

$$= \frac{e^{\alpha}}{(C^+_{bulk} - 1)} \sum_{i=1}^{\infty} C_i \frac{\partial N_i}{\partial \eta}\Big|_{\eta=1} e^{-\lambda_i^2 X^*} \tag{77}$$

For large values of X*, only the first term in the series will contribute significantly. Therefore, the fully developed Sherwood number is

$$Sh'_{\infty} = \frac{e^{\alpha} C_1 \frac{\partial N_1}{\partial \eta}\Big|_{\eta=1} e^{-\lambda_1^2 X^*}}{C_1 e^{-\lambda_1^2 X^*} \left(\frac{e^{\alpha}}{\lambda_1^2} \frac{\partial N_1}{\partial \eta}\Big|_{\eta=1}\right) / (\langle U \rangle / U_1)} \tag{78}$$

$$= \frac{\langle U \rangle}{U_1} \lambda_1^2 \tag{79}$$

Thus Sh'_∞ can be determined simply by knowing only the first eigenvalue and the average velocity. The total absorption rate per unit width, W_A, for an exposed film length, X, is calculated in terms of $\tilde{W}_A$:

$$\tilde{W}_A = e^{\alpha \Delta U_1} \sum_{i=1}^{\infty} C_i \frac{\partial N_i}{\partial \eta}\Big|_{\eta=1} \left[\frac{1}{\lambda_i^2} (e^{-\lambda_i^2 X^*} - 1)\right] \tag{80}$$

where $\tilde{W}_A = \frac{W_A}{C_S(T_1)}$. Equation 80 shows that the absorption rate will increase for an increase in the film thickness or the flow rate. For large contact times, the absorption rate will approach the saturation value:

$$\tilde{W}_{A\ sat.} = -e^{\alpha \Delta U_1} \sum_{i=1}^{\infty} C_i \frac{\partial N_i}{\partial \eta}\Big|_{\eta=1} \left(\frac{1}{\lambda_i^2}\right) \tag{81}$$

The above analysis therefore correctly accounts for the influence of the finite film thickness on absorption rate which is absent in the penetration theory, and useful results for intermediate and long contact times can be obtained relatively easily.

MASS TRANSFER WITH CHEMICAL REACTION

First-Order or Pseudo-First Order Reaction

The momentum and energy transport equations remain the same. The diffusion equation becomes

$$U(Y)\frac{\partial C}{\partial X} = \frac{\partial}{\partial Y}\left(D(T)\frac{\partial C}{\partial Y}\right) - k_1(T)C \tag{82}$$

where k_1 is the first-order or pseudo-first order reaction rate constant. All the rate constants are assumed to obey the Arrhenius relation. Using the same kind of reasoning in deriving $\mu(\eta)$, $D(\eta)$, and C_s, we arrive at (see Appendix A):

$$k_1 = k_{10}e^{p\alpha\eta} \tag{83}$$

where $p = \frac{\hat{E}}{R_g E_a}$ is a constant depending on the physical properties of the system, $\hat{E}$ is the activation energy, and k_{10} is the rate constant at T_0. The dimensionless form of Equation 82 is then

$$U^*\frac{\partial C^+}{\partial X^*} = \frac{\partial}{\partial \eta}\left(e^{\alpha\eta}\frac{\partial C^+}{\partial \eta}\right) - k_1^* e^{p\alpha\eta} C^+ \tag{84}$$

where $k_1^* = \frac{\Delta^2 k_{10}}{D_0}$ is the Damkohler Group II and the boundary conditions are the same as in Equations 32-34. Since the boundary condition Equation 34 is nonhomogeneous, the method of superposition is used to eliminate the nonhomogeneity. Let

$$C^+(X^*,\eta) = v(\eta) + u(X^*,\eta) \tag{85}$$

then Equation 84 can be reduced to two equivalent sets of equations:

(1) $$U^*\frac{\partial u}{\partial X^*} = \frac{\partial}{\partial \eta}\left(e^{\alpha\eta}\frac{\partial u}{\partial \eta}\right) - k_1^* e^{p\alpha\eta} u \tag{86}$$

with the boundary conditions

$$u = -v \qquad \text{at} \qquad X^* = 0 \tag{87}$$

$$\frac{\partial u}{\partial \eta} = 0 \qquad \text{at} \qquad \eta = 0 \tag{88}$$

$$u = 0 \qquad \text{at} \qquad \eta = 1 \tag{89}$$

$$(2)\quad \frac{d}{d\eta}\left(e^{\alpha\eta}\frac{dv}{d\eta}\right) - k_1^* e^{p\alpha\eta} v = 0 \tag{90}$$

with the boundary conditions

$$\frac{dv}{d\eta} = 0 \qquad \text{at} \qquad \eta = 0 \tag{91}$$

$$v = 1 \qquad \text{at} \qquad \eta = 1 \tag{92}$$

The first set of equations, which we shall designate the "transient part," still constitute a proper "Sturm-Liouville" system and can be solved by the same method of separation of variables as described for the case of physical absorption. The characteristic equation in this case is

$$\frac{d}{d\eta}\left(e^{\alpha\eta}\frac{dN_i}{d\eta}\right) + \left(\lambda_i^2 U^* - k_1^* e^{p\alpha\eta}\right) N_i = 0 \tag{93}$$

with the boundary conditions given by Equations 38 and 39. By employing the same kind of reasoning as in the case of physical absorption, Equation 93 can be transformed into the following initial value problem and integrated numerically:

$$N'(\eta) = Ve^{-\alpha\eta} \qquad N(0) = 1 \tag{94}$$

$$V'(\eta) = k_1^* e^{p\alpha\eta} N - \lambda^2 U^* N \qquad V(0) = 0 \tag{95}$$

$$\xi'(\eta) = \rho e^{-\alpha\eta} \qquad \xi(0) = 0 \tag{96}$$

$$\rho'(\eta) = (k_1^* e^{p\alpha\eta} - \lambda^2 U^*)\xi - 2\lambda U^* N \qquad \rho(0) = 0 \tag{97}$$

In order to simplify the solution of the second set of equations, which we shall designate the "steady part," a typical value of p = 1 is chosen for analysis. The solution is given by

$$v = \frac{m_2 e^{m_1 \eta} - m_1 e^{m_2 \eta}}{m_2 e^{m_1} - m_1 e^{m_2}} \tag{98}$$

where $$m_1 = \frac{-\alpha+(\alpha^2+4k_1^*)^{\frac{1}{2}}}{2} \tag{99}$$

$$m_2 = \frac{-\alpha-(\alpha^2+4k_1^*)^{\frac{1}{2}}}{2} \tag{100}$$

The expansion coefficients are obtained by applying Equation 87 and the orthogonality relationship:

$$C_i = \frac{\int_0^1 (-v)U^*N_i d\eta}{\int_0^1 U^*N_i^2 d\eta} \tag{101}$$

It can be shown, by following the same derivations in Appendix A of Jennis (37), that

$$\int_0^1 U^*N_i^2 d\eta = \frac{e^{\alpha}}{2\lambda_i}\left[\frac{\partial N_i}{\partial \eta}\ \frac{\partial N_i}{\partial \lambda_i}\right]_{\eta=1} \tag{102}$$

Then the expansion coefficients become

$$C_i = \frac{\frac{1}{m_2 e^{m_1}-m_1 e^{m_2}} \int_0^1 (m_1 e^{m_2\eta}-m_2 e^{m_1\eta})U^*N_i d\eta}{\frac{e^{\alpha}}{2\lambda_i}\left[\frac{\partial N_i}{\partial \eta}\frac{\partial N_i}{\partial \lambda_i}\right]_{\eta=1}} \tag{103}$$

The integral in the numerator is evaluated by Simpson's rule with extrapolation using step sizes of 0.025 and 0.0125 (see Lapidus (46), p. 54). The complete solution is

$$C^+ = \sum_{i=1}^{\infty} C_i N_i e^{-\lambda_i {}^2 X^*} + \frac{m_2 e^{m_1 \eta} - m_1 e^{m_2 \eta}}{m_2 e^{m_1} - m_1 e^{m_2}} \tag{104}$$

Equation 104 shows that the effect of chemical reactions with a linear order can be easily superimposed on the mean flow. The bulk concentration is computed as

$$C^+_{bulk} = \frac{\sum_{i=1}^{\infty} C_i e^{-\lambda_i {}^2 X^*} \left(\int_0^1 U^* N_i d\eta \right) + \frac{1}{m_2 e^{m_1} - m_1 e^{m_2}} \int_0^1 (m_2 e^{m_1 \eta} - m_1 e^{m_2 \eta}) U^* d\eta}{\langle U \rangle / U_1} \tag{105}$$

As $X^* \to \infty$, only the second term remains and an asymptotic situation has been reached. The integral, $\int_0^1 (m_2 e^{m_1 \eta} - m_1 e^{m_2 \eta}) U^* d\eta$, can be evaluated analytically by substituting the appropriate velocity profiles. For $\alpha = 0$:

$$\int_0^1 (m_2 e^{m_1 \eta} - m_1 e^{m_2 \eta}) U^* d\eta = (1 - \beta)(e^{\sqrt{k_1^*}} - e^{-\sqrt{k_1^*}}) + (2\beta - 2 - 2\sqrt{k_1^*} + \beta\sqrt{k_1^*}) \left(\frac{e^{\sqrt{k_1^*}}}{\sqrt{k_1^*}} - \frac{e^{\sqrt{k_1^*}}}{k_1^*} + \frac{1}{k_1^*} \right) + (2 - 2\beta - 2\sqrt{k_1^*} + \beta\sqrt{k_1^*}) \left(\frac{1}{k_1^*} - \frac{e^{-\sqrt{k_1^*}}}{\sqrt{k_1^*}} - \frac{e^{-\sqrt{k_1^*}}}{k_1^*} \right) \tag{106}$$

For $\alpha \neq 0$, the integral becomes, after a tedious calculation,

$$\int_0^1 (m_2 e^{m_1 \eta} - m_1 e^{m_2 \eta}) U^* d\eta = \frac{(1-\beta) m_2}{1 + \alpha - e^{\alpha}} \left[\frac{\alpha + 1}{m_1} (e^{m_1} - 1) + \frac{1}{m_1 + \alpha} \left(\frac{\alpha}{m_1 + \alpha} + \alpha + 1 \right) - \frac{1}{m_1 + \alpha} \left(\frac{\alpha}{m_1 + \alpha} + 1 \right) e^{(m_1 + \alpha)} \right] - \frac{(1-\beta) m_1}{1 + \alpha - e^{\alpha}} \left[\frac{\alpha + 1}{m_2} (e^{m_2} - 1) + \frac{1}{m_2 + \alpha} \left(\frac{\alpha}{m_2 + \alpha} + \alpha + 1 \right) - \frac{1}{m_2 + \alpha} \left(\frac{\alpha}{m_2 + \alpha} + 1 \right) e^{(m_2 + \alpha)} \right] + \frac{\beta m_1}{e^{\alpha} - 1} \left[\frac{1}{m_2 + \alpha} (e^{(m_2 + \alpha)} - 1) - \frac{1}{m_2} (e^{m_2} - 1) \right] + \frac{\beta m_2}{e^{\alpha} - 1} \left[\frac{1}{m_1 + \alpha} (e^{(m_1 + \alpha)} - 1) - \frac{1}{m_1} (e^{m_1} - 1) \right] \tag{107}$$

The dimensionless mass flux is given by

$$\frac{N_A|_{\eta=1}^{\Delta}}{D_0 C_S(T_1)} = e^{\alpha} \left[\sum_{i=1}^{\infty} C_i \frac{\partial N_i}{\partial \eta}\Big|_{\eta=1} e^{-\lambda_i^2 \chi^*} + \frac{m_1 m_2 (e^{m_1} - e^{m_2})}{m_2 e^{m_1} - m_1 e^{m_2}} \right] \tag{108}$$

It is convenient to define an average isothermal and nonisothermal enhancement factor respectively as:

$$\Phi_I = \left(\frac{W_{A,\text{reaction}}}{W_{A,\text{physical}}}\right)_{\alpha=0} \tag{109}$$

$$\Phi_N = \left(\frac{W_{A,\text{reaction}}}{W_{A,\text{physical}}}\right)_{\alpha\neq 0} \tag{110}$$

where the ratio is based on the same α and β for W_A, and for a first-order reaction,

$$\Phi = \frac{\left[\sum_{i=1}^{\infty} C_i \frac{\partial N_i}{\partial \eta}\Big|_{\eta=1} \left[\frac{1}{\lambda_i^2}(1-e^{-\lambda_i^2 \chi^*})\right] + \chi^* \frac{m_1 m_2 (e^{m_1} - e^{m_2})}{m_2 e^{m_1} - m_1 e^{m_2}} \right]_{\text{reaction}}}{\left[\sum_{i=1}^{\infty} C_i \frac{\partial N_i}{\partial \eta}\Big|_{\eta=1} \left[\frac{1}{\lambda_i^2}(1-e^{-\lambda_i^2 \chi^*})\right] \right]_{\text{physical}}} \tag{111}$$

It should be noted that the nonisothermal enhancement factor, Φ_N, is the ratio of the chemical absorption rate at a certain α and β to the physical absorption rate at the same α and β.

Asymptotic solutions have been obtained for the isothermal, zero interfacial shear case in the light of the penetration theory. We define

$$Sh = \frac{-D_0}{C_S - C_0} \frac{\partial C}{\partial Y}\Big|_{Y=\Delta} \tag{112}$$

where C_0 is the inlet concentration. The Sherwood number is defined with respect to $(C_S - C_0)$ and the solution is given as (20):

$$Sh = \sqrt{k_1^*}\ \operatorname{erf}(\sqrt{k_1^* X^*}) + \frac{e^{-k_1^* X^*}}{(\pi X^*)^{\frac{1}{2}}} \tag{113}$$

The asymptotes are:

(1) short θ_c, small k_1^* $\qquad Sh = \dfrac{1}{(\pi X^*)^{\frac{1}{2}}}$ (114)

(2) long θ_c, small k_1^* Sh approaches that of physical absorption

(3) short θ_c, large k_1^* $\qquad Sh = \dfrac{e^{-k_1^* X^*}}{(\pi X^*)^{\frac{1}{2}}}$ (115)

(4) long θ_c, large k_1^* $\qquad Sh = (k_1^*)^{\frac{1}{2}}$ (116)

Zero-Order or Pseudo-Zero Order Reaction

The diffusion equation with zero-order kinetics is given in dimensionless form as

$$U^* \frac{\partial C^+}{\partial X^*} = \frac{\partial}{\partial \eta}\left(e^{\alpha\eta} \frac{\partial C^+}{\partial \eta}\right) - k_0^* e^{p\alpha\eta} \tag{117}$$

where $k_0^* = \dfrac{k_{00}\Delta^2}{D_0 C_S(T_1)}$ and k_{00} is the rate constant at T_0. Introducing Equation 85 again reduces Equation 117 into two equivalent sets of equations:

(1) $$U^* \frac{\partial u}{\partial X^*} = \frac{\partial}{\partial \eta}\left(e^{\alpha\eta} \frac{\partial u}{\partial \eta}\right) \tag{118}$$

with the boundary conditions given by Equations 87-89.

(2) $$\frac{d}{d\eta}\left(e^{\alpha\eta} \frac{dv}{d\eta}\right) - k_0^* e^{p\alpha\eta} = 0 \tag{119}$$

with the boundary conditions given by Equations 91 and 92. The first set of equations are identical to the case for physical absorption and hence the solutions are the same except the expansion coefficients which have to be computed from Equation 101 instead. To simplify the solution procedure

for v, the same typical value of p = 1 is chosen. For $\alpha = 0$,

$$v = 1 - \frac{k_0^*}{2} + \frac{k_0^*}{2}\eta^2 \qquad \text{if} \quad k_0^* < \frac{2}{(1-\eta^2)}$$

$$= 0 \qquad \text{if} \quad k_0^* \geq \frac{2}{(1-\eta^2)} \tag{120}$$

For $\alpha \neq 0$,

$$v = \frac{k_0^*}{\alpha^2}(e^{-\alpha\eta}-e^{-\alpha}) + \frac{k_0^*}{\alpha}(\eta-1) + 1 \quad \text{if} \quad k_0^* < \left(\frac{e^{-\alpha}-e^{-\alpha\eta}}{\alpha^2} + \frac{1-\eta}{\alpha}\right)^{-1}$$

$$= 0 \qquad \text{if} \quad k_0^* \geq \left(\frac{e^{-\alpha}-e^{-\alpha\eta}}{\alpha^2} + \frac{1-\eta}{\alpha}\right)^{-1} \tag{121}$$

From the complete solution $C^+ = u + v$, the bulk concentration can easily be calculated from Equation 73. The dimensionless mass flux at the interface is

$$\frac{N_A|_{\eta=1}^{\Delta}}{D_0 C_S(T_1)} = \sum_{i=1}^{\infty} C_i \left.\frac{\partial N_i}{\partial \eta}\right|_{\eta=1} e^{-\lambda_i^2 X^*} + k_0^* \qquad \alpha = 0 \tag{122}$$

$$= e^{\alpha}\left[\sum_{i=1}^{\infty} C_i \left.\frac{\partial N_i}{\partial \eta}\right|_{\eta=1} e^{-\lambda_i^2 X^*} + \frac{k_0^*}{\alpha}(1-e^{-\alpha})\right] \quad \alpha \neq 0 \tag{123}$$

This enables the chemical absorption rate as well as the average enhancement factors to be obtained in a similar manner as for the first-order reactions:

$$\Phi_I = \frac{\left[\sum_{i=1}^{\infty} C_i \left.\frac{\partial N_i}{\partial \eta}\right|_{\eta=1} \left[\frac{1}{\lambda_i^2}(1-e^{-\lambda_i^2 X^*})\right] + k_0^* X^*\right]}{\left[\sum_{i=1}^{\infty} C_i \left.\frac{\partial N_i}{\partial \eta}\right|_{\eta=1} \left[\frac{1}{\lambda_i^2}(1-e^{-\lambda_i^2 X^*})\right]\right]_{\text{physical},\alpha=0}} \tag{124}$$

$$\Phi_N = \frac{\left[\sum_{i=1}^{\infty} C_i \left.\frac{\partial N_i}{\partial \eta}\right|_{\eta=1} \left[\frac{1}{\lambda_i^2}(1-e^{-\lambda_i^2 X^*})\right] + \frac{k_0^*}{\alpha}(1-e^{-\alpha})X^*\right]}{\left[\sum_{i=1}^{\infty} C_i \left.\frac{\partial N_i}{\partial \eta}\right|_{\eta=1} \left[\frac{1}{\lambda_i^2}(1-e^{-\lambda_i^2 X^*})\right]\right]_{\text{physical},\alpha\neq 0}} \tag{125}$$

Certain asymptotic solutions can again be evaluated for the isothermal, zero interfacial shear case:

(1) short θ_c, small k_0^* $\quad Sh = \frac{1}{(\pi X^*)^{\frac{1}{2}}}$ (126)

(2) long θ_c, small k_0^* $\quad$ Sh approaches that of physical absorption

(3) short θ_c, large k_0^* $\quad Sh = \frac{1}{(\pi X^*)^{\frac{1}{2}}} + 2k_0^*(X^*)^{\frac{1}{2}}$ (127)

(4) long θ_c, large k_0^* $\quad Sh = k_0^*$ (128)

Pseudo-n-th Order and Instantaneous Reaction

Although it is no longer possible to solve the general pseudo-n-th order reaction in a laminar falling film by the method of superposition, it can be inferred from the analysis for n = 0 and n = 1 that a "steady-state" situation should be approached at large values of X*. This asymptotic situation is practically independent of the details of the hydrodynamics in the liquid film, that is, it is independent of the velocity profile and hence the interfacial shear. However, it is still influenced by heat transfer because the molecular diffusion coefficient and kinetic rate constants are functions of temperature. The length of the film in which the "transient part" is important will depend on the reaction rate. If the reaction rate is high, it can be expected that the "transient part" will be relatively small, and vice versa. Under isothermal condition for a semi-infinite liquid, a limiting solution was given by Porter and Roberts (64) who proved the existence of a "steady-state" solution. The solution and the conclusions should be equally applicable to the falling film considered here.

Some of the important chemical reactions encountered in industrial processes such as the absorption of carbon dioxide into sodium hydroxide are practically instantaneous. A complete analysis for an instantaneous irreversible reaction in a falling film would be quite complex. However, certain asymptotic solutions can be obtained for the case of small contact times where the enhancement factor is given by (20):

$$\Phi_I = \frac{1}{\text{erf}(\gamma'/D_A)} \tag{129}$$

and γ' is defined by

$$e^{\gamma'^2/D_B}\ \text{erfc}(\gamma'/\sqrt{D_B}) = \frac{C_{Bo}}{zC_{As}}\sqrt{\frac{D_B}{D_A}}\, e^{\gamma'^2/D_A}\ \text{erf}(\gamma'/\sqrt{D_A}) \tag{130}$$

The reaction plane is located at a distance $2\gamma'\sqrt{\theta_c}$ from the interface. D_A and D_B are the respective molecular diffusivities of gaseous A and liquid reactant B. C_{Bo} is the initial concentration of B and z moles of it react with each mole of A. When Φ_I is much greater than unity, Φ_I reduces to

$$\Phi_I = \sqrt{\frac{D_A}{D_B}} + \frac{C_{Bo}}{zC_{As}}\sqrt{\frac{D_B}{D_A}} \tag{131}$$

If $D_A = D_B$, then

$$\Phi_I = 1 + \frac{C_{Bo}}{zC_{As}} \tag{132}$$

Equations 129 and 131 hold only for isothermal conditions where D_A and D_B are constant. However, Equation 132 is true also for nonisothermal conditions and irrespective of the geometry or fluid flow model as shown by Brunson and Wellek (12). This means that it is applicable to all the film flow regimes regardless of whether it is laminar, wavy or turbulent. It is also independent of interfacial shear but is influenced by heat trans-

fer because of the dependence of C_{As} on interfacial temperature. Equation 132 shows that when α increases, the nonisothermal enhancement factor will increase over that for isothermal conditions. Danckwerts (20) has quoted some reactions that can be regarded as instantaneous and some that may be diffusion-controlled. He established that the criterion for the reaction to be considered as instantaneous should be

$$\frac{Q_0}{2C_{As}}\sqrt{\frac{\pi}{D_A\theta_c}} \gg 1 + \frac{C_{B0}}{zC_{As}} \tag{133}$$

where Q_0 was the amount of gas which would be absorbed in time θ_c if there were no depletion of B in the neighborhood of the interface. Astarita (2) has also provided such a criterion in terms of the reaction time and diffusion time.

HYDRODYNAMIC STABILITY OF LIQUID FILMS FLOWING DOWN AN INCLINED PLANE WITH ACCOMPANYING HEAT TRANSFER AND INTERFACIAL SHEAR

Since surface waves appear at small Reynolds number for film flow and enhance the momentum, heat, and mass transfer rates considerably over that predicted for smooth laminar flow, it is desirable to study the stability characteristics of these liquid films under various operating conditions. This has important application to some industrial processes such as coating where the surface rippling may lead to product nonuniformity. The hydrodynamic stability of an isothermal liquid film flowing down an inclined plane was first treated in detail by Benjamin (6) and Yih (87). Subsequent workers have followed these two lines with slight modifications, such as incorporating the influence of airflow (75), surface contamination (75,85), and evaporative flux (5). In the present work, the influence of heat transfer and interfacial shear on the hydrodynamic stability of falling liquid films is investigated. This not only has a direct bearing on the first part of our work on heat and mass transfer analysis, but also has related applications to the more common processes of film condensation, evaporation, cooling and heating.

General Formulation

The system considered is one of two-dimensional plane parallel flow under the action of gravity similar to that shown in Figure 2. Heat transfer occurs as a linear temperature drop across the film. All the physical properties are assumed to be a negligible function of temperature with the exception of the liquid viscosity which is assumed to follow the

exponential-temperature relationship. The gas flow exerts a constant tangential stress on the free surface, the latter being restrained also by surface tension. Under these conditions, the primary flow is the same as described in the previous section on mass transfer in laminar liquid films. The velocity profile of the primary flow is

$$\overline{U} = \frac{U}{\langle U \rangle} = \frac{(1-\beta)\left[\frac{\alpha\eta e^{\alpha\eta} - \alpha e^{\alpha\eta} - e^{\alpha\eta} + \alpha + 1}{1+\alpha-e^{\alpha}}\right] + \beta\left[\frac{e^{\alpha\eta}-1}{e^{\alpha}-1}\right]}{z_1} \tag{134}$$

where

$$z_1 = (1-\beta)\left[\frac{\alpha^2+2\alpha+2-2e^{\alpha}}{\alpha^2+\alpha-\alpha e^{\alpha}}\right] + \beta\left[\frac{e^{\alpha}-\alpha-1}{\alpha e^{\alpha}-\alpha}\right] \tag{135}$$

The velocity profile has been nondimensionalized with respect to the average velocity. If an arbitrarily small two-dimensional harmonic disturbance is imposed on the primary flow, the disturbance will either grow or decay in time or space. The condition in which there is no growth or decay defines the condition for neutral stability. The usual assumptions are that the Fourier components of an arbitrary disturbance are dynamically independent and that it is sufficient to consider only two-dimensional disturbance if any three-dimensional disturbance is represented by the same equations as a two-dimensional disturbance. In the presence of gas flow, surface perturbation stresses are formed by the interaction of the mean gas flow with the harmonic disturbance at the gas-liquid interface. The two-dimensional equations of motion which include the effect of variable viscosity, together with the kinematic and surface stress boundary conditions at the interface and the no-slip boundary conditions at the wall, form a complete boundary-value problem. From the solution of

this problem under an arbitrary imposed disturbance, the stability criteria can be deduced from the relationship between the disturbance and the mean flow.

The two-dimensional equations of motion are, in dimensionless form,

$$\frac{\partial u_1}{\partial \tau} + u_1\frac{\partial u_1}{\partial x} + v_1\frac{\partial u_1}{\partial \eta} = -\frac{\partial p_1}{\partial x} + \frac{\sin\theta}{F^2} + \frac{1}{R}\left[2\tilde{\mu}\frac{\partial^2 u_1}{\partial x^2} + \frac{d\tilde{\mu}}{d\eta}\left(\frac{\partial u_1}{\partial \eta} + \frac{\partial v_1}{\partial x}\right) + \tilde{\mu}\left(\frac{\partial^2 u_1}{\partial \eta^2} + \frac{\partial^2 v_1}{\partial x \partial \eta}\right)\right] \tag{136}$$

$$\frac{\partial v_1}{\partial \tau} + u_1\frac{\partial v_1}{\partial x} + v_1\frac{\partial v_1}{\partial \eta} = -\frac{\partial p_1}{\partial \eta} + \frac{\cos\theta}{F^2} + \frac{1}{R}\left[\tilde{\mu}\left(\frac{\partial^2 v_1}{\partial x^2} + \frac{\partial^2 u_1}{\partial x \partial \eta} + 2\frac{\partial^2 v_1}{\partial \eta^2}\right) + 2\frac{d\tilde{\mu}}{d\eta}\frac{\partial v_1}{\partial \eta}\right] \tag{137}$$

The dimensionless continuity equation is

$$\frac{\partial u_1}{\partial x} + \frac{\partial v_1}{\partial \eta} = 0 \tag{138}$$

The dimensionless energy equation for the temperature field is

$$\frac{\partial \hat{T}}{\partial \tau} + u_1\frac{\partial \hat{T}}{\partial x} + v_1\frac{\partial \hat{T}}{\partial \eta} = \frac{1}{Pe}\left[\frac{\partial^2 \hat{T}}{\partial x^2} + \frac{\partial^2 \hat{T}}{\partial \eta^2}\right] \tag{139}$$

The nomenclature used here is similar in many respects to that of Yih's (87):

$$u_1 = \frac{\hat{u}}{\langle U\rangle},\ v_1 = \frac{\hat{v}}{\langle U\rangle},\ x = \frac{X}{\Delta},\ \eta = \frac{Y}{\Delta},\ p_1 = \frac{\hat{p}}{\rho_1\langle U\rangle^2},\ \tau = \frac{t\langle U\rangle}{\Delta},$$
$$\tilde{\mu} = \frac{\mu}{\mu_0},\ R = \frac{\Delta\langle U\rangle\rho_1}{\mu_0},\ F = \frac{\langle U\rangle}{(g\Delta)^{\frac{1}{2}}},\ \hat{T} = \frac{T-T_1}{T_0-T_1},\ Pe = \frac{\langle U\rangle\Delta}{\alpha_t} \tag{140}$$

where $\hat{u}$, $\hat{v}$ = velocity components in the X and Y directions

p = pressure

t = time

μ_0 = viscosity of liquid at reference temperature T_0

R = Reynolds number, $\frac{1}{4}$ Re

F = Froude number

α_t = thermal diffusivity

Pe = Peclet number

Let

$$u_1 = \bar{U} + u' \ , \ v_1 = v' \ , \ p_1 = \bar{P} + p' \ , \ \hat{T} = \bar{T} + T' \tag{141}$$

where the primed quantities represent perturbations and $\bar{U}$, $\bar{P}$, $\bar{T}$ represent the velocity, pressure and temperature of the primary flow respectively.

It is assumed that the stream function for an infinitesimal disturbance is given in dimensionless form as

$$\psi = \phi(\eta)\exp[ik(x-c\tau)] \tag{142}$$

$$p' = f(\eta)\exp[ik(x-c\tau)] \tag{143}$$

$$T' = \hat{F}(\eta)\exp[ik(x-c\tau)] \tag{144}$$

where k is the dimensionless wave number, and $c = c_r + ic_i$ is the complex wave velocity. c_r is the real wave velocity and kc_i is the rate of amplification or decay. By defining

$$u' = \psi_\eta \ , \quad v' = -\psi_x \tag{145}$$

the continuity equation is automatically satisfied. Equation 145 is substituted into the equations of motion. After linearization and elimination of $f'(\eta)$, a fourth-order, linear, homogeneous ordinary differential equation is obtained which is the modified Orr-Sommerfeld equation with inclusion of the effect of variable viscosity (henceforth referred to as the modified O-S equation):

$$ikR[(\bar{U} - c)(\phi''-k^2\phi) - \bar{U}''\phi] = \tilde{\mu}(\phi''''-2k^2\phi''+k^4\phi)$$

$$+2\frac{d\tilde{\mu}}{d\eta}(\phi'''-k^2\phi') + \frac{d^2\tilde{\mu}}{d\eta^2}(\phi''+k^2\phi) \tag{146}$$

This equation has also been used to study shear wave instability for plane Poiseuille flow (65) and boundary-layer flow (84) under heat transfer. The modified O-S equation contains extra viscosity derivative terms arising from the effect of variable viscosity and is particularly important for the study of liquids. The energy equation becomes, after the same kind of manipulation,

$$(\hat{F}'' - k^2\hat{F}) = ikPe[(\bar{U} - c)\hat{F} - \phi\bar{T}'] \tag{147}$$

Since the velocity perturbations vanish at the wall, the boundary conditions at the wall are

(1) $u'(0) = \psi_\eta(0) = 0$ (148)

(2) $v'(0) = -\psi_x(0) = 0$ (149)

The two boundary conditions at the gas-liquid interface concern the balance of the tangential and normal stresses. Following a similar procedure by Craik (19) and Smith (75) in defining stress perturbation components for airflow, the tangential and normal stress boundary conditions at the surface $\eta = 1 + a$ are respectively:

(3) $\tilde{\mu}[\frac{\partial v'}{\partial x} + \frac{\partial u'}{\partial \eta}] = \frac{\tau_t a\Delta}{\mu_0 \langle U\rangle} = R\Sigma a$ (150)

(4) $-p_1 + \frac{2}{R}\tilde{\mu}\frac{\partial v'}{\partial \eta} - S\frac{\partial^2 a}{\partial x^2} = \frac{\tau_n a}{\rho_1 \langle U\rangle^2} = \Pi a$ (151)

where $S = \frac{\sigma}{\rho_1 \langle U\rangle^2 \Delta}$, $\Sigma = \frac{\tau_t}{\rho_1 \langle U\rangle^2}$, $\Pi = \frac{\tau_n}{\rho_1 \langle U\rangle^2}$ are dimensionless. $\tau_t a$ and $\tau_n a$ are the respective tangential and normal stress perturbations exerted by the gas flow, σ is the surface tension and $a\Delta$ is the displacement of the liquid surface. The boundary conditions for the energy equation are simply

(5) $T'(0) = 0$ (152)

(6) $\hat{T}(1 + a) = 0$ (153)

Equations 150, 151 and 153 apply only at $\eta = 1 + a$ and have to be linearized so that they apply at $\eta = 1$. The four boundary conditions for the modified O-S equation can be expressed as, after substituting Equations 142 and 145,

(1) $\phi'(0) = 0$ (154)

(2) $\phi(0) = 0$ (155)

$$(3)e^{-\alpha}[\phi''(1) + (k^2 + \frac{\bar{U}''|_{\eta=1}}{c-\bar{U}(1)})\phi(1)] = R\Sigma \frac{\phi(1)}{c-\bar{U}(1)} \quad (156)$$

$$(4) \quad -\left[k\left[\frac{R\cos\theta}{F^2} + k^2RS - R\bar{U}'(1) - \frac{R\Pi}{c-\bar{U}(1)}\right]\right]\phi(1) + k[R(c-\bar{U}(1)) + 3ike^{-\alpha}] \cdot$$

$$\phi'(1) - ie^{-\alpha}\phi'''(1) + i\alpha e^{-\alpha}[\phi''(1) + k^2\phi(1)] = 0 \quad (157)$$

The two boundary conditions for the energy equation become

(5) $\hat{F}(0) = 0$ (158)

$$(6) \quad \hat{F}(1) + \frac{\bar{T}'(1)\phi(1)}{c-\bar{U}(1)} = 0 \quad (159)$$

A remaining condition, the linearized kinematic condition at the gas-liquid interface is

$$v' = -\psi_x = a_\tau + \bar{U}a_x \quad (160)$$

or

$$a = [\frac{\phi(1)}{c-\bar{U}(1)}] \exp [ik(x - c\tau)] \quad (161)$$

Equation 146, together with Equations 154-157, constitute a complete eigenvalue problem. For temporal growth, the complex wave velocity c is solved in terms of the wave number and other governing parameters. The

harmonic disturbance of wave number k will grow and amplify in time if c_i is positive and damp or decay when c_i is negative. The equation

$$c_i(R,F,k,\theta,S,\alpha,\beta,\Sigma,\Pi) = 0 \tag{162}$$

depicts a relation between the wave number and other parameters that influence the flow and is defined as the neutral stability condition. Since the modified O-S equation and the boundary conditions do not depend on the energy equation, the stability criteria can be obtained without solving the energy equation.

Since the commonly observed wavelengths of the harmonic disturbances on thin liquid films are usually large compared to the film thickness, the wave number can be assumed to be small. Provided $k^2 \ll 1$ and $kR \ll 1$, a successive perturbation method can be used to solve the modified O-S equation. Yih (87) has shown that only two perturbations will be accurate enough to solve the governing O-S equation at small wave number and to obtain the condition for neutral stability. Since the velocity profile of the primary flow differs for $\alpha = 0$ and $\alpha \neq 0$, it is necessary to analyze the isothermal and nonisothermal cases separately.

Stability Characteristics in the Presence of Interfacial Shear Only

In the limit of $\alpha = 0$, the velocity profile of the primary flow reduces to

$$\bar{U} = \frac{6(\beta-1)\eta^2}{4-\beta} + \frac{6(2-\beta)\eta}{4-\beta} \tag{163}$$

and the governing equation is the original Orr-Sommerfeld equation without the viscosity derivative terms. For the first approximation in the solution for long waves, k can be set equal to zero and the O-S equation becomes simply

$$\phi'''' = 0 \tag{164}$$

with the boundary conditions

$$(1)\quad \phi'(0) = 0 \tag{165}$$

$$(2)\quad \phi(0) = 0 \tag{166}$$

$$(3)\quad \phi''(1) + \frac{\bar{U}''|_{\eta=1}}{c-\bar{U}(1)}\phi(1) = 0 \tag{167}$$

$$(4)\quad \phi'''(1) = 0 \tag{168}$$

where Σ is neglected in the first approximation. A general solution of Equation 164 can be expressed as

$$\phi = \bar{A} + \bar{B}\eta + \bar{C}\eta^2 + \bar{D}\eta^3 \tag{169}$$

Boundary condition Equations 165, 166 and 168 require $\bar{A}$, $\bar{B}$, and $\bar{D}$ to be zero. Equation 167 yields

$$c_0 = \frac{12 - 6\beta}{4-\beta} \tag{170}$$

where c_o is the first approximation for c. Since the system is linear and homogeneous, the eigenfunction is determined by arbitrarily setting $\bar{C}$ equal to one and the first approximation for ϕ is

$$\phi_0 = \eta^2 \tag{171}$$

Equation 170 shows that $c_0 = 3$ when $\beta = 0$ and $c_0 = 2$ when $\beta = 1$.

In the second approximation, only terms containing k and S are retained, terms with higher order in k and terms with $k\phi_1$ are negelected. The O-S equation is reduced to, by setting $\phi = \phi_0 + \phi_1$,

$$\phi'''' = ikR[(\bar{U}-c_0)\phi_0'' - \bar{U}''\phi_0] \tag{172}$$

$$= ikR[\frac{12(2-\beta)(\eta-1)}{4-\beta}] \tag{173}$$

The boundary conditions are

(1) $\phi_1'(0) = 0$ (174)

(2) $\phi_1(0) = 0$ (175)

(3) $$\phi_1''(1) + \frac{\bar{U}''|_{\eta=1}}{c_0'}\phi_1(1) - \frac{\bar{U}''|_{\eta=1}}{(c_0')^2}\phi_0(1) = R\Sigma \cdot \frac{\phi_0(1)}{c_0'} \tag{176}$$

(4) $$-\left[k\left[\frac{R\cos\theta}{F^2} + k^2RS}{c_0'} - R\bar{U}'(1) - \frac{R\Pi}{c_0'}\right]\right]\phi_0(1) + kRc_0'\phi_0'(1) - i\phi_1'''(1) = 0 \tag{177}$$

where $c_0' = c_0-\bar{U}(1)$, c_1 is the second approximation for c and terms of the order $\phi_1\Sigma$ and $c_1\Sigma$ are neglected. The general solution of Equation 173 can be expressed as

$$\phi_1 = \bar{A} + \bar{B}\eta + \bar{C}\eta^2 + \bar{D}\eta^3 + ikR\frac{(2-\beta)}{4-\beta}(\frac{\eta^5}{10} - \frac{\eta^4}{2}) \tag{178}$$

Equations 174 and 175 require $\bar{A}$ and $\bar{B}$ to be zero. Since the first approximation for ϕ contains the term η^2, $\bar{C}$ in ϕ_1 can be set to zero. From Equation 177, the constant $\bar{D}$ is found to be

$$\bar{D} = ikR\left[\frac{(\frac{\cos\theta}{F^2} + k^2S)}{c_0'} - 12\frac{(1-\beta)}{4-\beta} - \frac{\Pi}{c_0'} - 2c_0'\right]/6 \tag{179}$$

Since $\phi = \phi_0 + \phi_1$, the complete solution for ϕ is

$$\phi = \eta^2 + \bar{D}\eta^3 + ikR\frac{(2-\beta)}{4-\beta}(\frac{\eta^5}{10} - \frac{\eta^4}{2}) \tag{180}$$

with $\bar{D}$ given by Equation 179 and $c_0' = \frac{6(1-\beta)}{4-\beta}$. Then c_1 can be obtained by applying Equation 176 and is given by

$$c_1 = \frac{-R\Sigma}{E} - ikR\left(\frac{6+E}{6E}\right)\Pi + ikR\left[\frac{c_0'}{E}\left[2(6+E)\frac{(1-\beta)}{4-\beta} - \frac{(6+E)c_0'}{3}\right.\right.$$

$$\left.\left. -(4+\frac{2}{5}E)\frac{(2-\beta)}{4-\beta}\right] + \frac{(6+E)}{6E}\left(\frac{\cos\theta}{F^2} + k^2S\right)\right] \qquad (181)$$

where $E = \bar{U}''|_{\eta=1}/c_0'$. For $\alpha = 0$, $E = -2$ and is a constant. The perturbation stresses are complex and can be written as

$$\Sigma = \Sigma_r + i\Sigma_i \ , \ \Pi = \Pi_r + i\Pi_i \qquad (182)$$

Since $c = c_0 + c_1 = c_r + ic_i$

$$c_r = \frac{6(2-\beta)}{4-\beta} + \frac{R\Sigma_r}{2} - \frac{kR\Pi_i}{3} \qquad (183)$$

$$c_i = \frac{R\Sigma_i}{2} + \frac{kR\Pi_r}{3} + kR\left[\frac{48(1-\beta)(2-\beta)}{5(4-\beta)^2}\right] - \frac{kR}{3}\left(\frac{\cos\theta}{F^2} + k^2S\right) \qquad (184)$$

Instability occurs when c_i is positive, that is, when

$$\frac{3\Sigma_i}{2k} + \Pi_r + \left[\frac{144(1-\beta)(2-\beta)}{5(4-\beta)^2}\right] > \frac{\cos\theta}{F^2} + k^2S \qquad (185)$$

For small k, or $k^2S \ll \frac{\cos\theta}{F^2}$, the above criterion reduces to

$$F^2\left[\frac{3\Sigma_i}{2k} + \Pi_r + \frac{144(1-\beta)(2-\beta)}{5(4-\beta)^2}\right] > \cos\theta \qquad (186)$$

Equations 185 and 186 indicate that when $\beta = 1$, that is plane Couette flow, the flow in thin liquid films may not be stable at all Reynolds number when $\theta<90°$, in contrast to the plane Couette flow in confined geometries where it is well-known that the flow is always hydrodynamically stable. This is because of the perturbation stresses Σ_i and Π_r, and possibly some additional stresses arising from turbulence, which are formed by the interaction of the gas flow with the arbitrary disturbances. It also helps to explain why waves are still present in many experimental

observations of film flow where the gas or vapor velocity is extremely high such that the condition approaches that of plane Couette flow. Equation 185 shows that in the presence of interfacial shear, the Froude number becomes the governing parameter which is different from the zero interfacial shear case where the Reynolds number is the governing parameter. This is because when $\beta = 0$, a unique relation exists between the Reynolds number and the Froude number for a falling film but not for the cases $\beta \neq 0$. Since Σ_i and Π_r are positive, Equation 185 indicates that interfacial shear is a destabilizing factor.

In order to compare the results with other workers, it is necessary to convert the dimensionless wave velocities into dimensional quantities:

$$\hat{c}_r = c_r\langle U\rangle = \frac{-m\Delta^2}{\mu} + \frac{\tau_1\Delta}{\mu} + \frac{G_r\Delta^2}{2\mu} - \frac{kH_i\Delta^2}{3\mu} \tag{187}$$

$$\hat{c}_i = c_i\langle U\rangle = \frac{G_i\Delta^2}{2\mu} - k(\rho_l g\cos\theta + \frac{k^2\sigma}{\Delta^2} - H_r)(\frac{\Delta^2}{3\mu}) + \frac{2kg\sin\theta\Delta^4}{15\nu^2}$$

$$(\frac{\tau_1}{\mu} + \frac{\rho_l g\sin\theta\Delta}{\mu}) \tag{188}$$

where $G = \frac{\rho_l\langle U\rangle^2\Sigma}{\Delta}$ and $H = \frac{\rho_l\langle U\rangle^2\Pi}{\Delta}$. Instability occurs when

$$\frac{3G_i}{2k} + H_r + \frac{2}{5}\frac{g\sin\theta\Delta^2}{\nu^2}(\tau_1 + \rho_l g\sin\theta\Delta) > \rho_l g\cos\theta + \frac{k^2\sigma}{\Delta^2} \tag{189}$$

Equation 188 is in tentative agreement with the analysis of Smith (75) on three-dimensional film flow. When $\theta = 0$, the above result reduces to Craik's analysis on wind-generated waves in horizontal liquid films (19):

$$H_r + \frac{3G_i}{2k} > \rho_l g + \frac{k^2\sigma}{\Delta^2} \tag{190}$$

When G_i and H_r are negligible or equal to zero, Equation 189 becomes

$$\frac{2}{5}\frac{\sin\theta\Delta^2}{\nu^2\rho_1}(\tau_1 + \rho_1 g \sin\theta\Delta) > \cos\theta + \frac{k^2\sigma}{\rho_1 g\Delta^2} \tag{191}$$

for small k, or $\frac{k^2\sigma}{\rho_1 g\Delta^2} << \cos\theta$, this further reduces to

$$\frac{2}{5}\frac{\tan\theta\Delta^2}{\nu^2\rho_1}(\tau_1 + \rho_1 g \sin\theta\Delta) > 1 \tag{192}$$

which is in agreement with the results of Smith (75).

Stability Characteristics in the Presence of Both Heat Transfer and Interfacial Shear

The velocity profile of the primary flow is given in a general form by Equations 134 and 135. The solution procedure is similar to that in the previous section. In the first approximation, k is set equal to zero and the modified O-S equation becomes

$$\tilde{\mu}\phi'''' + 2\frac{d\tilde{\mu}}{d\eta}\phi''' + \frac{d^2\tilde{\mu}}{d\eta^2}\phi'' = 0 \tag{193}$$

Since $\tilde{\mu} = e^{-\alpha\eta}$, this is equivalent to solving

$$\phi'''' - 2\alpha\phi''' + \alpha^2\phi'' = 0 \tag{194}$$

which is a fourth-order, linear differential equation with constant coefficients. The boundary conditions are

(1) $\phi'(0) = 0$ (195)

(2) $\phi(0) = 0$ (196)

(3) $\phi''(1) + \frac{\bar{U}''|_{\eta=1}}{c-\bar{U}(1)}\phi(1) = 0$ (197)

(4) $\phi'''(1) - \alpha\phi''(1) = 0$ (198)

where Σ is neglected in the first approximation as before. A general solution of Equation 194 can easily be shown to be

$$\phi = \bar{A} + \bar{B}\eta + \bar{C}e^{\alpha\eta} + \bar{D}\eta e^{\alpha\eta} \tag{199}$$

Boundary condition Equation 198 demands $\bar{D} = 0$. Applying the remaining boundary conditions with suitable substitution results in $\bar{B} = \alpha$, $\bar{C} = -1$ and

$$c_0 = \frac{(2-\beta) + \beta\frac{(1+\alpha-e^{\alpha})}{e^{\alpha}-1}}{z_1} \tag{200}$$

It can be shown that Equation 200 readily reduces to Equation 170 when $\alpha = 0$. Since the eigenfunction is determined only up to a multiplicative constant, $\bar{A}$ can be arbitrarily set equal to one and the first approximation for ϕ becomes

$$\phi_0 = 1 + \alpha\eta - e^{\alpha\eta} \tag{201}$$

As usual, only terms containing k and S are retained in the second approximation. The equation to be solved is

$$\tilde{\mu}\phi'''' + 2\frac{d\tilde{\mu}}{d\eta}\phi''' + \frac{d^2\tilde{\mu}}{d\eta^2}\phi'' = ikR[(\bar{U}-c_0)\phi_0'' - \bar{U}''\phi_0] \tag{202}$$

or

$$\phi_1'''' - 2\alpha\phi_1''' + \alpha^2\phi_1'' = ikR[(\bar{U}-c_0)\phi_0'' - \bar{U}''\phi_0]e^{\alpha\eta} \tag{203}$$

The boundary conditions are

(1) $\phi_1'(0) = 0$ (174)

(2) $\phi_1(0) = 0$ (175)

(3) $$\phi_1''(1) + \frac{\bar{U}''|_{\eta=1}}{c_0'}\phi_1(1) - \frac{\bar{U}''|_{\eta=1}c_1}{(c_0')^2}\phi_0(1) = \frac{R\Sigma}{e^{-\alpha}}\frac{\phi_0(1)}{c_0'} \tag{204}$$

(4) $$-\left[k\left[\frac{(\frac{R\cos\theta}{F^2} + k^2RS)}{c_0'} - R\bar{U}'(1) - \frac{R\Pi}{c_0'}\right]\right]\phi_0(1) + kRc_0'\phi_0'(1)$$

$$- ie^{-\alpha}\phi_1'''(1) + i\alpha e^{-\alpha}\phi''(1) = 0 \tag{205}$$

where terms of order $k\phi_1$, $\phi_1\Sigma$, and $c_1\Sigma$ are neglected. The right hand side of Equation 203 can be expanded, after substituting the appropriate $\bar{U}$, c_0, and ϕ_0, into

$$ikR[(\bar{U}-c_0)\phi_0'' - \bar{U}''\phi_0]e^{\alpha\eta} = ikR[(c_0\alpha^2 - 2B_1\alpha^2)e^{2\alpha\eta} + (B_1\alpha^4-2B_1\alpha^3-B_2\alpha^3)\eta e^{2\alpha\eta} - B_1\alpha^4\eta^2e^{2\alpha\eta} + 2B_1\alpha^2e^{3\alpha\eta}] \quad (206)$$

where $B_1 = \frac{1-\beta}{(1+\alpha-e^{\alpha})z_1}$, and $B_2 = \frac{\beta}{(e^{\alpha}-1)z_1}$. The general solution of Equation 203 may be expressed as the sum of a complementary solution and a particular solution:

$$\phi_1 = \bar{A} + \bar{B}\eta + \bar{C}e^{\alpha\eta} + \bar{D}\eta e^{\alpha\eta} + ikR(A'e^{2\alpha\eta} + B'\eta e^{2\alpha\eta} + C'\eta^2e^{2\alpha\eta} + D'e^{3\alpha\eta}) \quad (207)$$

The constants A', B', C', and D' are determined respectively as

$$A' = \frac{c_0 + 3B_2 - 3B_1\alpha - 7.5B_1}{4\alpha^2} \quad (208)$$

$$B' = \frac{4B_1 + B_1\alpha - B_2}{4\alpha} \quad (209)$$

$$C' = -\frac{B_1}{4} \quad (210)$$

$$D' = \frac{B_1}{18\alpha^2} \quad (211)$$

Since ϕ_0 contains the constant 1 which is set arbitrarily, $\bar{A}$ in ϕ_1 can be set equal to zero. By applying Equations 202-205, and after long and tedious substitution and manipulation, $\bar{B}$, $\bar{C}$, $\bar{D}$ and c_1 can be determined respectively as

$$\bar{B} = -\alpha\bar{C} - \bar{D} - ikR(2\alpha A' + B' + 3\alpha D') \quad (212)$$

$$\bar{C} = -ikR(A' + D') \quad (213)$$

$$\bar{D} = \frac{i}{\alpha^2}\left[kR\left[\frac{\cos\theta}{F^2} + k^2S}{c_0'} - \bar{U}'(1) - \frac{\Pi}{c_0'} \right](1+\alpha-e^{\alpha}) - kRc_0'\alpha(1-e^{\alpha}) \right.$$

$$- kRe^{-\alpha}[8\alpha^3e^{2\alpha}(A'+B'+C') + 12\alpha^2e^{2\alpha}(B'+2C') + 12\alpha C'e^{2\alpha}+27\alpha^3D'e^{3\alpha}]$$

$$\left. + kR\alpha e^{-\alpha}[4\alpha^2e^{2\alpha}(A'+B'+C') + 4\alpha e^{2\alpha}(B'+2C') + 2C'e^{2\alpha}+9\alpha^2D'e^{3\alpha}] \right] \quad (214)$$

$$c_1 = \frac{-R\Sigma}{e^{-\alpha}E} + ikRb_2 - ikRb_3\left(\frac{\cos\theta}{F^2} + k^2S - \Pi\right) \quad (215)$$

where

$$b_2 = \frac{c_0'}{E(1+\alpha-e^{\alpha})}\left[4\alpha^2e^{2\alpha}(A'+B'+C') + 4\alpha e^{2\alpha}(B'+2C') + 2C'e^{2\alpha} \right.$$

$$+ 9\alpha^2D'e^{3\alpha} - E(A'+D') - E(2\alpha A'+B'+3\alpha D') + E(A'e^{2\alpha} + B'e^{2\alpha}$$

$$+ C'e^{2\alpha} + D'e^{3\alpha}) - (A'+D')(\alpha^2e^{\alpha} - E - E\alpha + Ee^{\alpha})$$

$$- \frac{(2\alpha e^{\alpha}+\alpha^2e^{\alpha}-E+Ee^{\alpha})}{\alpha^2}\left[\frac{\beta\alpha e^{\alpha}(1+\alpha-e^{\alpha})}{(e^{\alpha}-1)z_1} + c_0'\alpha(1-e^{\alpha}) + 4\alpha^3e^{\alpha} \right.$$

$$\left.\left. (A'+B'+C') + 8\alpha^2e^{\alpha}(B'+2C') + 10\alpha C'e^{\alpha}+18\alpha^3D'e^{2\alpha} \right] \right] \quad (216)$$

$$b_3 = \frac{E-Ee^{\alpha}-2\alpha e^{\alpha}-\alpha^2e^{\alpha}}{\alpha^2E} \quad (217)$$

$$E = \frac{\bar{U}''|_{\eta=1}}{c_0'} = \frac{\alpha^2e^{\alpha}}{1+\alpha-e^{\alpha}} \qquad \text{for } \alpha \neq 0 \quad (218)$$

Since $\phi = \phi_0 + \phi_1$, the complete solution for ϕ is

$$\phi = 1 + (\alpha+\bar{B})\eta + (\bar{C}-1)e^{\alpha\eta} + \bar{D}\eta e^{\alpha\eta} + ikR[A'e^{2\alpha\eta} + B'\eta e^{2\alpha\eta} + C'\eta^2e^{2\alpha\eta} + D'e^{3\alpha\eta}] \quad (219)$$

with $\bar{B}$, $\bar{C}$, $\bar{D}$ given by Equations 212-214, and A', B', C', D' given by Equations 208-211. The complex wave velocity, $c = c_0 + c_1 = c_r + ic_i$, is expressed as

$$c_r = \frac{(2-\beta) + \beta \frac{1+\alpha-e^{\alpha}}{e^{\alpha}-1}}{z_1} - \frac{R\Sigma_r}{e^{-\alpha_E}} - b_3 kR\Pi_i \tag{220}$$

$$c_i = \frac{-R\Sigma_i}{e^{-\alpha_E}} + b_2 kR - b_3 kR\left[\frac{\cos\theta}{F^2} + k^2 S - \Pi_r\right] \tag{221}$$

Instability occurs when

$$\frac{-\Sigma_i}{e^{-\alpha} E k b_3} + \Pi_r + \frac{b_2}{b_3} > \frac{\cos\theta}{F^2} + k^2 S \tag{222}$$

For small k, or $k^2 S << \frac{\cos\theta}{F^2}$, the above criterion becomes

$$F^2 \left[\frac{-\Sigma_i}{e^{-\alpha} E k b_3} + \Pi_r + \frac{b_2}{b_3}\right] > \cos\theta \tag{223}$$

Equations 220-223 are in a similar form as Equations 183-186 and it can be shown that in the limit of $\alpha = 0$, they are identical. This provides a check on the numerical procedure for the above mathematical analysis. Values of b_2, b_3 and E can be computed for various values of α and β. For an isothermal, zero interfacial shear liquid film, $\Sigma_i = 0$, $\Pi_r = 0$, $b_2 = \frac{6}{5}$, $b_3 = \frac{1}{3}$ and $E = -2$. Equation 222 reduces to

$$\frac{18}{5} > \frac{\cos\theta}{F^2} + k^2 S \tag{224}$$

If $k \to 0$, the above criterion becomes

$$R > \frac{5}{6} \cot\theta \tag{225}$$

where the relation $3F^2 = R\sin\theta$ has been substituted. Equation 225 is the one originally obtained by Benjamin (6) and Yih (87). When only heat transfer is involved and $\beta = 0$, Equation 222 becomes

$$\frac{b_2}{b_3} > \frac{\cos\theta}{F^2} + k^2 S \tag{226}$$

where b_2, b_3 and F are now functions of α only. In most experiments on film flow, it is much easier to vary the film Reynolds number than the Froude number. In order to compare the stability characteristics of liquid films accompanied by heat transfer and interfacial shear with the isothermal, zero interfacial shear films, it is necessary to compare them under the same Reynolds number. For a given flow rate, the film thickness can be calculated from either one of Equations 27-30 if the physical properties of the liquid, the angle of inclination, α and β (or τ_1) are known. Then the Froude number can be evaluated for each different case of α and β. If Σ_i and Π_r are known or can be calculated from hydrodynamic parameters of the gas flow, the stability criterion Equation 222 can be compared with Equation 224 under the same film Reynolds number. The perturbation stresses have already been shown to be destabilizing. For a given Reynolds number, F increases when α and/or β increase. b_2/b_3 also increases when α increases. Therefore, Equation 226 indicates that an increase in α is also a destabilizing factor. The stability criteria show that a decrease in θ or an increase in surface tension is stabilizing.

MASS TRANSFER IN TURBULENT FALLING FILMS WITH OR WITHOUT CHEMICAL REACTION

A number of models concerning mass transfer in a turbulent falling liquid film have appeared in the literature (e.g., 4, 48, 66). Most of them postulated that some type of surface renewal or eddy diffusion governs the transport processes. The surface renewal models usually require a determination of the surface renewal rate from experiments. King (43) introduced a surface-renewal-damped-eddy diffusivity model which also required two unknown parameters to be determined. The large eddy cell model of Fortescue and Pearson (27) assumes that square roll cells at the gas-liquid interface govern the mass transfer process. Although they found good agreement with experimental data in open channel flow, the model was not applicable to thin film flow. In contrast, Banerjee et al. (4) assumed that small eddies dominated the mass transfer in turbulent falling films because of the small thickness of the film. The rate of viscous dissipation was related to the turbulence and wave properties of the flow by a semi-empirical approach. Out of the various models proposed, the damped turbulence model of Levich (48) and Davies (22) seems to be a more realistic one and it is supported by some experimental findings (22). Its advantage also lies in the fact that no unknown empirical parameters have to be determined. However, the mass transfer coefficient deduced from this model underestimates the dependence of k_L on Re when compared with experiments. This is mainly because in the damped turbulence model, the friction velocity is used as a characteristic velocity, whereas in actual turbulent flow, a spectrum of eddy velocities exists.

The turbulent or eddy diffusivity was postulated as

$$D_{turb} = \frac{0.4 v_0}{\bar{\lambda}} \bar{Y}^2 = a' \bar{Y}^2 \tag{227}$$

where v_0, $\bar{\lambda}$, and $\bar{Y}$ have been previously defined. Since the use of a single representative velocity in a thin film is a quite doubtful assumption, the constant a' does not give the correct dependence of k_L on Re. Lamourelle and Sandall (45) experimentally determined the value of a' for falling water films in a long wetted-wall column. The expression was given by Equation 5. In the following, the solution procedure used in the previous sections on mass transfer in laminar falling films is extended to turbulent falling films by incorporating the eddy diffusivity model Equation 227. Analytical solutions for physical and chemical absorption with linear reaction kinetics are presented. The results are compared to the numerical solution and experimental data of Sandall and co-workers (41, 54,70).

Physical Absorption

The analysis is carried out for isothermal conditions. The species mass balance equation for a developing concentration profile is, in dimensionless form,

$$\frac{\partial C^+}{\partial X^*} = \frac{\partial}{\partial \eta} \left[(1+\beta^*(1-\eta)^2) \frac{\partial C^+}{\partial \eta} \right] \tag{228}$$

with the same boundary conditions as given by Equations 32-34. $\beta^* = \frac{a'\Delta^2}{D}$ is a dimensionless parameter characterizing the degree of turbulence. Large β^* denotes high turbulence level. The main assumptions in arriving at Equation 228 were embodied in the work of Sandall (70):

1. The velocity profile is approximated by the surface velocity, U_1, when absorption is for short to intermediate contact times since the turbulent velocity profile is rather flat near the interface.
2. The eddy diffusivity expression, originally established for the zone of damped turbulence, is assumed to apply over the whole film.
3. The average film thickness is assumed to be constant.
4. Diffusion-induced velocity is neglected.

The first three assumptions were justified by calculations made by Lamourelle and Sandall (45) and Menez and Sandall (54).

Equation 228 can again be solved by means of the separation of variables. The eigen-equation in this case becomes

$$[(1+\beta^*(1-\eta)^2)N_i']' + \lambda_i^2 N_i = 0 \tag{229}$$

with the boundary conditions given by Equations 38 and 39. By the same token as in the laminar flow analysis, the eigenvalues are computed by the fourth-order Runge-Kutta-Gill method and Newton's iteration. The coefficients, C_i, are again given by Equation 43. The Sherwood number for intermediate contact times, θ_c, is

$$Sh = -\sum_{i=1}^{\infty} C_i e^{-\lambda_i^2 X^*} \frac{\partial N_i}{\partial \eta}\Big|_{\eta=1} \tag{230}$$

For short θ_c, the penetration theory is again valid. For long θ_c, the Sherwood number was found to be (45)

$$Sh = \frac{2}{\pi}(\beta^*)^{\frac{1}{2}} \tag{231}$$

First-Order or Pseudo-First Order Reaction

It is implicitly understood that the assumptions made in the previous section on physical absorption also apply to the chemical absorption cases considered in the following. The dimensionless governing equation can be reduced to two equivalent sets of equations by linear superposition:

$$(1)\quad \frac{\partial u}{\partial X^*} = \frac{\partial}{\partial \eta}\left[(1+\beta^*(1-\eta)^2)\,\frac{\partial u}{\partial \eta}\right] - k_1^* u \tag{232}$$

with the boundary conditions given by Equations 87-89.

$$(2)\quad \frac{d}{d\eta}\left[(1+\beta^*(1-\eta)^2)\,\frac{dv}{d\eta}\right] - k_1^* v = 0 \tag{233}$$

with the boundary conditions given by Equations 91 and 92. k_1^* is the same Damkohler Group II as defined before. The first set of equations can again be separated and cast into a Sturm-Liouville system. The eigen-equation in this case has the form

$$[(1+\beta^*(1-\eta)^2)N_i']' + (\lambda_i^2 - k_1^*)N_i = 0 \tag{234}$$

with the boundary conditions given by Equations 38 and 39. Employing the fourth-order Runge-Kutta-Gill method, the initial-value system to be integrated is

$$N'(\eta) = \frac{V}{1+\beta^*(1-\eta)^2} \qquad N(0) = 1 \tag{235}$$

$$V'(\eta) = (k_1^* - \lambda^2)N \qquad V(0) = 0 \tag{236}$$

$$\xi'(\eta) = \frac{\rho}{1+\beta^*(1-\eta)^2} \qquad \xi(0) = 0 \tag{237}$$

$$\rho'(\eta) = (k_1^* - \lambda^2)\xi - 2\lambda N \qquad \rho(0) = 0 \tag{238}$$

The coefficients, C_i, are computed from the orthogonality relationship

$$C_i = \frac{\int_0^1 (-v)N_i\,d\eta}{\int_0^1 N_i^2\,d\eta} \tag{239}$$

The solution for v can either be obtained numerically, or more conveniently, by means of a general hypergeometric series. Let $\bar{\eta} = 1 - \eta$ where $\bar{\eta} = 0$ at the interface and substitute into Equations 233, 91, and 92, the resulting system of equations have been solved recently by Stepanek and Achwal (77) in terms of the Gauss hypergeometric series. The solution for v is

$$v = A(1-z')^{-b}\ {}_2F_1(b,b;\ \tfrac{1}{2};\ \tfrac{z'}{z'-1}) + B(1-z')^{-b}\ (\tfrac{z'}{z'-1})^{\frac{1}{2}}\ {}_2F_1(b+\tfrac{1}{2},\ b+\tfrac{1}{2};\ \tfrac{3}{2};\ \tfrac{z'}{z'-1}) \tag{240}$$

where $b = \frac{1}{4} - \sqrt{\frac{1}{16} + \frac{k_1^*}{4\beta^*}}$, $z' = -\beta^*\bar{\eta}^2 = -\beta^*(1-\eta)^2$, ${}_2F_1$ denotes a hypergeometric series (47). The integration constants can be determined from the boundary conditions as

$$A = 1 \tag{241}$$

$$B = \frac{b(\frac{\beta^*+1}{\beta^*})^{\frac{1}{2}}[{}_2F_1(b,b;\frac{1}{2};\frac{\beta^*}{\beta^*+1})] - (\frac{2b}{\beta^*+1}){}_2F_1(b+1,b+1;\frac{3}{2};\frac{\beta^*}{\beta^*+1})}{(\frac{1}{2\beta^*} - b){}_2F_1(b+\frac{1}{2},b+\frac{1}{2};\frac{3}{2};\frac{\beta^*}{\beta^*+1}) + \frac{2}{3}(b+\frac{1}{2})^2(\frac{1}{1+\beta^*}){}_2F_1(B+\frac{3}{2},b+\frac{3}{2};\frac{5}{2};\frac{\beta^*}{\beta^*+1})} \tag{242}$$

As $\beta^* \to \infty$,

$$B \doteq -\frac{{}_2F_1(b,\ b;\ \frac{1}{2};\ 1)}{{}_2F_1(b+\frac{1}{2},\ b+\frac{1}{2};\ \frac{3}{2};\ 1)} \tag{243}$$

in which ${}_2F_1$ can be converted into simple Gamma functions under certain conditions. The complete solution is therefore

$$C^+ = u + v = \sum_{i=1}^{\infty} C_i N_i e^{-\lambda_i^2 X^*} + \text{Equation 240} \tag{244}$$

The Sherwood number for intermediate contact times and reaction rates is

$$Sh = \sum_{i=1}^{\infty} C_i \frac{\partial N_i}{\partial \eta}\Big|_{\eta=1} e^{-\lambda_i^2 X^*} - B\beta^{*\frac{1}{2}} \tag{245}$$

If the concentration profile is fully developed at a distance sufficiently far downstream, then there is no need to solve the first set of equations. Certain asymptotic solutions have also been given by Menez and Sandall (54). These are rearranged and stated here:

(1) short θ_c, small k_1^* $\qquad Sh = \frac{1}{(\pi X^*)^{\frac{1}{2}}}$ (114)

(2) long θ_c, small k_1^* $\qquad Sh = \frac{2}{\pi}(\beta^*)^{\frac{1}{2}}$ (231)

(3) short θ_c, large k_1^* $\qquad Sh = \frac{e^{-k_1^* X^*}}{(\pi X^*)^{\frac{1}{2}}}$ (115)

(4) long θ_c, large k_1^* $\qquad Sh = (k_1^*)^{\frac{1}{2}}$ (116)

Zero-Order or Pseudo-Zero Order Reaction

As usual, the dimensionless governing equation can be transformed into two sets of equations by linear superposition:

(1) $$\frac{\partial u}{\partial X^*} = \frac{\partial}{\partial \eta}\left[(1+\beta^*(1-\eta)^2)\frac{\partial u}{\partial \eta}\right] \tag{246}$$

with the boundary conditions given by Equations 87-89.

(2) $$\frac{d}{d\eta}\left[(1+\beta^*(1-\eta)^2)\frac{dv}{d\eta}\right] - k_0^* = 0 \tag{247}$$

with the boundary conditions given by Equations 91 and 92. The first set of equations is identical to that of physical absorption, so the solution is the same except the coefficients C_i which have to be computed from Equation 239. Let $\bar{\eta} = 1 - \eta$, then the solution for v is, after two integrations and applying the boundary conditions:

$$v = 1 - \frac{k_0^*}{(\beta^*)^{\frac{1}{2}}} \arctan[(\beta^*)^{\frac{1}{2}}(1-\eta)] + \frac{k_0^*}{2\beta^*} \ln[1+\beta^*(1-\eta)^2]$$

$$\text{for } \eta \text{ satisfying } \frac{1}{(\beta^*)^{\frac{1}{2}}} \arctan[(\beta^*)^{\frac{1}{2}}(1-\eta)] - \frac{1}{2\beta^*} \ln[1+\beta^*(1-\eta)^2] < \frac{1}{k_0^*}$$

$$v = 0 \text{ if vice versa} \tag{248}$$

The Sherwood number for intermediate contact times and reaction rates is

$$Sh = \sum_{i=1}^{\infty} C_i \frac{\partial N_i}{\partial \eta}\Big|_{\eta=1} e^{-\lambda_i^2 X^*} + k_0^* \tag{249}$$

For a fully developed concentration profile, it is only necessary to solve the second set of equations. The asymptotic solutions can easily be deduced as

(1) short θ_c, small k_0^* $\qquad Sh = \frac{1}{(\pi X^*)^{\frac{1}{2}}}$ (126)

(2) long θ_c, small k_0^* $\qquad Sh = \frac{2}{\pi} (\beta^*)^{\frac{1}{2}}$ (231)

(3) short θ_c, large k_0^* $\qquad Sh = \frac{1}{(\pi X^*)^{\frac{1}{2}}} + 2k_0^*(X^*)^{\frac{1}{2}}$ (127)

(4) long θ_c, large k_0^* $\qquad Sh = k_0^*$ (128)

Pseudo-n-th Order and Instantaneous Reaction

Although it is no longer feasible to use the method of superposition for a general pseudo-n-th order reaction in a turbulent falling film, it can still be inferred from the analysis for n=0 and n=1 that a "steady-state" situation should approach at large values of X*. At this asymptotic situation, for $k_n^* \gg \beta^*$, the Sherwood number will be independent of the turbulent characteristics of the flow and depends only on k_n^*. For

$k_n^* << \beta^*$, the Sherwood number will be primarily a function of the turbulence parameter β^*. The length of the film in which the "transient part" is important will depend both on β^* and k_n^*. If $k_n^* >> \beta^*$, the "transient part" is expected to be relatively small while the reverse will be true if $k_n^* << \beta^*$. This is in contrast to the case in laminar falling film where the "transient part" varies inversely only with k_n^*.

Mass transfer with an instantaneous reaction in a turbulent liquid has been analyzed by Stepanek and Achwal (78) using the damped turbulence model. Mendez and Sandall (53) also used their previously proposed eddy diffusivity expression Equation 5 to study instantaneous reaction in a turbulent falling film. Axial transport was neglected for a fully developed condition and they found good agreement between the theoretical results and the experimental absorption of carbon dioxide into sodium hydroxide. The details are not repeated here. It should be recalled that a limiting solution for short contact times in a laminar falling film, Equations 129-132, can still be applied here when the gas absorbed has only enough time to diffuse into the diffusion sublayer near the interface where the influence of the molecular diffusivity is predominant over that of the turbulent diffusivity.

RESULTS AND DISCUSSION

Mass Transfer in a Laminar Falling Film

The eigenvalues and eigenfunctions for the case of physical absorption are determined for various values of α and β using the series solution:

1. $\alpha = 0$, $\beta = 0$ (constant properties, no shear)
2. $\alpha = 0$, $\beta = 1$
3. $\alpha = 1$, $\beta = 0$
4. $\alpha = 1$, $\beta = 1$
5. $\alpha = 0.1$, $\beta = 1$
6. $\alpha = 0.3$, $\beta = 1$
7. $\alpha = 0.1$, $\beta = 0.5$

The first four cases are also analyzed by the quasi-numerical solution as a comparison to the series solution. The eigenvalues computed by the series solution are presented in Table 2. The eigenvalues and related quantities, $\frac{\partial N_i}{\partial \lambda_i}|\eta=1$, $\frac{\partial N_i}{\partial \eta}|\eta=1$, C_i, computed by the quasi-numerical solution are presented in Tables 3-6 for the first fifteen eigenvalues. It can be seen that there is a regularity in spacing among the eigenvalues for all the cases considered, and that the magnitude of the eigenvalues increases when α or β increases. Since numerical errors tend to build up in calculating the subsequent coefficients, a_n, in the series solution, only the lower eigenvalues can be obtained accurately. For $\alpha = 1$, $0 \leq \beta \leq 1$, because the velocity profile is approximated by a truncated series expansion, the truncated error in the term, $\lambda^2 U^* N$, tends to amplify for large

Table 2. Eigenvalues computed by the series solution for various values of α and β

i \ α,β	0,0	0,1	1,0	1,1	0.1,1.0	0.3,1.0	0.1,0.5
1	2.263111	2.799526	3.592302	4.790286	2.951099	3.281392	2.613427
2	6.297685	7.481780	9.098676	11.593983	7.807398	8.507878	7.074924
3	10.307726	12.186397	14.715327	18.606422	12.699082	13.799045	11.541416
4	14.312794	16.895272	20.353074	25.667432	17.597843	19.103833	16.008821
5	18.315927	21.605664	25.998648	32.747604	22.499229	24.413828	20.476507
6	22.318088	26.316766		39.837404	27.401886	29.726396	24.944303
7	26.319690	31.028257			32.305258	35.040437	29.412152
8	30.320951	35.739984			37.209073	40.355405	
9					42.113193	45.670970	

Table 3. Eigenvalues and related quantities for $\alpha = 0$, $\beta = 0$ (quasi-numerical solution, $\delta\eta = 0.005$)

i	λ_i	$\frac{\partial N_i}{\partial \lambda_i}\|_{\eta=1}$	$\frac{\partial N_i}{\partial \eta}\|_{\eta=1}$	C_i
1	2.263111	-0.660401	-2.014963	1.338187
2	6.297685	0.582159	4.713852	-0.545516
3	10.307726	-0.540625	-7.123505	0.358898
4	14.312794	0.513588	9.379770	-0.272076
5	18.315927	-0.493848	-11.532720	0.221109
6	22.318100	0.478440	13.608540	-0.187304
7	26.319733	-0.465873	-15.623206	0.163110
8	30.321011	0.455309	17.587470	-0.144870
9	34.322072	-0.446223	-19.508974	0.130588
10	38.322999	0.438269	21.393406	-0.119077
11	42.323852	-0.431206	-23.245113	0.109587
12	46.324683	0.424861	25.067478	-0.101618
13	50.325536	-0.419102	-26.863144	0.094825
14	54.326453	0.413830	28.634163	-0.088960
15	58.327478	-0.408962	-30.382080	0.083844

Table 4. Eigenvalues and related quantities for $\alpha = 0$, $\beta = 1$

i	λ_i	$\frac{\partial N_i}{\partial \lambda_i}\|_{\eta=1}$	$\frac{\partial N_i}{\partial \eta}\|_{\eta=1}$	C_i
1	2.799526	-0.519194	-2.180245	1.375992
2	7.481780	0.437942	4.914880	-0.610391
3	12.186397	-0.403417	-7.374308	0.406818
4	16.895273	0.381945	9.679588	-0.309931
5	21.605681	-0.366567	-11.879923	0.252528
6	26.316802	0.354691	14.001588	-0.214263
7	31.028331	-0.345074	-16.060785	0.186792
8	35.740125	0.337027	18.068414	-0.166039
9	40.452117	-0.330130	-20.032255	0.149763
10	45.164280	0.324107	21.958079	-0.136630
11	49.876607	-0.318769	-23.850273	0.125793
12	54.589110	0.313979	25.712217	-0.116687
13	59.301811	-0.309634	-27.546496	0.108921
14	64.014742	0.305656	29.355047	-0.102215
15	68.727944	-0.301981	-31.139231	0.096364

Table 5. Eigenvalues and related quantities for $\alpha = 1$, $\beta = 0$

i	λ_i	$\frac{\partial N_i}{\partial \lambda_i}\|_{\eta=1}$	$\frac{\partial N_i}{\partial \eta}\|_{\eta=1}$	C_i
1	3.587407	-0.387773	-1.477908	1.437713
2	9.065506	0.307105	3.021233	-0.718373
3	14.652242	-0.278843	-4.437974	0.489516
4	20.261025	0.262188	5.771499	-0.376492
5	25.878222	-0.250585	-7.046154	0.308419
6	31.499615	0.241778	8.275979	-0.262607
7	37.123439	-0.234734	-9.469927	0.229512
8	42.748822	0.228894	10.634134	-0.204395
9	48.375282	-0.223926	-11.773037	0.184630
10	54.002535	0.219614	12.889964	-0.168638
11	59.630409	-0.215814	-13.987484	0.155412
12	65.258796	0.212420	15.067610	-0.144276
13	70.887633	-0.209358	-16.131933	0.134763
14	76.516886	0.206568	17.181708	-0.126535
15	82.146545	-0.204006	-18.217907	0.119343

Table 6. Eigenvalues and related quantities for $\alpha = 1$, $\beta = 1$

i	λ_i	$\frac{\partial N_i}{\partial \lambda_i}\|_{\eta=1}$	$\frac{\partial N_i}{\partial \eta}\|_{\eta=1}$	C_i
1	4.787656	-0.279332	-1.664109	1.495500
2	11.580055	0.210124	3.265565	-0.821945
3	18.581973	-0.188192	-4.749372	0.571921
4	25.632783	0.175909	6.148458	-0.443554
5	32.702887	-0.167574	-7.486492	0.364953
6	39.782696	0.161348	8.777728	-0.311582
7	46.868132	-0.156419	-10.031389	0.272812
8	53.957158	0.152362	11.253847	-0.243278
9	61.048648	-0.148930	-12.449718	0.219974
10	68.141931	0.145964	13.622467	-0.201080
11	75.236589	-0.143358	-14.774758	0.185430
12	82.332360	0.141036	15.908667	-0.172238
13	89.429077	-0.138945	-17.025811	0.160957
14	96.526641	0.137042	18.127433	-0.151193
15	103.624999	-0.135294	-19.214456	0.142655

λ's. Therefore only five or six eigenvalues can be computed. In contrast, the exact velocity profile is used in the quasi-numerical solution and the higher eigenvalues can be obtained easily. The agreement between the two solutions is exact for $\alpha = 0$ although slight deviations are found for $\alpha = 1$. This is attributed to the fact that the approximate velocity profile is used in the series solution for $\alpha \neq 0$. The eigenvalues computed by the quasi-numerical solution for $\alpha = 0$, $\beta = 0$ agree exactly with those of Tamir and Taitel (81) and Rotem and Neilson (68), showing that the solution is accurate.

The eigenvalues for the last three cases are compared with the work by Jennis (37) who used the assumptions of linear dependency of viscosity and molecular diffusivity on temperature. Agreement is very close showing that for small α, preferably $0 \leq \alpha \leq 0.3$, the two models are invariably the same. However, the two models deviate considerably for increasing values of α and β. This can be seen from Figure 3 where the dimensionless average velocity is plotted for various values of α and β. The average velocity for a linear temperature dependency of μ and D can be derived as

$$\frac{\langle U \rangle}{U_1} = (1-\beta)\left[\frac{1.5\alpha^2 - \alpha - (1-\alpha)^2 \ln(1-\alpha)}{\alpha^2 + \alpha(1-\alpha)\ln(1-\alpha)}\right] - \beta\left[\frac{(1-\alpha)\ln(1-\alpha) + \alpha}{\alpha \ln(1-\alpha)}\right] \qquad (250)$$

Equation 250 is not valid for $\alpha \geq 1$. The analysis of Jennis is restricted only to small α's with relatively large β's. This is primarily because of the linear assumptions used. The present work represents a substantial improvement by employing a more realistic assumption--the exponential dependency of viscosity on temperature and the Stokes-Einstein relation for the molecular diffusivity. Also, by invoking a quasi-numerical solution, the analysis is applicable to all ranges of α and β.

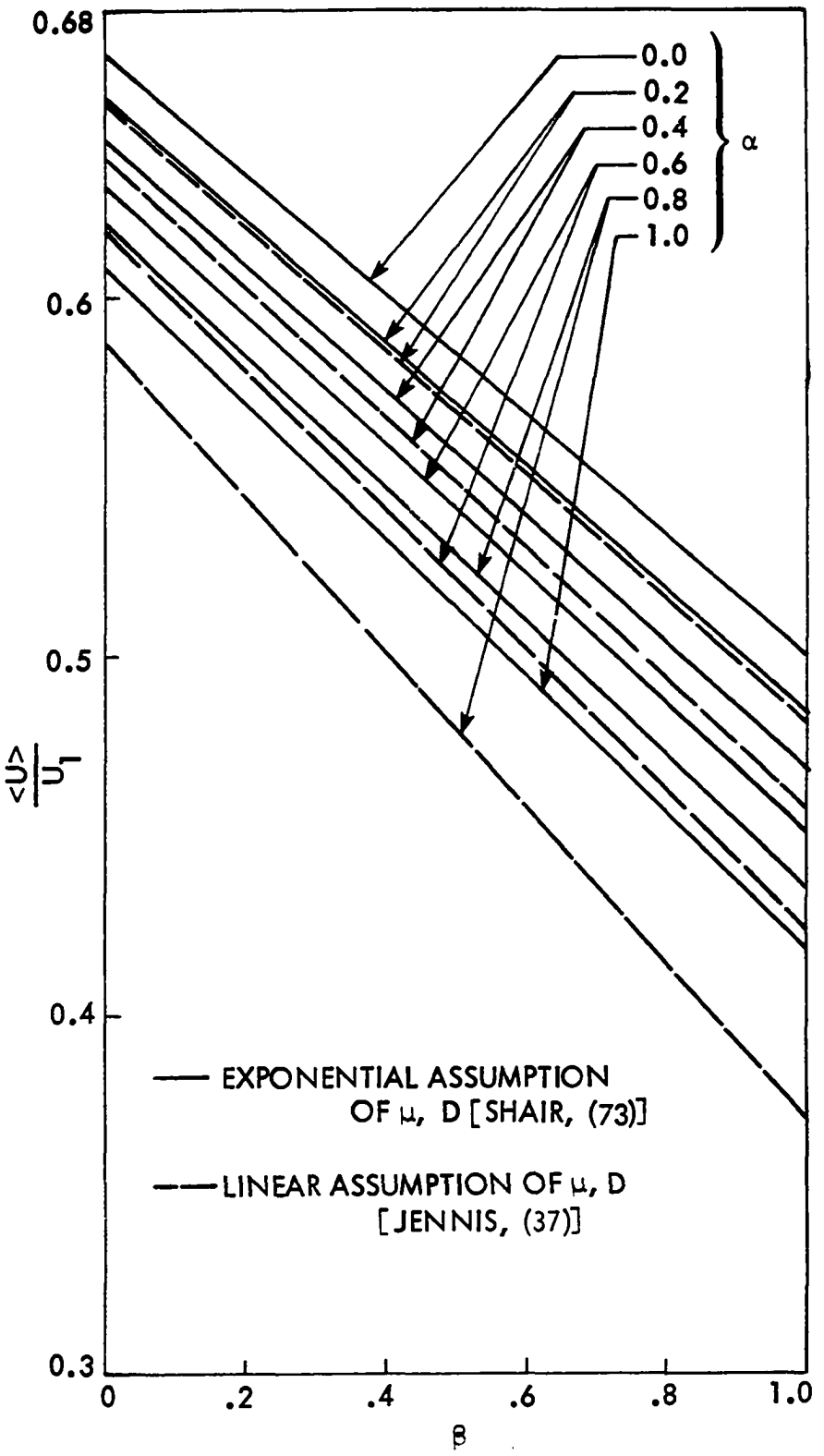

Figure 3. Average velocity in a falling film as a function of α and β

The concentration profile, bulk concentration, Sherwood number and total absorption rates can be computed using the first fifteen eigenvalues and associated eigenfunctions from the quasi-numerical solution. Four extreme operating conditions are analyzed:

1. $\alpha = 0, \beta = 0$
2. $\alpha = 0, \beta = 1$
3. $\alpha = 1, \beta = 0$
4. $\alpha = 1, \beta = 1$

The value of $\alpha = 1$ represents a 2.72 times change of viscosity across the film and is considered sufficient for most practical situations.

The variation of the bulk concentration with the dimensionless axial distance is presented in Figure 4. In order to compare absorption under nonisothermal conditions with that of isothermal conditions, the dimensionless bulk concentration with respect to the surface concentration at the reference temperature T_0 is also plotted for a typical value of $h = 0.6$ using Equation 35. When compared with the case of $\alpha = 0, \beta = 0$ under the same $C_s(T_0)$, it is observed that at a fixed X^* in the film, an increase in β increases the bulk concentration while an increase in α may increase or decrease the bulk concentration depending on the value of h. This shows that in order to correctly analyze the effects of heat transfer on the absorption rates, the variation of gas solubility with surface temperature must be accounted for. Since in most typical gas-liquid systems, the gas solubility decreases with increasing temperature and the value of α is usually greater than 0.5, an increase in α usually decreases the bulk concentration. High values of α and β cause saturation to be reached more quickly. Figure 5 gives the variation of the local Sherwood

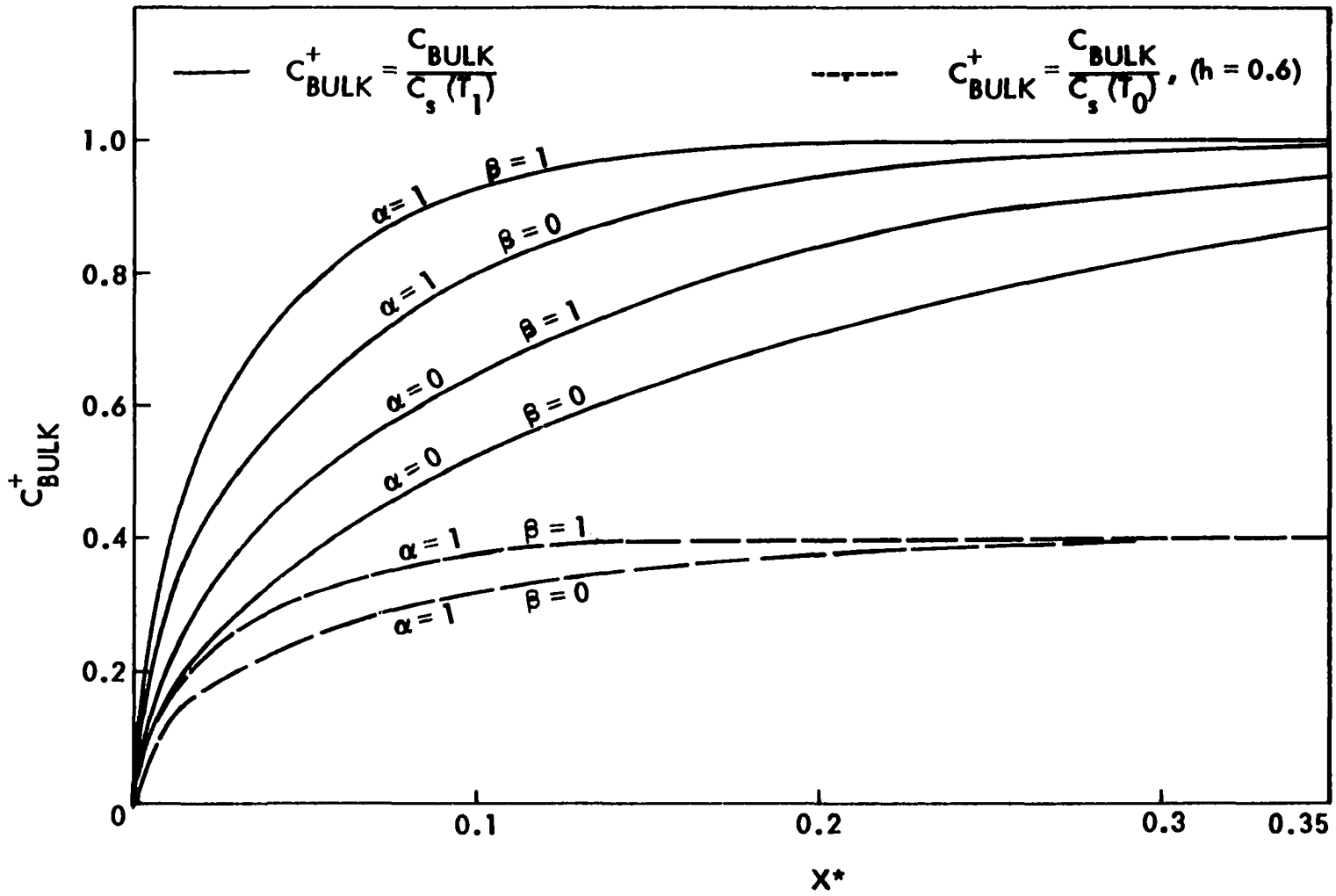

Figure 4. Dimensionless bulk concentration as a function of dimensionless axial length for various values of α and β

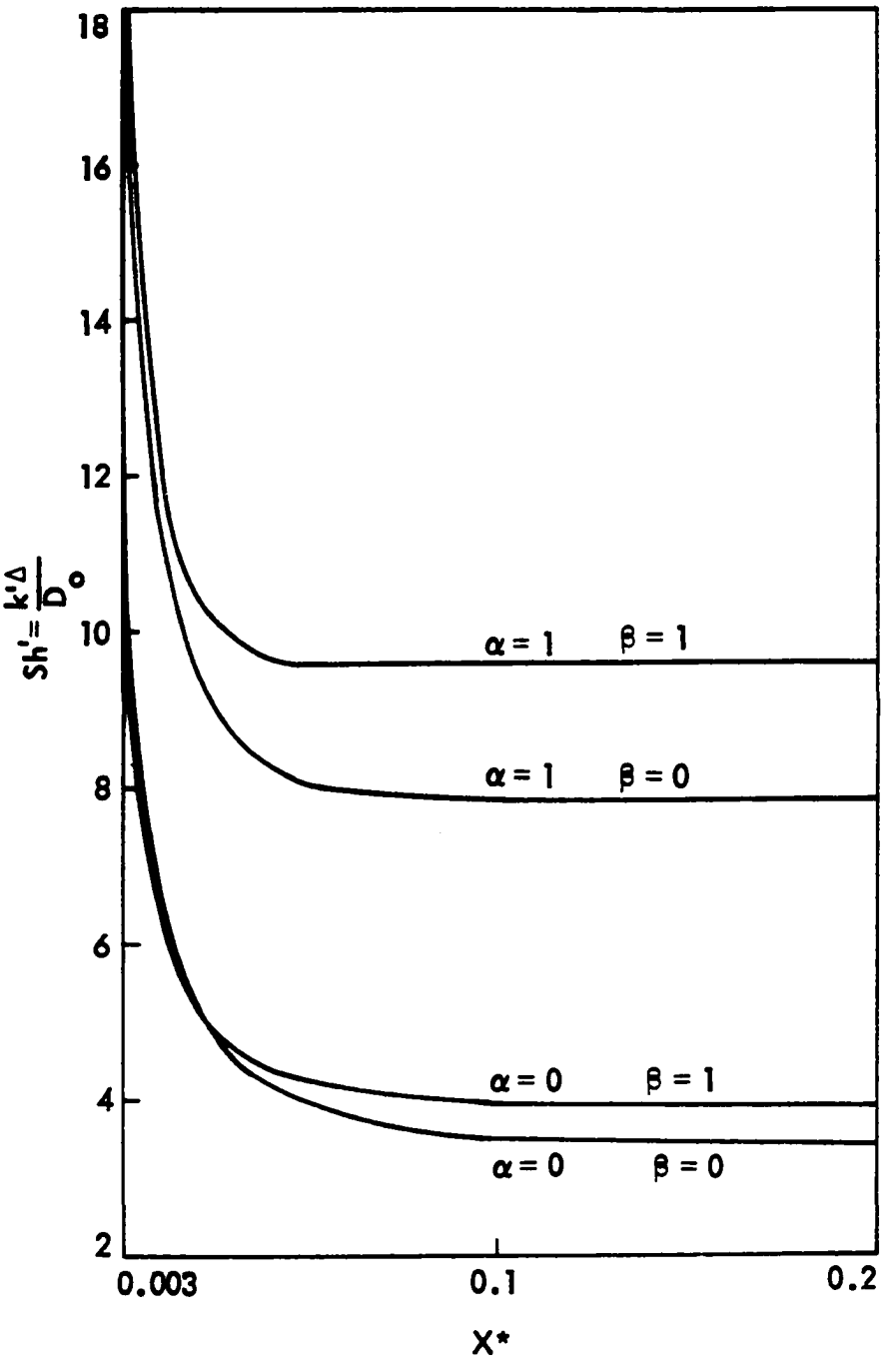

Figure 5. Local Sherwood number as a function of dimensionless axial length

number with the dimensionless axial length, X*. The Sherwood number here is defined with respect to the concentration difference ($C_s - C_{bulk}$). The higher the values of α and β, the faster the Sherwood number reaches its asymptotic value. The asymptotic Sherwood number as shown in Figure 5 is computed from Equation 79.

In order to assess the influence of heat transfer and cocurrent gas shear on the total absorption rate, it is necessary to compare several extreme operating conditions with the $\alpha = 0$, $\beta = 0$ case under the same flow rate. Since both the film thickness and surface velocity change under the same flow rate for different values of α and β, the dimensionless axial length, X*, cannot be used as a basis for comparison. In fact, no convenient dimensionless quantity can be used. Therefore, a comparison is made by plotting the dimensional total absorption rate, $\tilde{W}_A$, versus the exposed film length, X. For a given flow rate per unit width, Q, a given $\frac{-m}{\mu_0}$ (i.e., a given slope) and a given $\frac{\tau_1}{\mu_0}$ (i.e., a given β), the film thickness can be obtained from Equations 27-30. The average velocity, and hence the surface velocity, can be calculated. The parameter, $\Delta^2 U_1$, is plotted against the flow rate in Figure 6. It can be seen that the influence of β is much more pronounced than that of α on $\Delta^2 U_1$. This is also true for the film thickness. For a given X and D_0, X* is obtained at a given Q. From Figure 4, the appropriate values of C^+_{bulk} can thus be found. The total absorption rate $\tilde{W}_A = C^+_{bulk}\langle U\rangle$ is then plotted versus the exposed film length in Figures 7 and 8 for two different flow rates. It is evident that an increase in flow rate increases the absorption rate regardless of the values of α and β. The film reaches saturation more

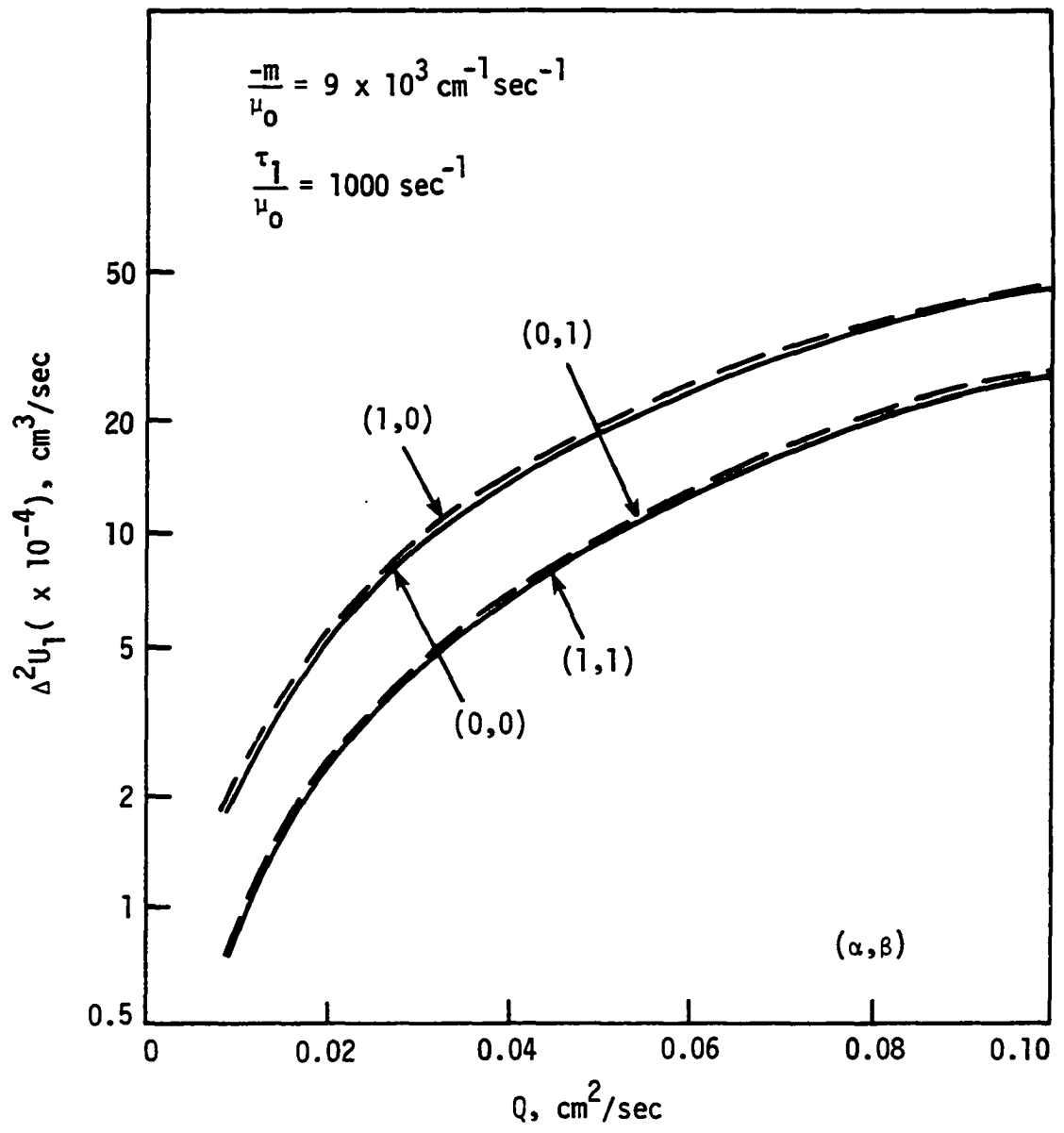

Figure 6. $\Delta^2 U_1$ as a function of flow rate per unit width for different values of α and β

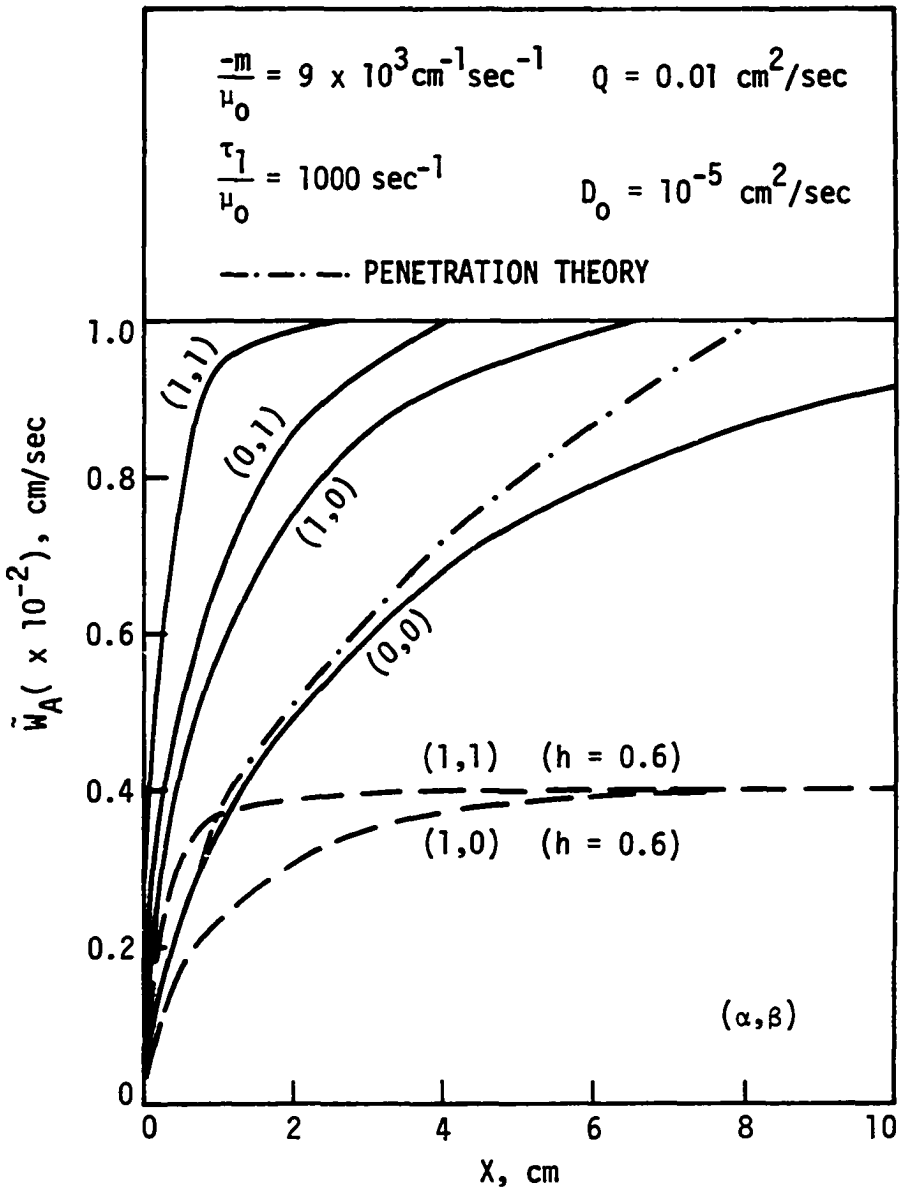

Figure 7. Total absorption rate as a function of exposed film length; Q = 0.01 cm^2/sec

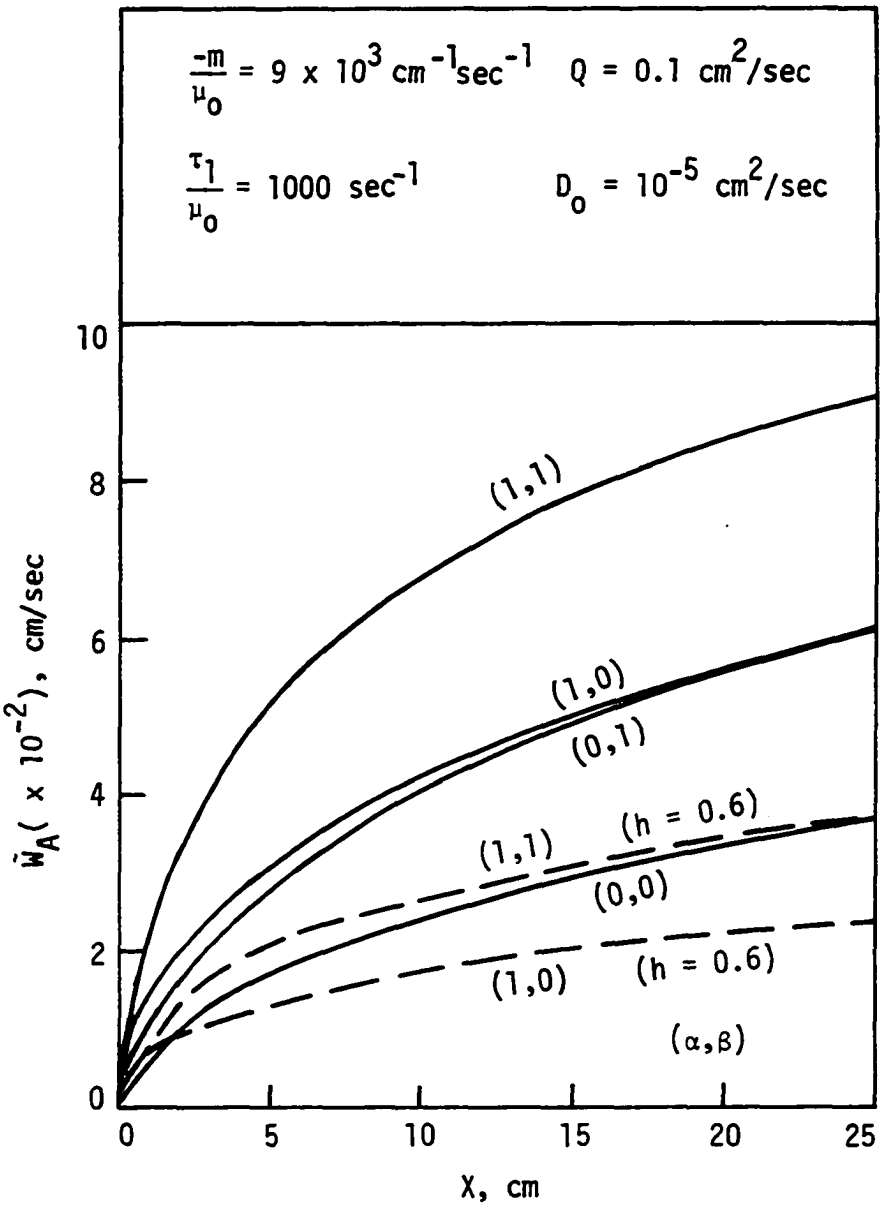

Figure 8. Total absorption rate as a function of exposed film length; Q = 0.1 cm^2/sec

quickly at lower Q. An increase in cocurrent gas shear decreases the film thickness and increases the absorption rate. An increase in α also decreases the film thickness and increases the molecular diffusivity, but may increase or decrease the absorption rate depending on the gas solubility-temperature relationship as expressed by the parameter h. For a countercurrent gas shear in which the film is still flowing downward or a temperature gradient in which $T_1 < T_0$ (i.e., $-\alpha$), the film thickness increases. Conclusions regarding their effects on mass transfer cannot readily be drawn because of the change in velocity profile in the liquid film. However, it can be reasoned from the above that a countercurrent gas shear (in which the film is still flowing downward) will decrease the mass transfer rate because of an increase in film thickness. A temperature gradient in which $T_1 < T_0$ will increase or decrease the mass transfer rate depending on the gas solubility-temperature relationship also.

Mass Transfer with Chemical Reaction in a Laminar Falling Film

For a first-order reaction, two cases, $\alpha = 0$, $\beta = 0$; $\alpha = 1$, $\beta = 1$, are analyzed with different values of the Damkohler Group II, k_1^*. The eigenvalues and the associated quantities are reported in Tables 7-11 for $k_1^* = 1$, 50 and 100. Obviously, the same kind of regularity in spacing among the eigenvalues appear. When k_1^* increases, the eigenvalues increase in magnitude showing that the "transient part" decays rapidly. A comparison between Tables 8 and 11 shows that at a given k_1^*, an increase in α or β again increases the magnitude of the eigenvalues as in physical absorption. The first five eigenfunctions for a typical case $\alpha = 0$, $\beta = 0$, $k_1^* = 50$ are shown in Figure 9. In Figure 10, the local dimension-

Table 7. Eigenvalues and related quantities for $\alpha = 0$, $\beta = 0$, $k_1^* = 1$ (quasi-numerical solution, $\delta\eta = 0.005$)

i	λ_i	$\frac{\partial N_i}{\partial \lambda_i}\|_{\eta=1}$	$\frac{\partial N_i}{\partial \eta}\|_{\eta=1}$	C_i
1	2.663279	-0.778609	-2.218629	-0.964482
2	6.454775	0.597204	4.777428	0.518831
3	10.404437	-0.545842	-7.158879	-0.352164
4	14.382572	0.516151	9.403706	0.269412
5	18.370492	-0.495350	-11.550581	-0.219785
6	22.362882	0.479418	13.622664	0.186547
7	26.357671	-0.466565	-15.634879	-0.162634
8	30.353989	0.455812	17.597303	0.144554
9	34.351208	-0.446607	-19.517469	-0.130366
10	38.349093	0.438571	21.400864	0.118915

Table 8. Eigenvalues and related quantities for $\alpha = 0$, $\beta = 0$, $k_1^* = 50$

i	λ_i	$\frac{\partial N_i}{\partial \eta}\|_{\eta=1}$	C_i
1	8.717104	-34.703869	-0.026171
2	11.311869	18.540428	0.075029
3	14.257060	-14.593301	-0.117436
4	17.478363	13.948615	0.139505
5	20.912751	-14.586208	-0.144688
6	24.499966	15.794844	0.140789
7	28.192514	-17.274363	-0.133231
8	31.957563	18.886790	0.124728
9	35.773440	-20.564597	-0.116435
10	39.625861	22.272882	0.108780

Table 9. Eigenvalues and related quantities for $\alpha = 0$, $\beta = 0$, $k_1^* = 100$

i	λ_i	$\frac{\partial N_i}{\partial \eta}\|_{\eta=1}$	C_i
1	11.610962	-154.319662	-0.004921
2	14.083877	61.016884	0.019497
3	16.867268	-36.466070	-0.041048
4	19.890363	27.300135	0.063039
5	23.100715	-23.486307	-0.080474
6	26.462294	22.068550	0.091584
7	29.946703	-21.889587	-0.097006
8	33.529317	22.404998	0.098324
9	37.189153	-23.329104	-0.097072
10	40.909224	24.501929	0.094381

Table 10. Eigenvalues and related quantities for $\alpha = 1$, $\beta = 1$, $k_1^* = 1$, $p = 1$

i	λ_i	$\frac{\partial N_i}{\partial \eta}\|_{\eta=1}$	C_i
1	5.369688	-1.829556	-1.178755
2	11.850322	3.327469	0.781215
3	18.753200	-4.784780	-0.560395
4	25.757530	6.172615	0.438791
5	32.800872	-7.504576	-0.362532
6	39.863330	8.792057	0.310182
7	46.936618	-10.043187	-0.271927
8	54.016670	11.263831	0.242683
9	61.101261	-12.458344	-0.219553
10	68.189075	13.630041	0.200772

Table 11. Eigenvalues and related quantities for $\alpha = 1$, $\beta = 1$, $k_1^* = 50$, $p = 1$

i	λ_i	$\frac{\partial N_i}{\partial \eta}\|_{\eta=1}$	C_i
1	15.455304	-30.149808	-0.037842
2	20.203396	14.388184	0.110398
3	25.494639	-10.711065	-0.177463
4	31.238910	9.832896	0.216354
5	37.337411	-9.981843	-0.229432
6	43.695594	10.585973	0.227118
7	50.236941	-11.410922	-0.217669
8	56.906721	12.348738	0.205685
9	63.667773	-13.345794	-0.193348
10	70.495088	14.373806	0.181595

less mass flux is plotted as a function of the dimensionless axial length for different values of k_1^*. For $k_1^* = 1$, the mass transfer rate is only slightly influenced by the presence of the chemical reaction and the transfer rate approaches that of physical absorption. For $k_1^* = 50$ and 100, the transfer rate reaches its "steady-state" value at a relatively small X^* implying that the length of the "transient part" varies inversely with the reaction rate. At such high values of k_1^*, the system is essentially governed by the process of steady diffusion with chemical reaction and the effect of hydrodynamics is unimportant.

For a zero-order reaction, the eigenvalues are the same as computed from the section on physical absorption. The only difference is the expansion coefficients which have to be obtained from Equation 101. In Table 12, the expansion coefficients are reported for $k_0^* = 0.1$ and 1. In

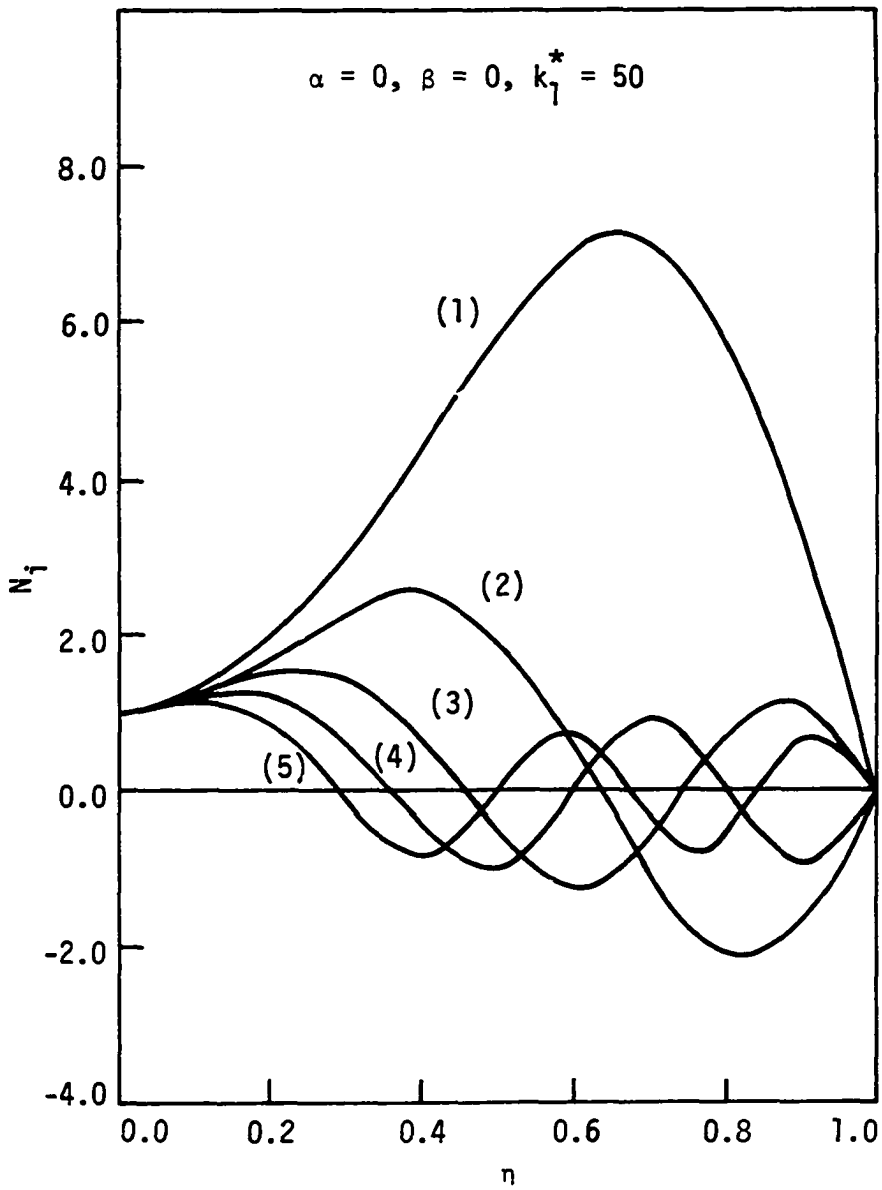

Figure 9. First 5 eigenfunctions for $\alpha = 0$, $\beta = 0$, $k_1^* = 50$; laminar flow

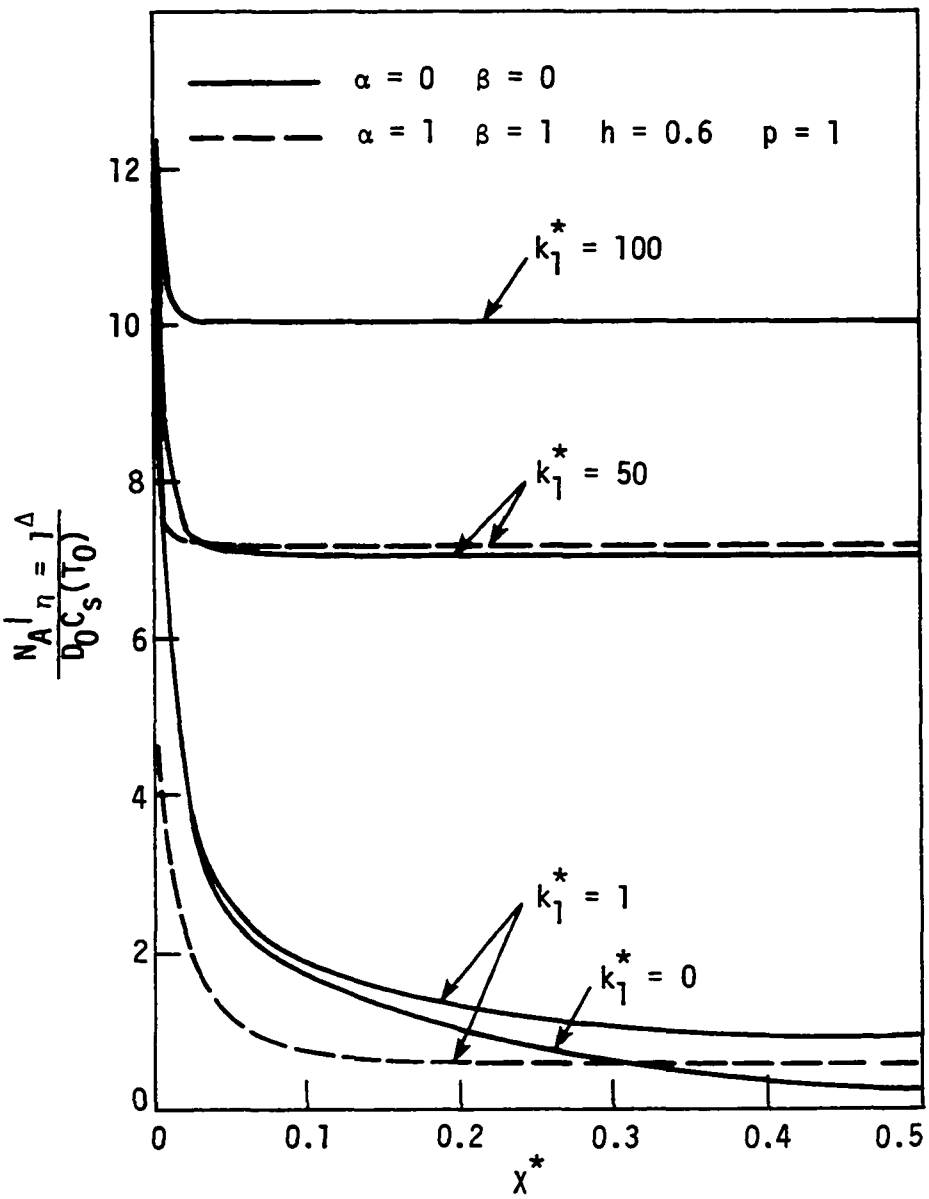

Figure 10. Local dimensionless mass flux as a function of dimensionless axial length for different values of Damkohler Group II, k_1*

Table 12. Expansion coefficients, C_i, for zero-order reactions

	$\alpha = 0, \beta = 0$		$\alpha = 1, \beta = 1, p = 1$
i	$k_0^* = 0.1$	$k_0^* = 1$	$k_0^* = 1$
1	-1.291444	-0.870757	-1.157568
2	0.546601	0.556374	0.828685
3	-0.357798	-0.347899	-0.559626
4	0.272303	0.274340	0.445431
5	-0.220842	-0.218438	-0.361922
6	0.187394	0.188202	0.312382
7	-0.163000	-0.162009	-0.271564
8	0.144917	0.145337	0.243708
9	-0.130531	-0.130011	-0.219322
10	0.119106	0.119358	0.201344

order to compare the reaction enhancement, the isothermal and nonisothermal enhancement factors based on Equations 109-111, 124-125 are plotted versus X* for some values of k_1^* and k_0^* in Figure 11. Evidently, the enhancement factors increase with X*. At a fixed X*, Φ_N is larger than the corresponding Φ_I for a given k_1^* or k_0^*. For example, Φ_N for $k_1^* = 50$ is about two to three times greater than Φ_I. This is probably due to the fact that an increase in α increases the molecular diffusivity, and above all, increases the Arrhenius reaction rate as expressed by the parameter p. It must be remembered, however, that Φ_N compares the total chemical absorption rate to the total physical absorption rate at the same α and β. It does not afford a comparison between the chemical absorption rate at a certain α and β with the physical absorption rate at $\alpha = 0$, $\beta = 0$. Such a comparison would have to be made on a dimensional basis such as under a given flow rate, slope and gas shear. Certain deductions, however, can be

Figure 11. Average isothermal and nonisothermal enhancement factors for first- and zero-order reactions

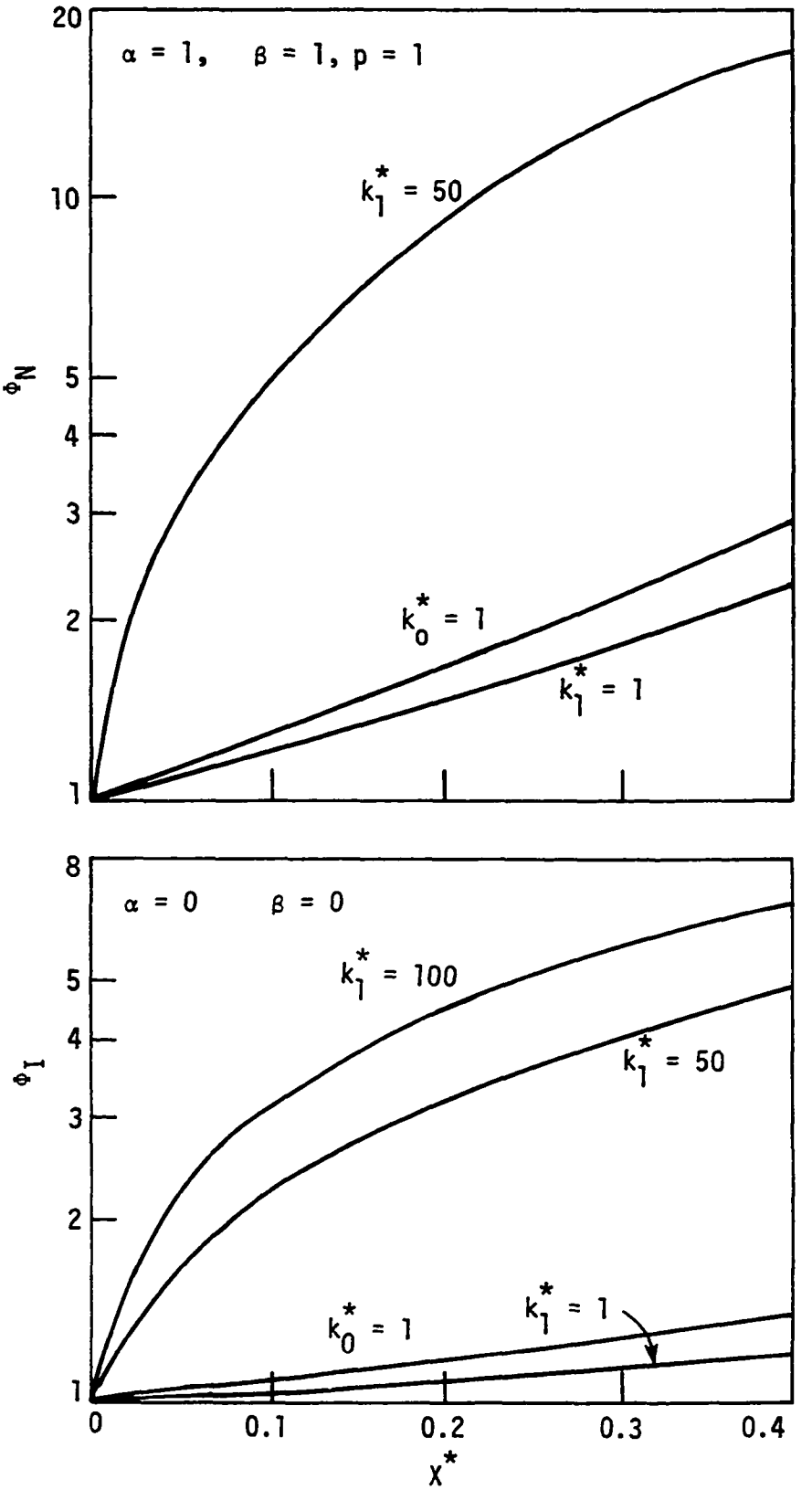
α = 1, β = 1, p = 1
$k_1^* = 50$
$k_0^* = 1$
$k_1^* = 1$
ϕ_N
20
10
5
4
3
2
1
α = 0 β = 0
$k_1^* = 100$
$k_1^* = 50$
$k_0^* = 1$
$k_1^* = 1$
ϕ_I
8
5
4
3
2
1
0
0.1
0.2
0.3
0.4
x^*

made regarding the effects of heat transfer and chemical reaction on the mass transfer rate. In physical absorption, heat transfer ($T_1 > T_0$) increases the molecular diffusivity and decreases the film thickness. This leads to an increase in mass transfer rate. However, the decrease of gas solubility with increasing α acts as an opposing factor in decreasing the mass transfer rate. So, an increase in α may increase or decrease the mass transfer rate depending on the value of h. In the presence of chemical reactions, heat transfer will further increase the Arrhenius reaction rate. The larger the rate constant, the more effective is the increase in mass transfer rate. Therefore, the reaction enhancement for a certain α and β as compared to $\alpha = 0$, $\beta = 0$ may be greater, less or even equal to 1.0 depending on the relative importance of several factors: the magnitudes of α, β, h and p.

For a general pseudo-n-th order reaction, a simple closed-form solution cannot be obtained. However, it is anticipated that some of the conclusions drawn for $n = 0$ and $n = 1$ should be valid here. The curves of the local dimensionless mass flux as a function of X* should be quite similar to those curves shown in Figure 10 which are composed of a "transient part" and a "steady part." The reaction enhancement will also depend on the relative magnitudes of α, β, h and p.

Hydrodynamic Stability

Interfacial shear

In the presence of interfacial shear only, the instability criterion is given, in dimensionless form, by Equation 185 or 186. When Σ_i, Π_r and

$\beta = 0$, this readily reduces to the Benjamin-Yih analysis Equation 225. When $\beta \neq 0$, the perturbation stresses, Π and Σ, have to be evaluated. In order to estimate these surface stresses, a shear-flow model due to Miles (55,56) and Benjamin (7) can be used which assumes a mean dimensional velocity profile in the gas phase where turbulent fluctuations are ignored. The main results of the estimate are summarized in the paper by Craik (19) and will not be repeated here. Craik studied the generation of surface waves on a horizontal thin liquid film of water by airflow. When the gas and liquid are different from air and water, a dimensional scaling of the physical properties can be applied. Simple calculations show that Σ_i and Π_r are positive and are functions of the wave number of the disturbance, and the physical and hydrodynamical parameters of the gas flow. Equations 185 and 186 therefore indicate that the presence of interfacial shear always creates additional instability through the perturbation stresses. Even when $\beta = 1$, the liquid film may still be unstable depending on the relative magnitudes of Σ_i, Π_r, θ and σ. This is in contrast to the situation of plane Couette flow found in confined geometries where the flow is always stable. The analysis here can also be applied to the case of countercurrent gas flow by setting τ_1 negative. Then β may become either positive or negative depending on the sign of U_1. For the first approximation, the dimensional wave velocity becomes

$$\hat{c}_0 = \frac{6(2-\beta)}{4-\beta}\langle U\rangle = \frac{6(2-\beta)}{4-\beta}\,\frac{(4-\beta)}{6}U_1 = 2U_1 + \frac{\tau_1\Delta}{\mu_0}$$

$$= 2\left[\frac{-m\Delta^2}{2\mu_0} - \frac{\tau_1\Delta}{\mu_0}\right] + \frac{\tau_1\Delta}{\mu_0} = \frac{-m\Delta^2}{\mu_0} - \frac{\tau_1\Delta}{\mu_0} \qquad (251)$$

As pointed out by Smith (75), when $-m\Delta > \tau_1$, the wave and the surface of the film travels down the slope even when the gas flow is countercurrent.

When $-m\Delta < \tau_1$, the wave and the surface of the film travel up the slope. If $-m\Delta = \tau_1$, then a stationary wave is generated. When Σ_i and Π_r are small and negligible, Equation 184 can be rearranged into a form that is similar to Benjamin and Yih's result:

$$c_i = kR\left[\frac{48(1-\beta)(2-\beta)}{5(4-\beta)^2}\right] - \frac{k}{3}\left[\frac{R\cos\theta}{F^2} + k^2RS\right] \quad (252)$$

$$= b_2kR - b_3kR\left[\frac{\cos\theta}{F^2} + k^2S\right] \quad (253)$$

The coefficients b_2 and b_3 are tabulated in Table 13. Obviously, b_2 decreases with increasing β while b_3 remains a constant.

Heat transfer

The solution of the modified O-S equation in the presence of only heat transfer can be obtained from Equation 219 by setting β, Σ_i and Π_r equal to zero. The instability criterion is given by Equation 226 where some typical values of b_2 and b_3 are shown in the first half of Table 14. It can be seen that an increase in α increases b_2, b_3 and the ratio b_2/b_3. Since the Froude number always increases for increasing α, Equation 226 indicates that an increase in α is destabilizing as compared to an isothermal liquid film. When α is positive, that is $T_1 > T_0$ or wall cooling, the film is more unstable. When α is negative, that is $T_1 < T_0$ or wall heating, the film becomes more stable provided that natural convection effects are negligible. An explanation is that when $T_1 > T_0$, the liquid viscosity at the film surface will be less than the liquid viscosity at the wall or $\mu_1 < \mu_0$. If a reference temperature T_0 is used for an isothermal film, then a cooled film will be less viscous at the film surface than the corresponding isothermal film. Therefore a cooled film will be more susceptible to surface wave formation and hence more

Table 13. Values of b_2 and b_3 for different values of $\beta(\alpha = 0)$

β	b_2	b_3
0.0	1.2000	0.3333
0.1	1.0793	0.3333
0.2	0.9573	0.3333
0.3	0.8345	0.3333
0.4	0.7111	0.3333
0.5	0.5879	0.3333
0.6	0.4148	0.3333
0.7	0.3438	0.3333
0.8	0.2250	0.3333
0.9	0.1099	0.3333
1.0	0.0000	0.3333

unstable. The reverse is true for $T_1 < T_0$ in which $\mu_1 > \mu_0$, the film surface exhibits higher viscosity and so the surface is more resistant to external disturbances. Obviously, viscosity is a stabilizing factor in liquid film flow.

Neutral stability curves for a typical liquid water with a given kinematic surface tension and kinematic viscosity are shown in Figures 12-14 for three different angles of inclination: 90°, 60° and 10°. The axis k = 0 is also a part of the neutral stability curve. The upper part above each curve represents a stable region where infinitesimal harmonic disturbances are damped. When S = 0, a vertical falling film is always unstable for positive values of α. For θ less than 90°, bifurcation

Table 14. Values of b_2 and b_3 for different values of α and β

α	β	b_2	b_3
-3.0	0.0	0.376810	0.181497
-2.0	0.0	0.517131	0.216166
-1.0	0.0	0.757566	0.264241
0.0	0.0	1.200000	0.333333
0.2	0.0	1.329386	0.350690
0.4	0.0	1.478100	0.369522
0.6	0.0	1.649548	0.389989
0.8	0.0	1.847804	0.412269
1.0	0.0	2.077748	0.436564
2.0	0.0	3.955008	0.597264
3.0	0.0	8.259626	0.858188
0.0	1.0	0.000000	0.333333
0.2	1.0	-0.103984	0.350690
0.4	1.0	-0.202550	0.369522
0.6	1.0	-0.295638	0.389989
0.8	1.0	-0.383222	0.412269
1.0	1.0	-0.465307	0.436564

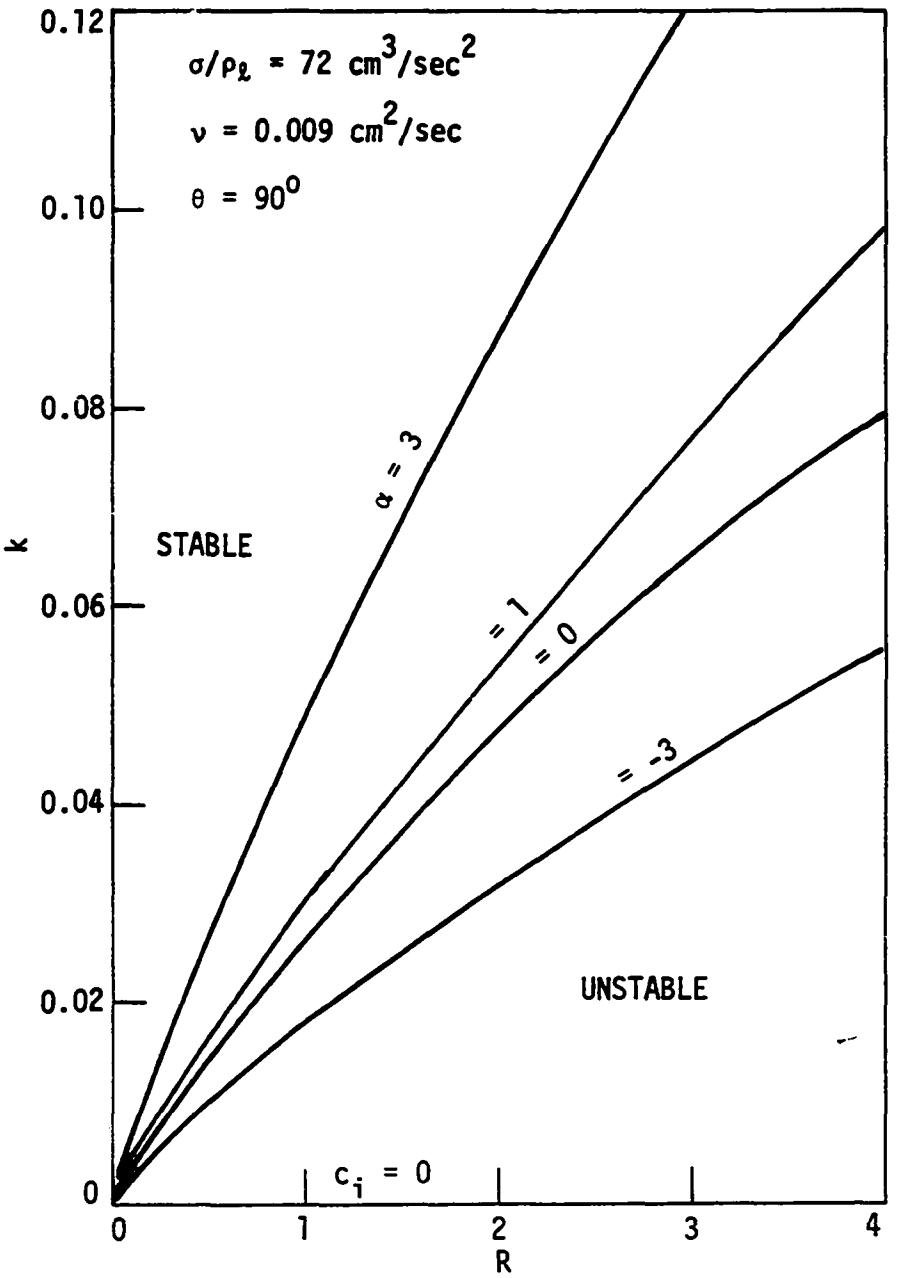

Figure 12. Neutral stability curves for various α's in vertical film flow, $\theta = 90°$

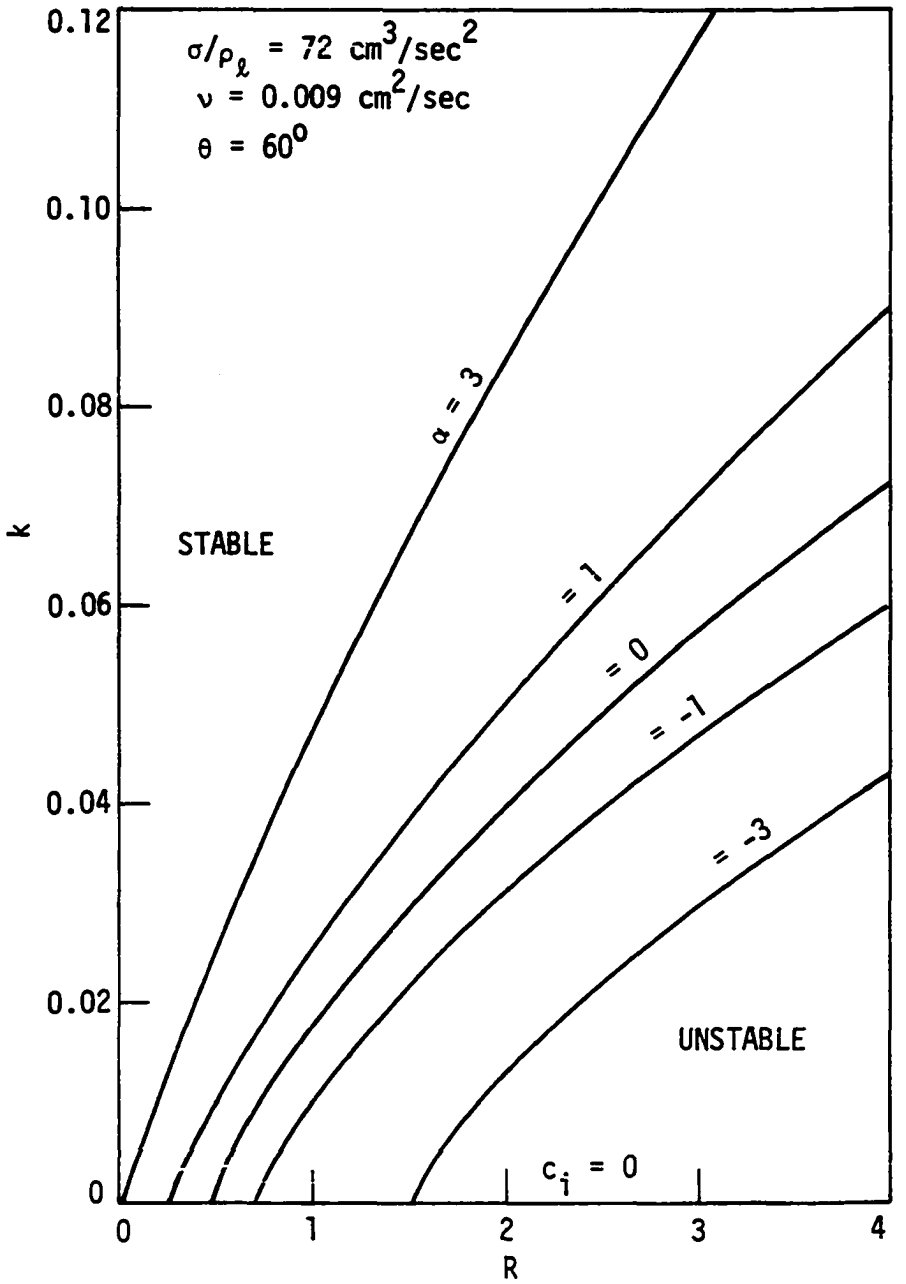

Figure 13. Neutral stability curves for various α's, θ = 60°

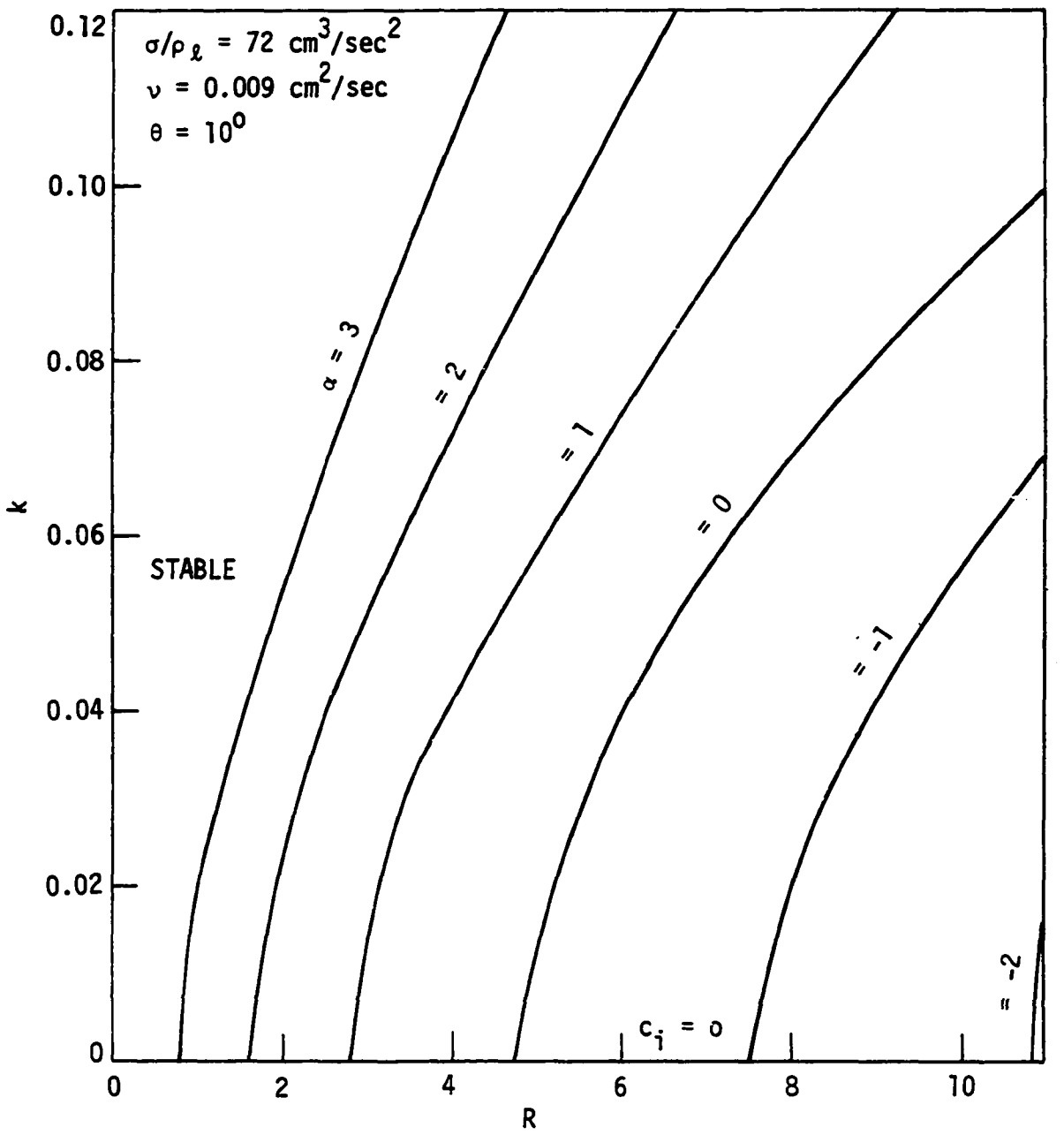

Figure 14. Neutral stability curves for various α's, θ = 10°

points are usually formed depending on the values of α. As θ is decreasing, the neutral stability curves shift to the right and the critical Reynolds number, R_{cr}, also shifts to the right. It seems that a negative α shifts the R_{cr} more in magnitude than a positive α as can be seen from Figures 13 and 14. The values of R_{cr} are obtained from Equation 226 by solving F_{cr} using trial and error. Obviously, heating of the wall is more stable than cooling and the angle of inclination is a stabilizing factor. Figure 14 shows that, at $\theta = 10°$, practically high flow rates can be achieved without any surface wave formation. The possibility of achieving high flow rates increases with increased heating but decreases with increased cooling. In Figures 15-17, the dimensionless amplification factor is plotted as a function of the dimensionless wave number for different α's. Figure 15 shows that at a small Reynolds number of $R = 1.111$, the growth rate of the disturbance is very small at $\theta = 90°$ whereas at $\theta = 10°$, the disturbance decays for all k. As the Reynolds number increases to 5.555, the amplification rate increases substantially for positive α's, as shown in Figure 16. Again, the angle of inclination proves to be a stabilizing factor by decreasing the amplification. In Figure 17, a comparison is made between the amplification rate of two different flow rates at a fixed angle of inclination. Higher values of α and flow rate exhibit higher amplification rates. In order to assess the influence of heat transfer on the stability of falling liquid films, a comparison is made between the nonisothermal film and the isothermal film under the same Reynolds number and fixed dimensional wave number. This is shown in Figure 18 by replotting Figure 13. The shape of the curves in the two

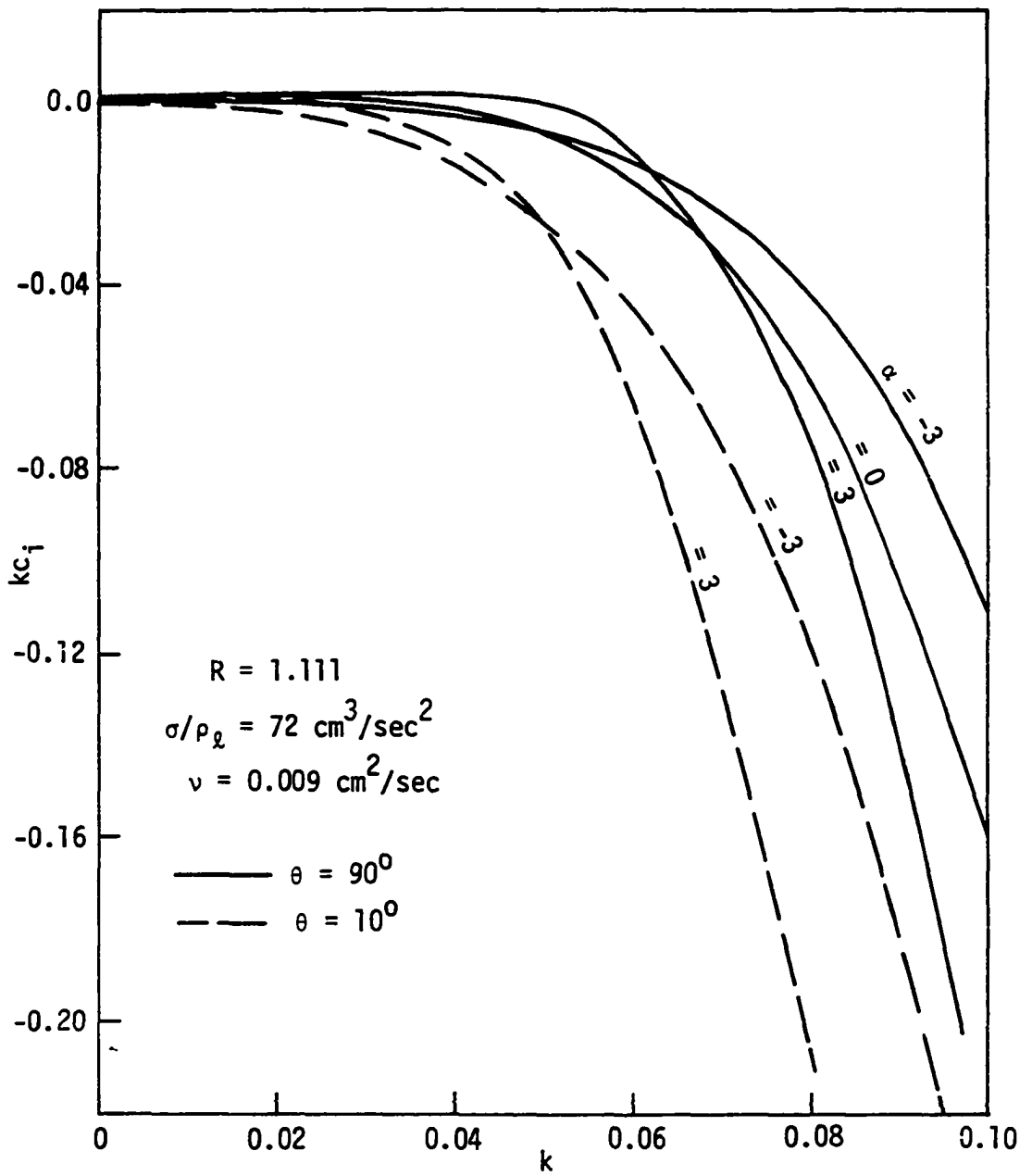

Figure 15. Amplification factor as a function of wave number for different α's

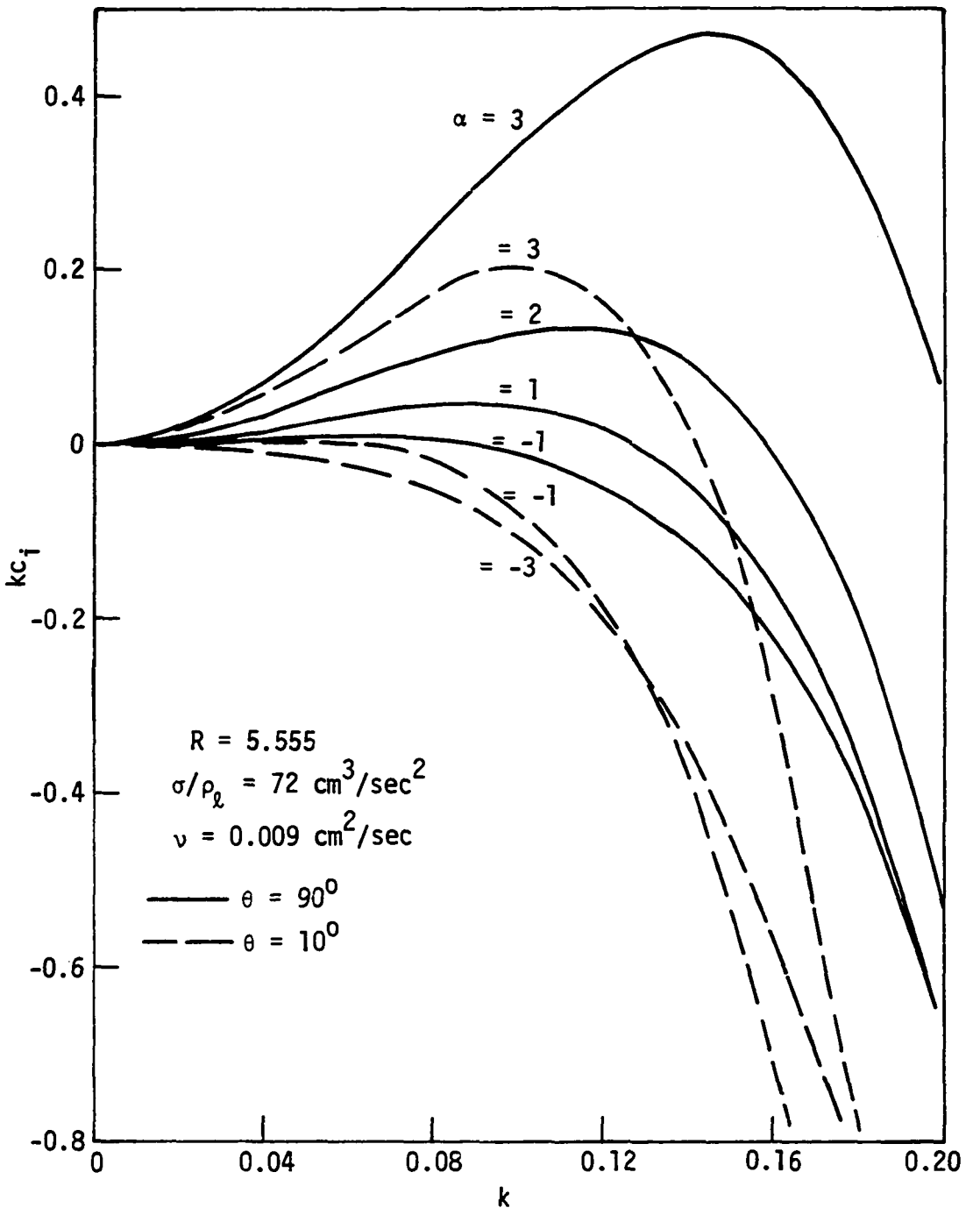

Figure 16. Amplification factor as a function of wave number for different α's

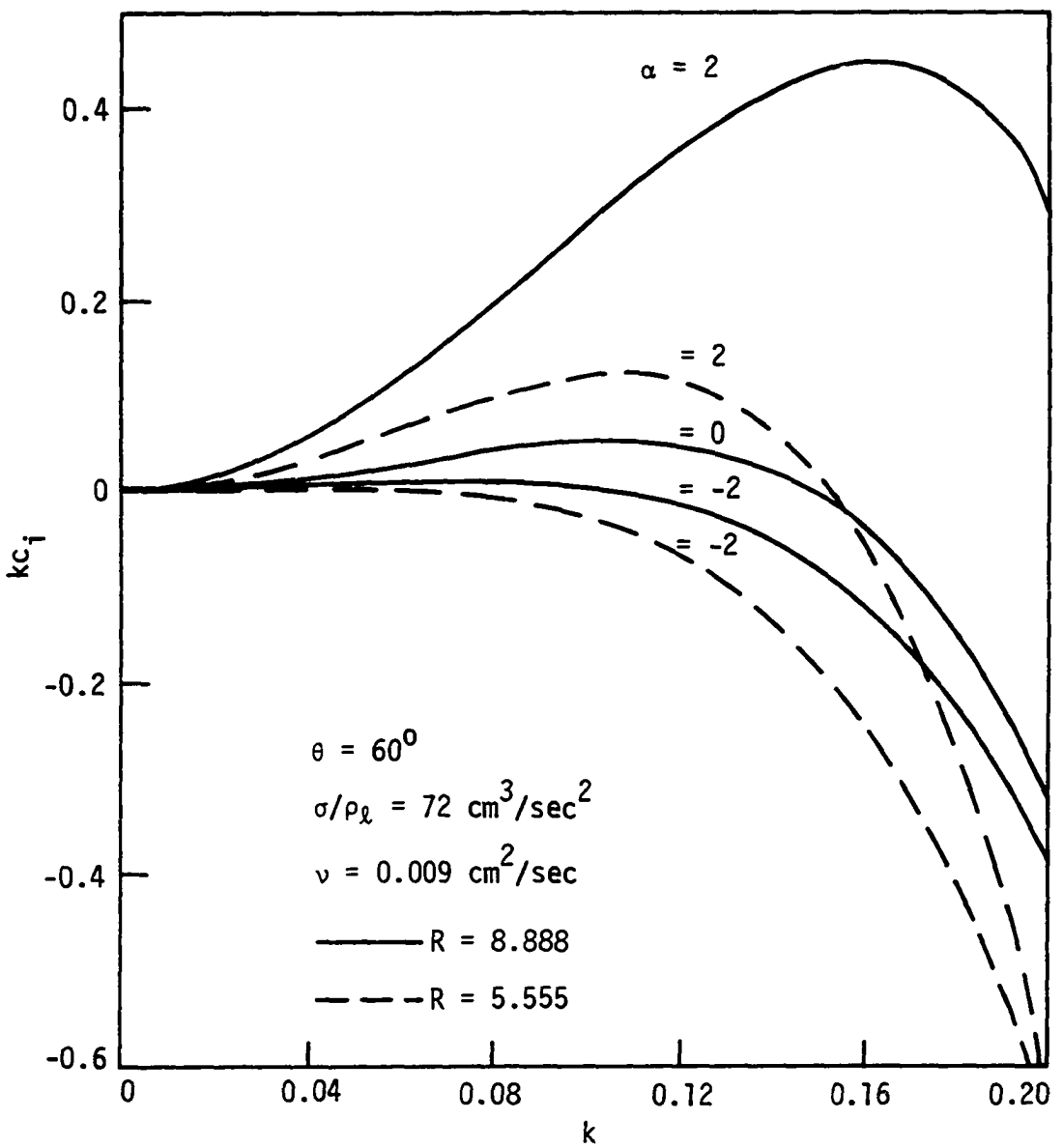

Figure 17. Amplification factor as a function of wave number for different α's

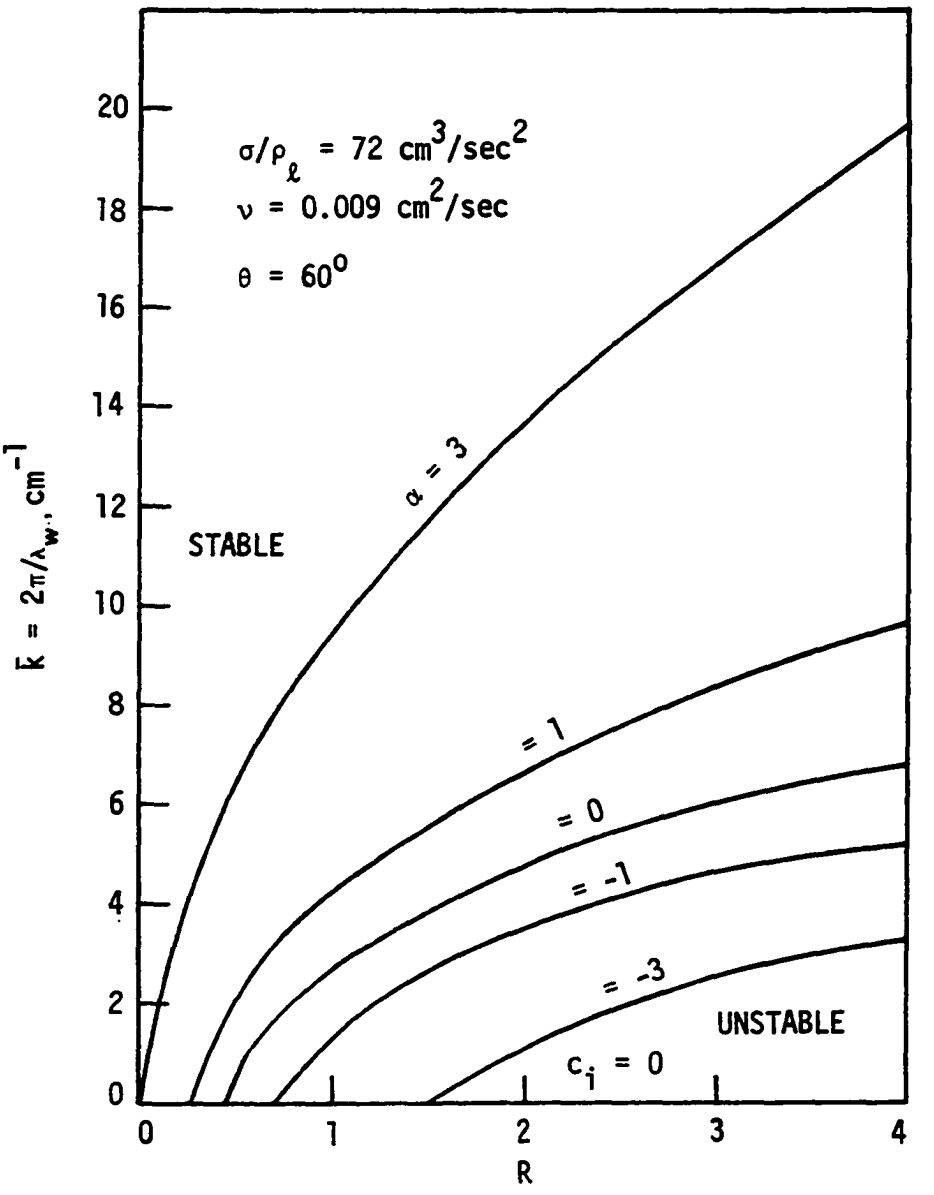

Figure 18. Neutral stability curves for various α's in terms of dimensional wave number, $\bar{k}$

figures does not change appreciably. An advantage of using the dimensional wave number instead of the dimensionless wave number for comparison is that the film thickness, which is a function of α, is not involved. Figure 19, which is replotted from Figure 17, compares the dimensional amplification factor of different α's with the case of $\alpha = 0$ under the same dimensional wave number. Although the curves do not have the same shape as the curves in Figure 17, the same trend is observed, namely, higher flow rates and α's exhibit higher amplification rates and flows with positive α's are more unstable than those with negative α's.

It is of interest to compare the effects of heat transfer on surface wave instability in falling liquid films with that of shear wave instability in laminar boundary-layer flow (84) and plane Poiseuille flow (65). The flow of a falling liquid film can be visualized as one-half of a plane Poiseuille flow with a free surface. Gravity and surface tension forces are dominant in falling films whereas in plane Poiseuille flow, the pressure gradient is usually the driving force. While only shear waves appear in confined flows, both surface waves and shear waves may exist on a liquid film at small Reynolds number. The surface waves are usually unstable whereas the shear waves are highly damped. The surface waves commonly observed usually have long wavelengths and are more unstable than short waves which are damped by surface tension. In the presence of heat transfer, the temperature gradient induces a viscosity variation across the flowing liquid and so additional viscosity gradient terms appear in the O-S equation. A comparison of the effects of heat transfer on surface wave and shear wave instability is shown in Table 15. Although there is a fundamental difference between surface wave and shear wave instability,

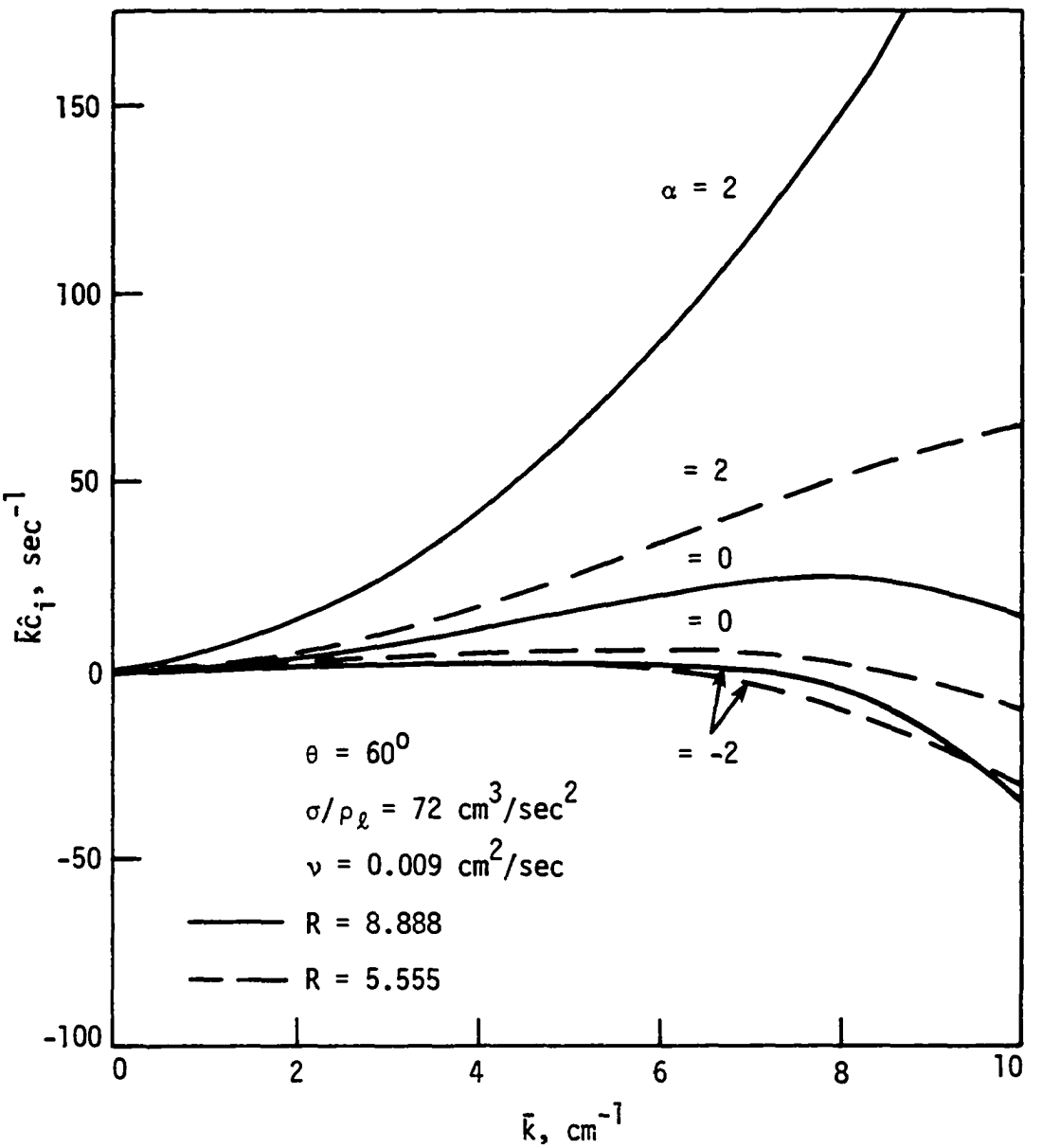

Figure 19. Dimensional amplification factor as a function of dimensional wave number for different α's

Table 15. Comparison of the effects of heat transfer on surface wave and shear wave instability

	Falling film flow	Plane Poiseuille flow (65)	Laminar boundary-layer flow (84)
Wave formation	Surface wave and shear wave, appear at small Re	Shear wave, appears at large Re	Shear wave, appears at large Re
Modified O-S equation	Same	Same	Same
Boundary conditions	Influenced by heat transfer	Not influenced	Not influenced
Mean velocity profile	$\frac{d}{dY}(\mu \frac{dU}{dY}) = -\rho_1 g \sin\theta$, deviates from semi-parabolic	$\frac{d}{dY}(\mu \frac{dU}{dY}) = \frac{dP}{dX}$, skew-symmetric	Solution of boundary-layer equations of momentum, deviates from Blasius profile
Solution method	Successive perturbation	Numerical integration	Numerical integration
Cooling of wall	Destabilizing	A temperature difference between the two walls is always destabilizing	Destabilizing
Heating of wall	Stabilizing		Stabilizing, but an optimum is found in which further heating decreases the Re_{cr}
Causes of instability	Increased cooling produces inflection points in mean velocity profile, viscosity gradient terms destabilizing	Viscosity gradient terms destabilizing	Increased cooling produces inflection points in mean velocity profile, viscosity gradient terms destabilizing

the effects of heat transfer on them are in many respects similar. A major cause of instability in these flows is the extra viscosity gradients which appear in the modified O-S equation. Another cause of instability is probably due to the modification of the mean velocity profile by heat transfer. As can be seen from Figure 20, at $\alpha = 2$ and 3 ($\beta = 0$), wall cooling produces an inflection point in the mean velocity profile while wall heating does not produce this kind of inflection point. This type of phenomena is also found in laminar boundary-layer flows. As pointed out by Potter and Graber (65) and further illustrated in this study, although the viscosity gradient terms may be small, their effects cannot be neglected. It should also be noticed that the instability of falling film flow and laminar boundary-layer flow both depend on the direction of heat transfer whereas the plane Poiseuille flow does not. This further indicates that the inflection points found in the mean velocity profile are a cause of instability. In the plane Poiseuille flow studied by Potter and Graber, water was used as the flowing liquid. A linear temperature difference was imposed and they also used the exponential viscosity-temperature relationship as used in this study. The value of the activation energy for viscosity, E_a, was given as 3233°R or 1741°K. Iyer's (34) experimental correlation of 87 liquids gave E_a as 1832°K for water, and the E_a for other liquids ranged from a few hundred to 3000. In a falling film of water, if T_0 is 300°K and the temperature drop, $T_1 - T_0$, is 10°K, then this will give an α approximately equal to 0.2. If $T_1 - T_0$ is 100°K, then α is approximately 2. Therefore the ranges of α reported in this study are sufficient for most practical operating conditions.

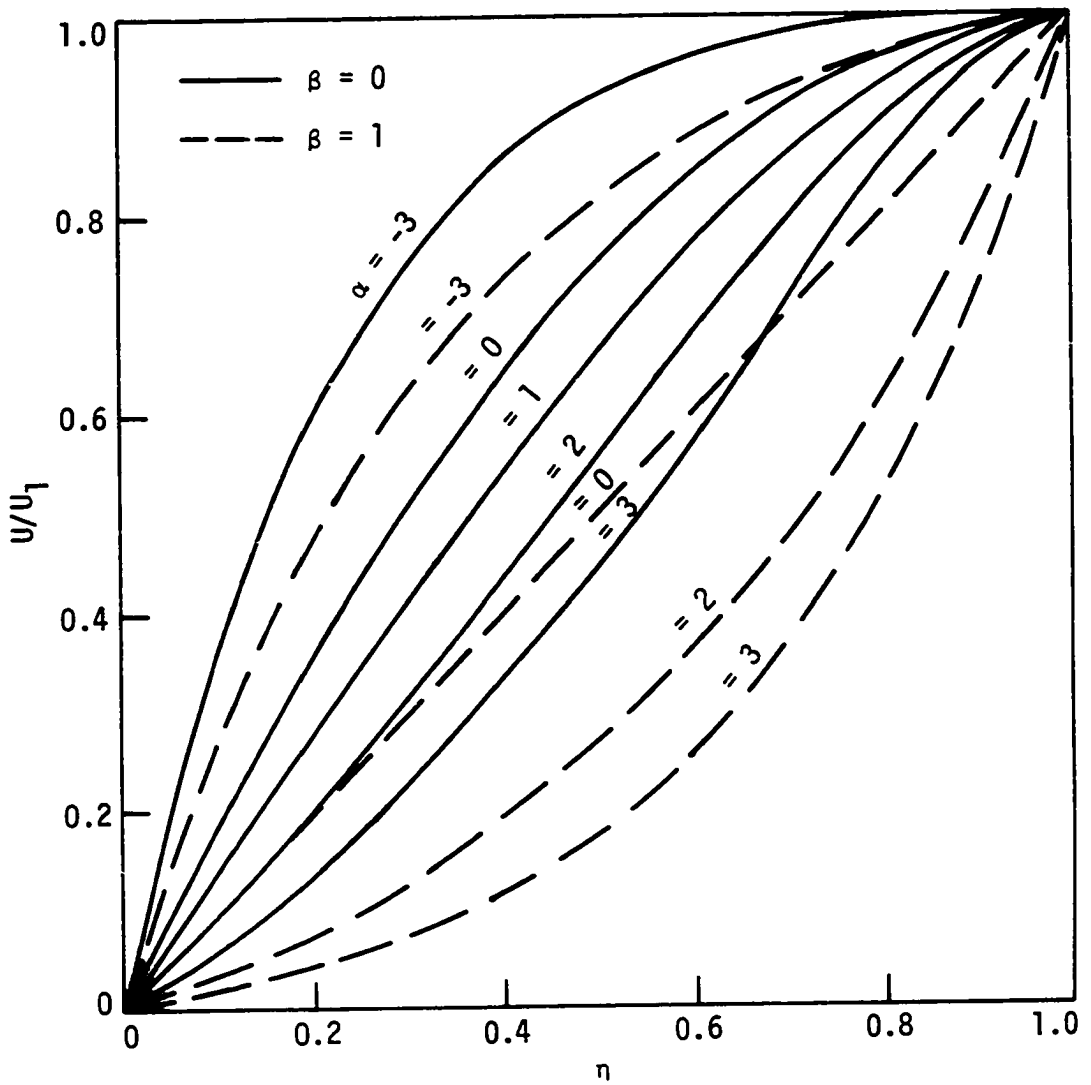

Figure 20. Dimensionless velocity profiles as a function of α and β [Shair (73)]

Both heat transfer and interfacial shear

In the first approximation, the dimensionless wave velocity as given by Equation 200 is plotted as a function of α and β in Figure 21. At a fixed α, an increase in β decreases c_0. At a fixed β, an increase in α increases c_0 for small β's and decreases c_0 for large β's. This is due to the variation of the velocity profile and hence the average velocity. In the second approximation, some of the values of b_2 and b_3 in Equation 222 are computed for $\beta = 1$ in the second half of Table 14. A contrasting difference with the case of $\beta = 0$ is observed, the values of b_2 and b_2/b_3 decrease with increasing α. The value of b_3 is independent of β and is only a function of α. It can be recalled that b_2/b_3 increases for increasing α when $\beta = 0$ and decreases for increasing β when $\alpha = 0$. Thus the ratio b_2/b_3 may increase or decrease depending on the relative magnitudes and signs of α and β. The first two terms of Equation 222 both increase for increasing α or β but the third term may decrease and even be negative at large values of β which means that the destabilizing effects are not simply additive. All these imply that there is a certain interaction between heat transfer and interfacial shear. This probably arises from the mean velocity profile variation. Figure 20 shows that at $\beta=0$, inflection points may be formed at high values of α while at $\beta=1$, the velocity profiles are symmetrical at, say, $\alpha=3$ and -3. This kind of symmetry is also found for other α's and there are no inflection points. This means that an increase in β leads to a more stabilizing velocity profile. The same is true for increased wall heating, which also leads to a more stabilizing velocity profile. From the above discussion, it can be con-

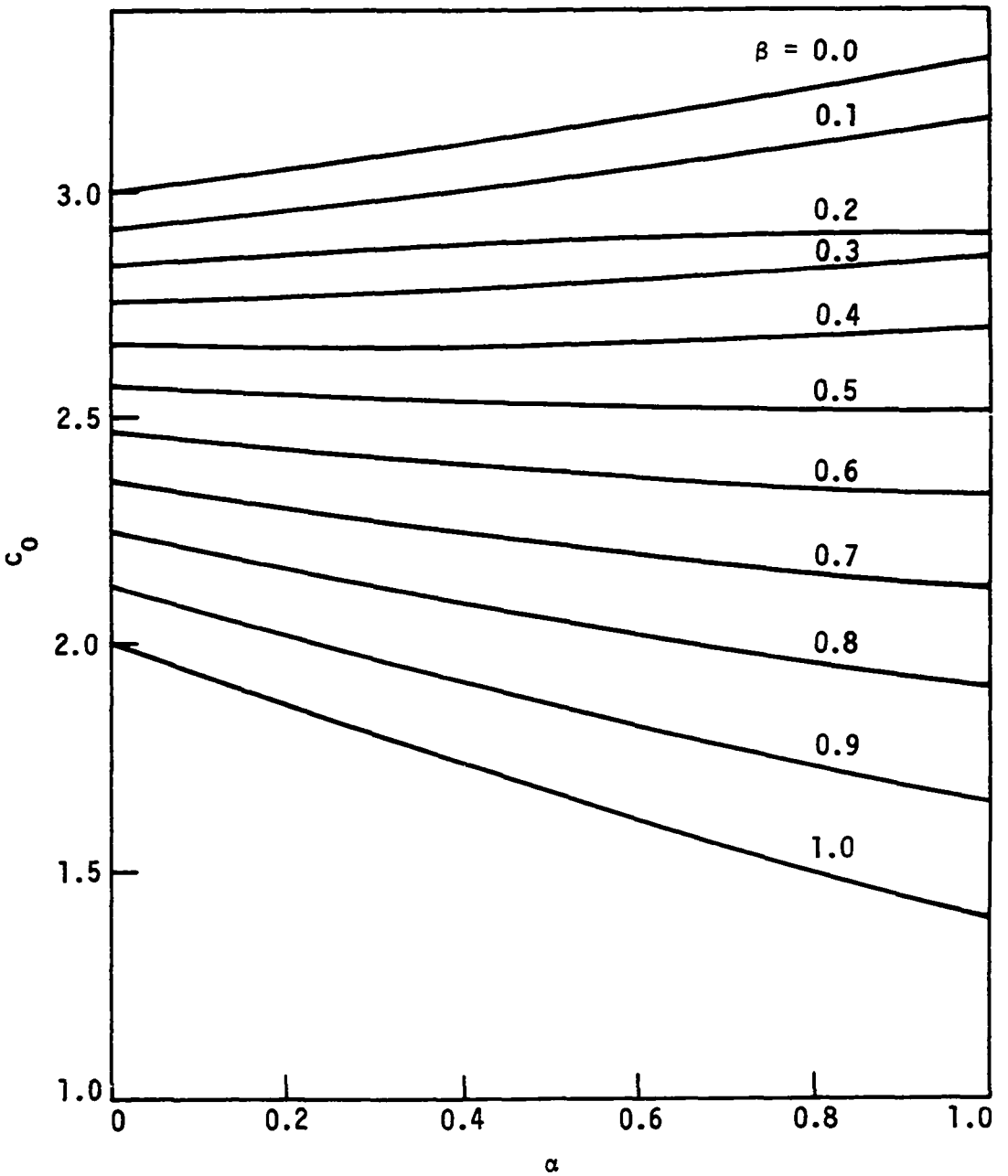

Figure 21. Dimensionless real wave velocity (first approximation) as a function of α and β

cluded that cocurrent and countercurrent interfacial shear are destabilizing factors because of the formation of surface perturbation stresses. Wall cooling is also a destabilizing factor because of the lower viscosity generated at the film surface. However, these two destabilizing effects are not simply additive and have some interactions between them primarily through the mean velocity profile variation. Wall heating is a stabilizing factor provided that natural convection effects are negligible. The analysis reported here is only valid for long waves where the wave number is small. For large wave number, a numerical solution by Whitaker (85) or an approximate analytical solution by Anshus and Goren (1) can be used.

Mass Transfer in a Turbulent Falling Film

The eigenvalues and the related quantities are solved by means of the quasi-numerical method for two values of the turbulence parameter, $\beta^* =$ 500 and 50000. They are reported in Table 16 and 17 respectively, for the first ten eigenvalues. The magnitudes of the eigenvalues are considerably larger than those found in laminar flow. Again, the higher eigenvalues assume a regularity in spacing. It is found that as β^* increases, it becomes necessary to decrease the integration step size for the Runge-Kutta-Gill-4 method in order to insure accuracy of the integration. This is because when β^* increases, increasing turbulence causes a steepening of the concentration gradient near the interface and so a much finer grid size has to be used. In Figures 22 and 23, the first five eigenfunctions are plotted for $\beta^* = 500$ and 50000 respectively. The eigenfunctions oscillate rapidly near the interface which is a result of the steep concentration

Table 16. Eigenvalues and related quantities for turbulent film flow, $\beta^* = 500$ (quasi-numerical solution, $\delta\eta = 0.0025$)

i	λ_i	$\frac{\partial N_i}{\partial \lambda_i}\|_{\eta=1}$	$\frac{\partial N_i}{\partial \eta}\|_{\eta=1}$	C_i
1	4.105010	-0.465493	-0.156436×10^{2}	1.046651
2	28.143091	0.932255	1.258407×10^{2}	-7.622954×10^{-2}
3	46.498874	-0.849076	-2.159197×10^{2}	5.065719×10^{-2}
4	64.896403	0.826089	3.044308×10^{2}	-3.730632×10^{-2}
5	83.330017	-0.817091	-3.923239×10^{2}	2.937366×10^{-2}
6	101.781306	0.812726	4.800073×10^{2}	-2.417786×10^{-2}
7	120.243724	-0.810170	-5.675753×10^{2}	2.053011×10^{-2}
8	138.711862	0.808549	6.550755×10^{2}	-1.783241×10^{-2}
9	157.184574	-0.807372	-7.424897×10^{2}	1.575965×10^{-2}
10	175.661109	0.806392	8.297764×10^{2}	-1.411913×10^{-2}

Table 17. Eigenvalues and related quantities for turbulent film flow, $\beta^* = 50000$ (quasi-numerical solution, $\delta\eta = 0.001$)

i	λ_i	$\frac{\partial N_i}{\partial \lambda_i}\|_{\eta=1}$	$\frac{\partial N_i}{\partial \eta}\|_{\eta=1}$	C_i
1	12.097581	-0.163787	-1.444681×10^{2}	1.009374
2	189.184306	0.612179	2.547388×10^{3}	-1.726897×10^{-2}
3	298.504450	-0.478394	-4.245087×10^{3}	1.400533×10^{-2}
4	410.770620	0.443072	5.990462×10^{3}	-1.098896×10^{-2}
5	524.177389	-0.428410	-7.726520×10^{3}	8.906192×10^{-3}
6	638.207775	0.420808	9.448194×10^{3}	-7.447046×10^{-3}
7	752.627165	-0.415816	-1.115032×10^{4}	6.390715×10^{-3}
8	867.324414	0.411426	1.281723×10^{4}	-5.604757×10^{-3}
9	982.247715	-0.406367	-1.441857×10^{4}	5.010608×10^{-3}
10	1097.371620	0.399544	1.590519×10^{4}	-4.561539×10^{-3}

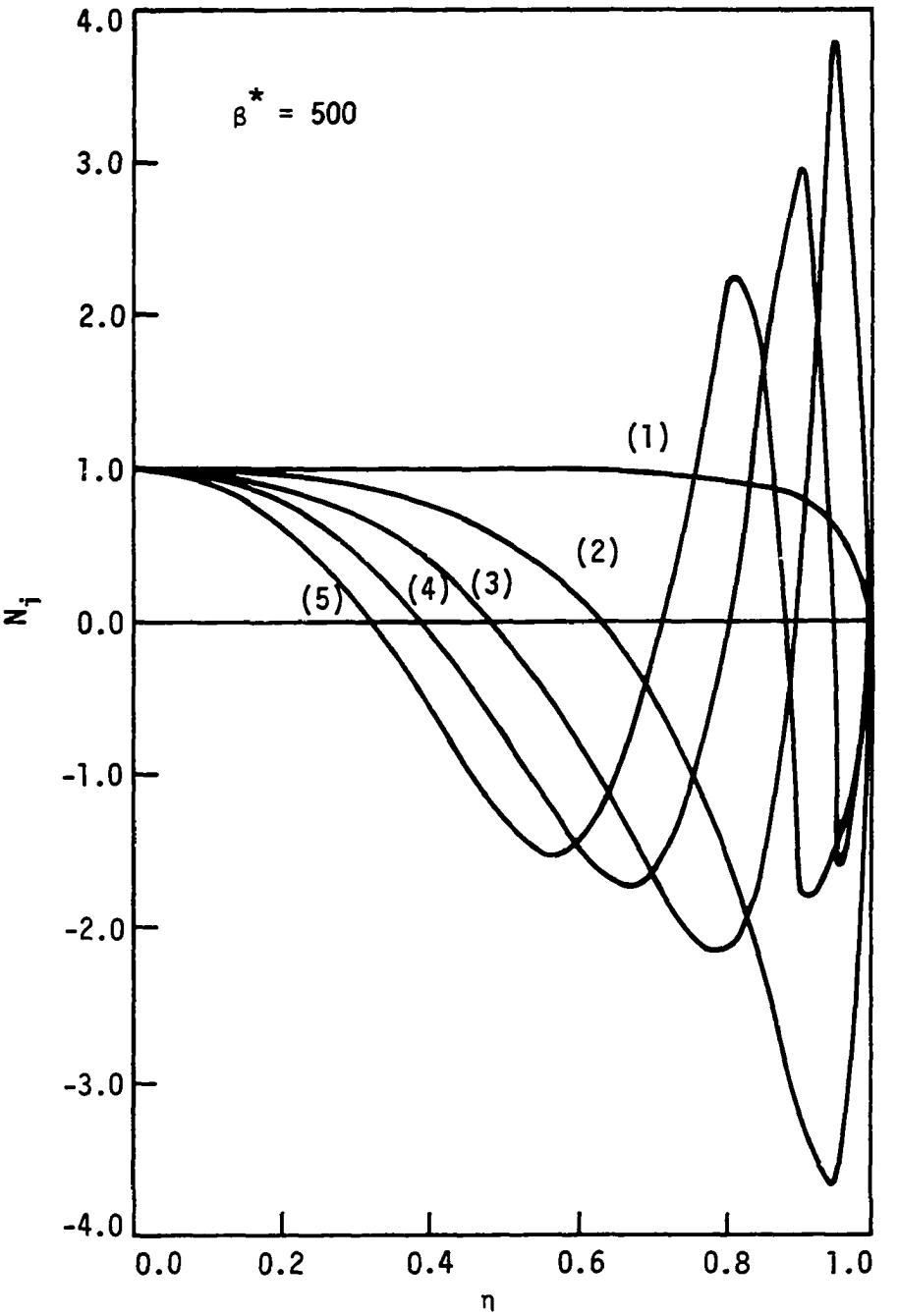

Figure 22. First 5 eigenfunctions for turbulent film flow, $\beta^* = 500$

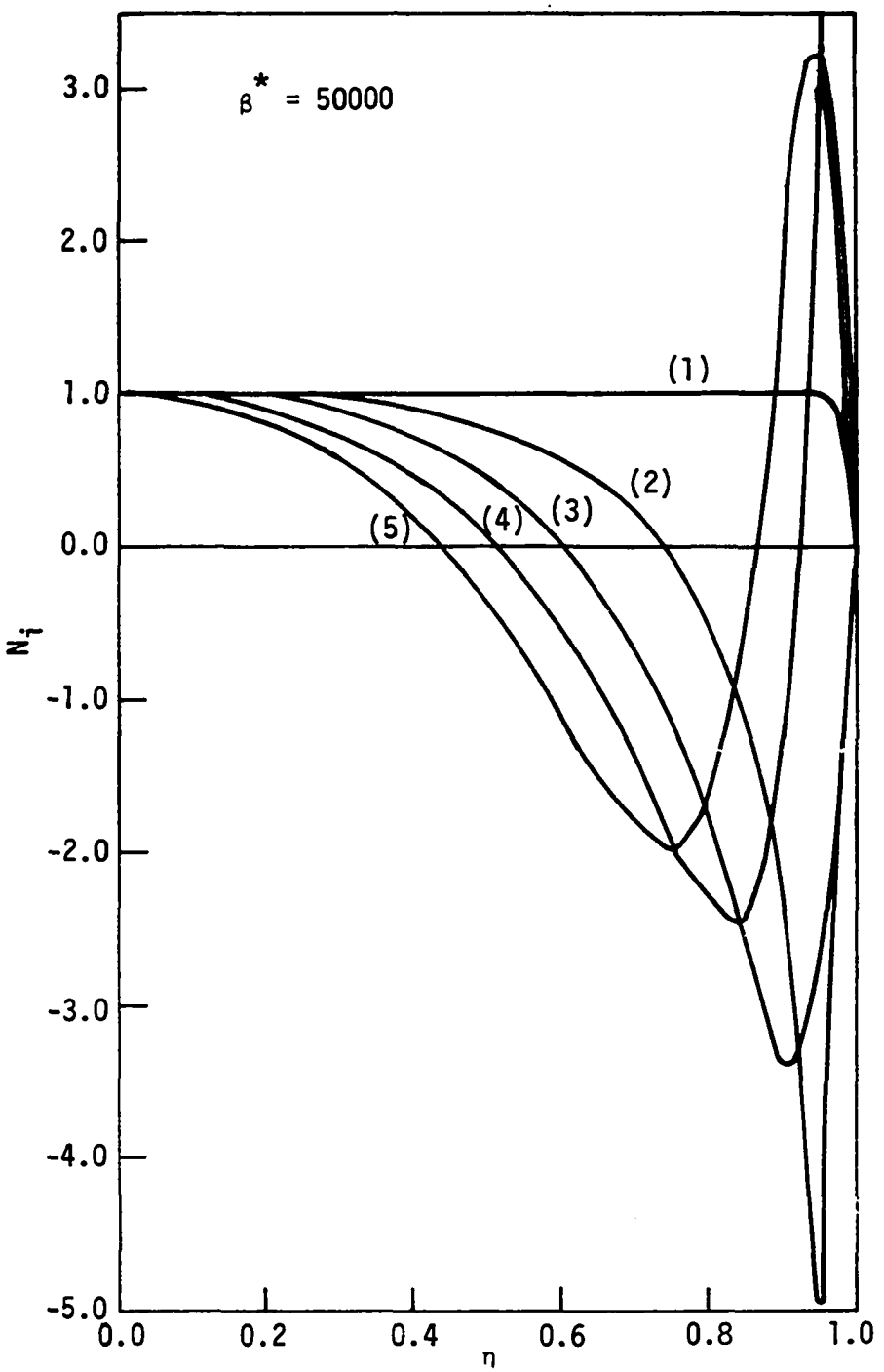

Figure 23. First 5 eigenfunctions for turbulent film flow, $\beta^* = 50000$

gradient generated. Furthermore, the amplitude of oscillation of the eigenfunctions for $\beta^* = 50000$ is higher than that for $\beta^* = 500$ with the eigenfunctions shifted more towards the interface. This indicates that a much steeper concentration gradient is being developed for $\beta^* = 50000$ than $\beta^* = 500$. In Figures 24 and 25, a comparison is made between the present analytical solution based on Equation 230 with the numerical finite difference solution of Sandall (70) for $\beta^* = 500$ and 50000. The agreement is excellent. Sandall has also provided an approximate formula which is valid for small X^*:

$$Sh = \frac{1}{2\sqrt{X^*}} \left[\frac{2}{\sqrt{\pi}} + 0.5642\ \beta^* X^*\right] \tag{254}$$

This formula is also shown in Figures 24 and 25. The fully developed asymptote is given by Equation 231.

Mass Transfer with Chemical Reaction in a Turbulent Falling Film

Since the major part of the results for a first-order reaction has already been provided in detail by Kayihan and Sandall (41), and Menez and Sandall (54), they will not be repeated here. In order to illustrate the usefulness of the present analysis using the method of separation of variables and linear superposition, a typical case of $\beta^* = 500$ and $k_1^* = 250$ is chosen for demonstration purposes. The first ten eigenvalues are shown in Table 18. The eigenvalues are larger in magnitude than those found in physical absorption. Again, a regularity in spacing among the higher eigenvalues is observed. It is quite clear that the convective-diffusion equation considered here for a falling film with its typical

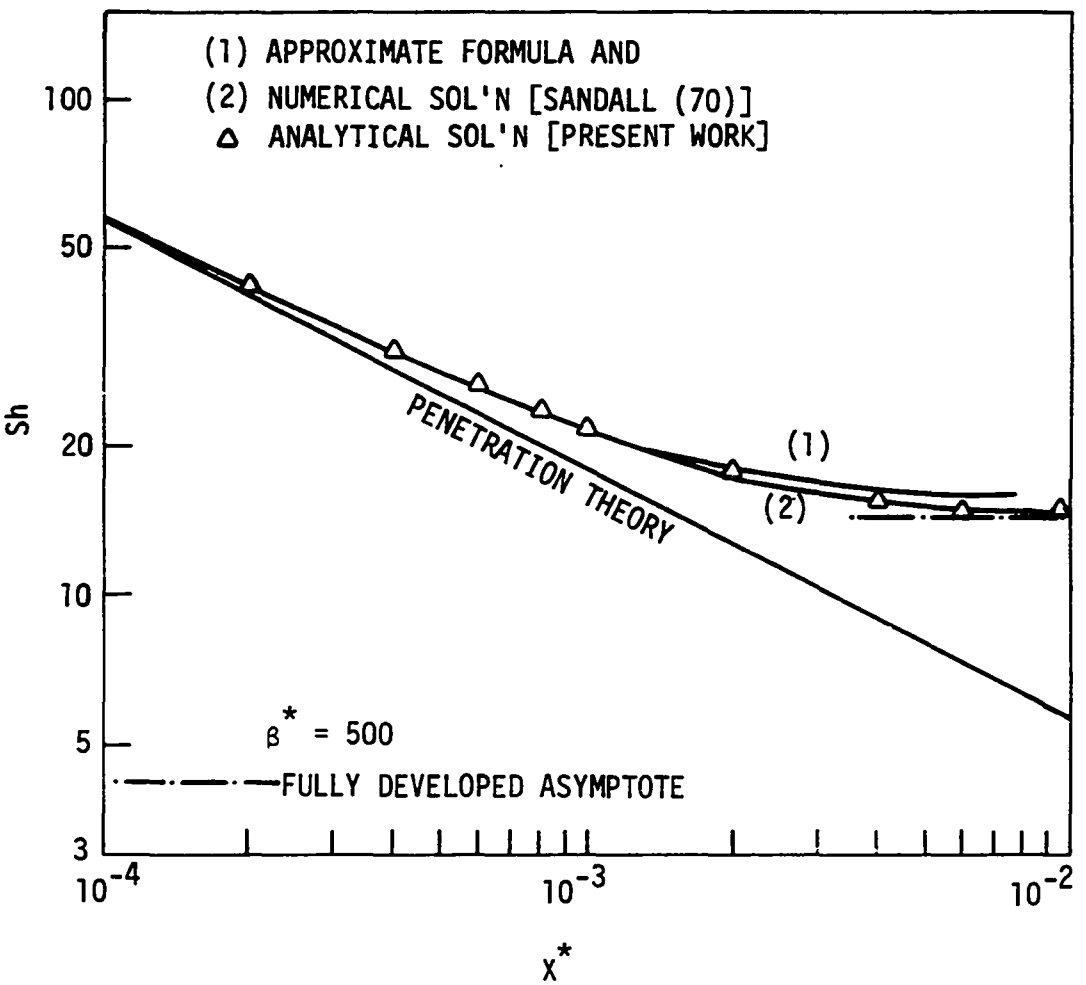

Figure 24. Comparison of the analytical solution with the numerical solution for a turbulent falling film, $\beta^* = 500$

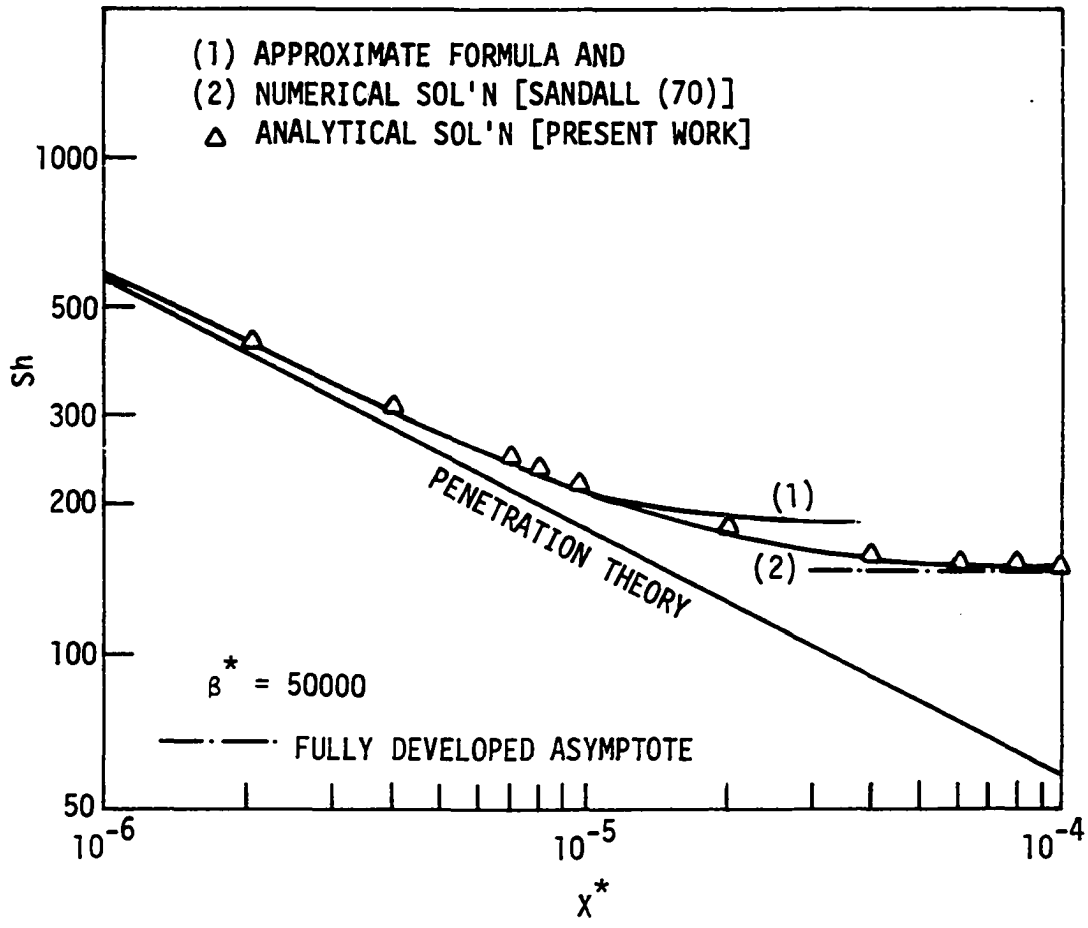

Figure 25. Comparison of the analytical solution with the numerical solution for a turbulent falling film, $\beta^* = 50000$

Table 18. First ten eigenvalues for a first-order reaction in a turbulent falling film, $\beta^* = 500$, $k_1^* = 250$ ($\delta\eta = 0.0025$)

i	λ_i
1	16.335578
2	32.280544
3	49.113597
4	66.794784
5	84.816813
6	103.002672
7	121.278824
8	139.610102
9	157.977816
10	176.371271

boundary conditions should have an asymptotic solution in which the higher eigenvalues can be obtained from relatively simple analytical relationships involving periodic functions. In Figure 26, a comparison is made between the hypergeometric series solution of Stepanek and Achwal (77) with the experimental data and finite difference numerical solution of Menez and Sandall (54). The agreement is quite good showing that the use of an eddy diffusivity concept permits a convenient description and solution of those problems involving chemical reactions in a turbulent falling film. The experimental data were taken at fully developed conditions such that the "transient part" in Equation 245 is zero. Stepanek and Achwal (77) concluded that their solution was highly insensitive to the choice of the boundary condition inside the liquid phase. Their conclusions were based on a calculation of k_1^*/β^* varying from 20 to 10100 which means that

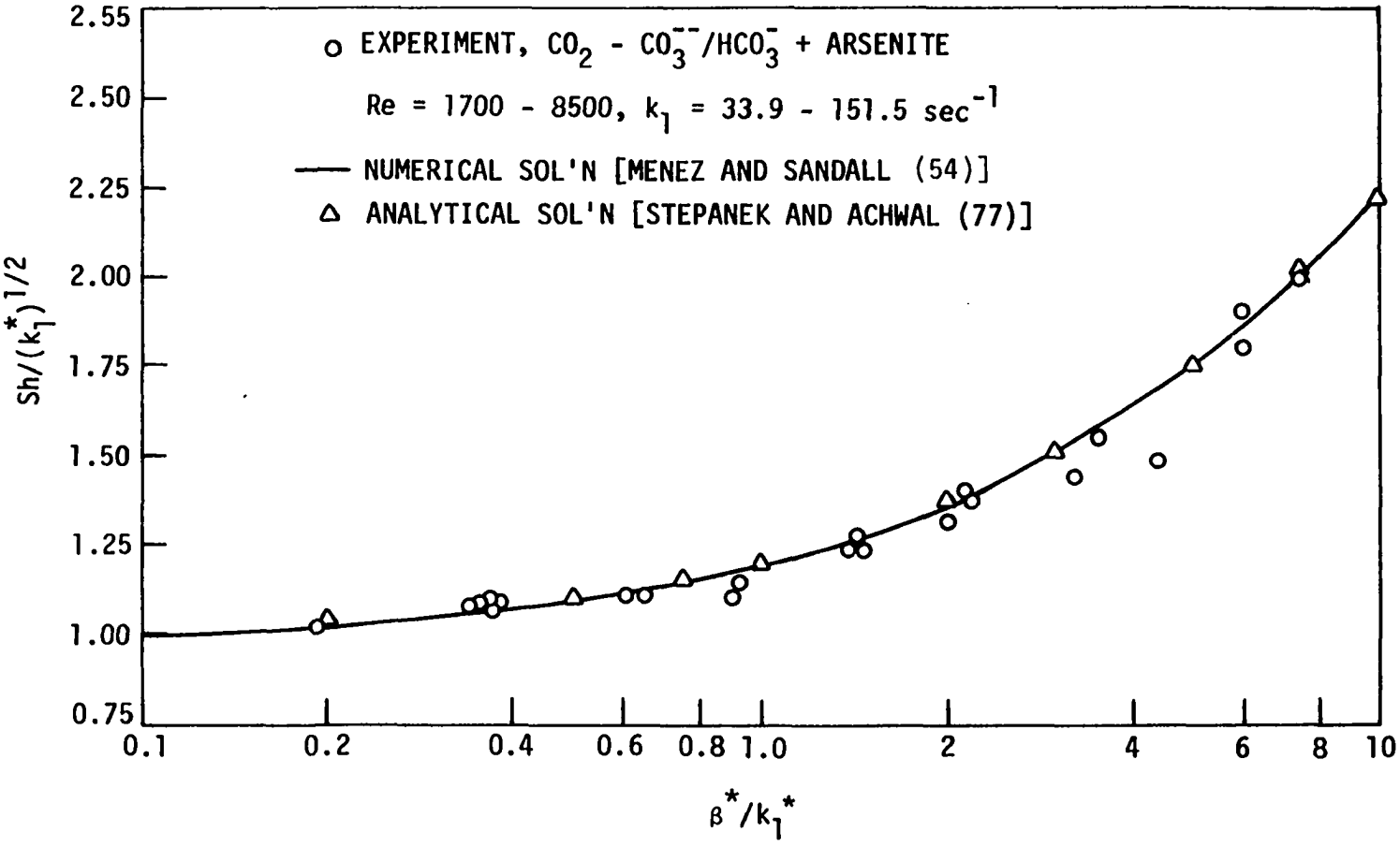

Figure 26. Absorption with first-order reaction in a turbulent falling film at fully developed concentration profile conditions

$\beta^*/k_1^* \leq 0.05$. Judging from Figure 26, when $\beta^*/k_1^* \leq 0.05$, the solution is essentially in the fast reaction region. Therefore their conclusions are only valid for fast reactions. For large values of β^*/k_1^*, the effect of the boundary condition inside the liquid phase should be important, especially for a liquid film whose thickness is small.

For a zero-order reaction, the eigenvalues and the related quantities are the same as in physical absorption, but the expansion coefficients are computed from Equation 239. The first ten expansion coefficients are reported in Table 19 for $\beta^* = 500$ and different k_0^*'s. The Sherwood number is plotted as a function of the dimensionless axial length in Figure 27. As k_0^* increases, the curves tend to flatten out and the "transient part" decays rapidly. Obviously, the effect of the chemical reaction is to enhance the absorption rate. From Figure 27, the enhancement factor for a zero-order reaction can easily be found for $\beta^* = 500$.

For a pseudo-n-th order reaction, it is expected that the same kind of curves which consist of a "transient part" and a "steady part" would appear as in Figure 27. However, the length of the "transient part" will depend both on β^* and k_n^*. If $k_n^* >> \beta^*$, the length of the "transient part" will be expected to be relatively small while the reverse will be true if $k_n^* << \beta^*$.

The analytical solution developed here using the simple method of separation of variables clearly offers substantial advantage over that of the finite difference numerical solution in describing the effects of operating variables. The method is also generally applicable to different kinds of continuous turbulent velocity profiles and eddy diffusivity profiles in a falling film.

Table 19. Expansion coefficients, C_i, for zero-order reactions in a turbulent falling film, $\beta^* = 500$

i \ k_0^*	20	30	40	50
1	-0.131189×10^{-1}	-0.410459×10^{-2}	-0.195170×10^{-2}	-0.138104×10^{-2}
2	0.373673×10^{-1}	0.132907×10^{-1}	0.654275×10^{-2}	0.465332×10^{-2}
3	-0.489583×10^{-1}	-0.218507×10^{-1}	-0.114370×10^{-1}	-0.820766×10^{-2}
4	0.435253×10^{-1}	0.270546×10^{-1}	0.155172×10^{-1}	0.112864×10^{-1}
5	-0.315195×10^{-1}	-0.288911×10^{-1}	-0.186937×10^{-1}	-0.138423×10^{-1}
6	0.224709×10^{-1}	0.279013×10^{-1}	0.208935×10^{-1}	0.158196×10^{-1}
7	-0.192064×10^{-1}	-0.250573×10^{-1}	-0.220876×10^{-1}	-0.171738×10^{-1}
8	0.189493×10^{-1}	0.215129×10^{-1}	0.223059×10^{-1}	0.178830×10^{-1}
9	-0.183845×10^{-1}	-0.183054×10^{-1}	-0.216348×10^{-1}	-0.179518×10^{-1}
10	0.169736×10^{-1}	0.161070×10^{-1}	0.202055×10^{-1}	0.174097×10^{-1}

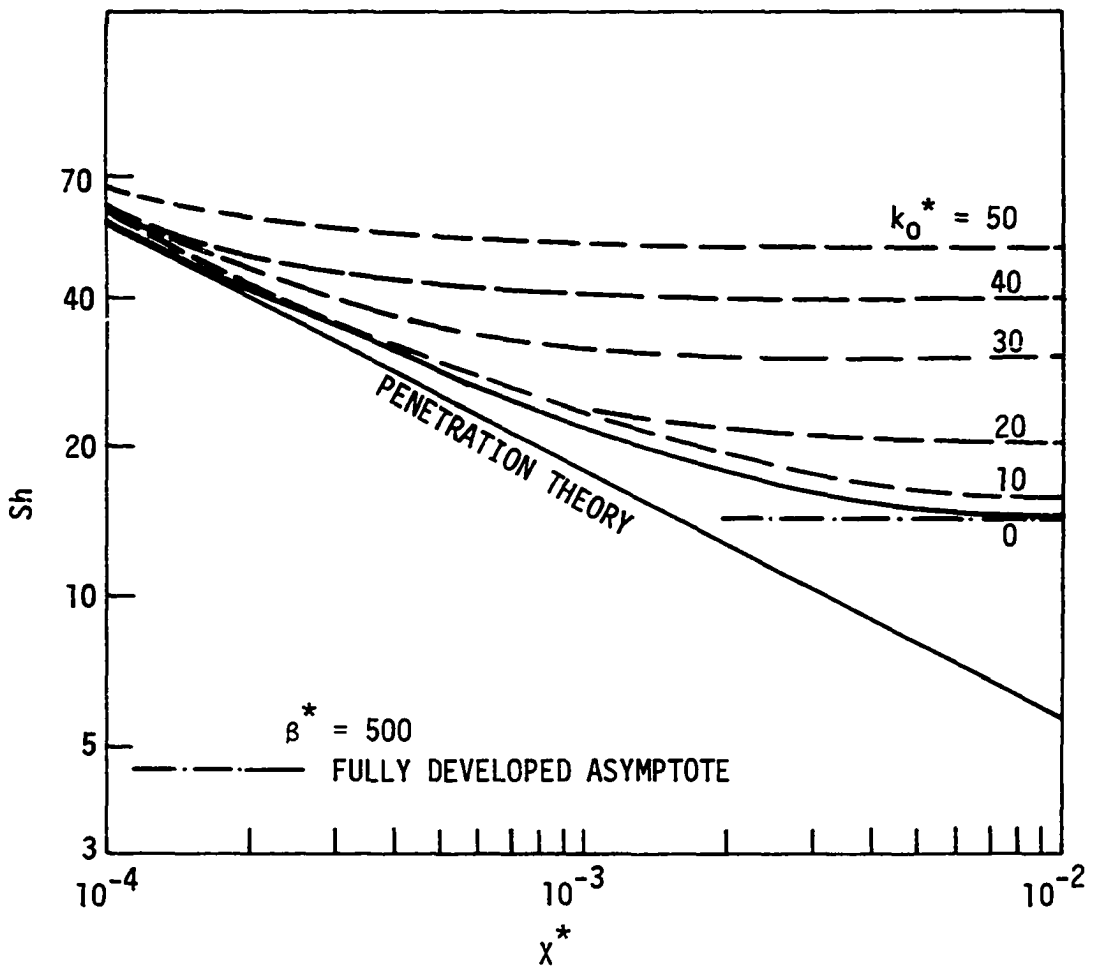

Figure 27. Sherwood number as a function of dimensionless axial length for a zero-order reaction in a turbulent falling film, $\beta^* = 500$

CONCLUSIONS

A model which incorporates the effects of heat transfer and interfacial shear is developed for mass transfer with or without chemical reaction in a laminar falling film. Effects of heat transfer on liquid viscosity, molecular diffusivity, reaction rate constant and gas solubility are explicitly taken into account. The analysis shows that the heat transfer and interfacial shear can have a profound influence on the mass transfer rate. A cocurrent gas shear decreases the film thickness and increases the mass transfer rate. A linear temperature drop in the liquid film in which the wall is cooled also decreases the film thickness but the mass transfer rate can be reduced or increased depending on the gas solubility-temperature relationship. For most gases under practical conditions, the gas solubility decreases with increasing temperature and so the mass transfer rate will be reduced. The assumptions that the viscosity varies exponentially with temperature and that $\frac{D\mu}{T}$ is constant represent a much better approximation than the assumptions of linear dependency of viscosity and molecular diffusivity on temperature as used by Jennis (37). Moreover, this enables the analysis to be carried out for all ranges of the temperature gradient and interfacial shear, which is not possible in the work by Jennis. In the presence of chemical reactions, the heat transfer increases the Arrhenius reaction rate such that the reaction enhancement for finite values of α and β as compared to an isothermal, zero interfacial shear film ($\alpha = 0$, $\beta = 0$) may be greater, less, or even equal to 1.0 depending on the relative importance of the dimensionless parameters α, β, h, and p. α, h, and p represent the effects of

heat transfer on liquid viscosity, gas solubility, and reaction rate respectively, and β represents the interfacial shear. The parametric study presented here should be a useful guide to the development of experimental testing of certain extreme operating conditions of mass transfer into falling films involving heat transfer and interfacial shear.

The linear stability of this flow is determined by a method using small disturbance theory. The governing Orr-Sommerfeld (O-S) equation, which is modified to include the effects of temperature on viscosity, is solved by a successive perturbation method. The analysis shows that wall cooling is destabilizing because of the lower viscosity generated at the film surface while the reverse is true for wall heating. The additional viscosity gradient terms in the modified O-S equation are shown to be important destabilizing factors. The stability of the flow is also influenced by the variation of the mean velocity profile in the liquid film. Thus, the effects of heat transfer on surface wave instability in falling films are in many respects similar to the shear wave instability in other types of flow. The neutral stability curves show that the angle of inclination is a stabilizing factor and the critical Reynolds number for surface wave formation is more influenced by wall heating than wall cooling. Interfacial shear is also shown to be a destabilizing factor because of the generation of surface perturbation stresses. However, the destabilizing effects of interfacial shear and wall cooling are not simply additive because of the coupling and interaction in the mean velocity profile. The linear stability analysis enables one to determine the critical conditions under which waves will appear and has important application to processes dealing with heat and mass transfer in falling films.

An analytical solution is developed for mass transfer with or without chemical reaction in a turbulent falling film using an eddy diffusivity expression previously derived. The solutions for intermediate contact times and reaction rates can be obtained in a relatively simple manner. The results on physical absorption agree well with the numerical finite difference solution. The results on chemical absorption also agree with the numerical solution and experimental data for a first-order reaction. New results are presented for a zero-order reaction. The chemical absorption rate for a pseudo-n-th order reaction is shown to be comprised of a "transient part" and a "steady part," the relative importance of which depends on the degree of turbulence and the reaction rate. Thus, the exact solution makes it possible not only to generalize the results easily, but also permits a better understanding of the effect of variations in flow conditions and reaction rates on mass transfer in turbulent falling films.

REFERENCES

1. Anshus, B. E., and S. L. Goren. 1966. A method of getting approximate solutions to the Orr-Sommerfeld equation for flow on a vertical wall. A. I. Ch. E. J. 12: 1004-1008.

2. Astarita, G. 1967. Mass transfer with chemical reaction. Elsevier Publishing Co., Amsterdam.

3. Banerjee, S., E. Rhodes, and D. S. Scott. 1967. Mass transfer to falling wavy liquid films at low Reynolds numbers. Chem. Eng. Sci. 22: 43-48.

4. Banerjee, S., D. S. Scott, and E. Rhodes. 1968. Mass transfer to falling wavy liquid films in turbulent flow. I&EC Fundamentals 7: 22-27.

5. Bankoff, S. G. 1971. Stability of liquid flow down a heated inclined plane. Int. J. Heat Mass Transfer 14: 377-385.

6. Benjamin, T. B. 1957. Wave formation in laminar flow down an inclined plane. J. Fluid Mech. 2: 554-574.

7. Benjamin, T. B. 1959. Shearing flow over a wavy boundary. J. Fluid Mech. 6: 161-205.

8. Bennett, J. P., and R. E. Rathbun. 1972. Reaeration in open-channel flow. USGS Professional Paper No. 737, 75 pp.

9. Berbente, C. P., and E. Ruckenstein. 1968. Hydrodynamics of wave flow. A. I. Ch. E. J. 14: 772-782.

10. Brumfield, L. K., and T. G. Theofanous. 1976. On the prediction of heat transfer across turbulent liquid films. J. Heat Transfer (Trans. ASME) 98: 496-502.

11. Brumfield, L. K., R. N. Houze, and T. G. Theofanous. 1975. Turbulent mass transfer at free, gas-liquid interfaces, with applications to film flows. Int. J. Heat Mass Transfer 18: 1077-1081.

12. Brunson, R. J., and R. M. Wellek. 1970. Determination of the enhancement factor for mass transfer with an instantaneously fast chemical reaction. Chem. Eng. Sci. 25: 904-906.

13. Cerro, R. L., and S. Whitaker. 1971. Entrance region flows with a free surface: The falling liquid film. Chem. Eng. Sci. 26: 785-798.

14. Chavan, V. V., and R. A. Mashelkar. 1972. Gas absorption in falling non-Newtonian films. Chem. Eng. J. 4: 223-228.

15. Chiang, S. H., and H. L. Toor. 1964. Gas absorption accompanied by a large heat effect and volume change of the liquid phase. A. I. Ch. E. J. 10: 398-402.

16. Chun, K. R., and R. A. Seban. 1971. Heat transfer to evaporating liquid films. J. Heat Transfer (Trans. ASME) 93: 391-396.

17. Chung, D. K., and A. F. Mills. 1976. Experimental study of gas absorption into turbulent falling films of water and ethylene glycol-water mixtures. Int. J. Heat Mass Transfer 19: 51-59.

18. Cook, A. E., and E. Moore. 1972. Gas absorption with a first order chemical reaction and large heat effect. Chem. Eng. Sci. 27: 605-613.

19. Craik, A. D. D. 1966. Wind-generated waves in thin liquid films. J. Fluid Mech. 26: 369-392.

20. Danckwerts, P. V. 1970. Gas-liquid reactions. McGraw-Hill, New York.

21. Davidson, J. F., and E. J. Cullen. 1957. The determination of diffusion coefficients for sparingly soluble gases in liquids. Trans. Instn. Chem. Engrs. 35: 51-60.

22. Davies, J. T. 1972. Turbulence phenomena. Academic Press, Inc., New York.

23. Davies, J. T., and K. V. Warner. 1969. The effect of large-scale roughness in promoting gas absorption. Chem. Eng. Sci. 24: 231-240.

24. Dukler, A. E. 1972. Characterization, effects and modeling of the wavy gas-liquid interface. Progress in heat and mass transfer. Proceedings of the International Symposium on Two-Phase Systems, edited by G. Hetsroni, S. Sideman, and J. P. Hartnett, pp. 207-234.

25. Dukler, A. E., and O. P. Bergelin. 1952. Characteristics of flow in falling liquid films. Chem. Eng. Prog. 48: 557-563.

26. Emmert, R. E., and R. L. Pigford. 1954. A study of gas absorption in falling liquid films. Chem. Eng. Prog. 50: 87-93.

27. Fortescue, G. E., and J. R. A. Pearson. 1967. On gas absorption into a turbulent liquid. Chem. Eng. Sci. 22: 1163-1176.

28. Fulford, G. D. 1964. The flow of liquids in thin films. Pages 151-236 in T. B. Drew, J. W. Hoopes, Jr., and T. V. Vermeulen. Advances in chemical engineering. Academic Press, New York.

29. Goodridge, F., and G. Gartside. 1965. Mass transfer into near-horizontal liquid films. Part 1: Hydrodynamic studies. Trans. Instn. Chem. Engrs. 43: T62-T67.

30. Goodridge, F., and G. Gartside. 1965. Mass transfer into near-horizontal liquid films. Part 2: The measurement of rates of gas absorption. Trans. Instn. Chem. Engrs. 43: T74-T77.

31. Gottfredi, J. C., A. A. Yeramian, and J. J. Ronco. 1972. Mass transfer into a sheared interface with and without chemical reaction. Chem. Eng. J. 3: 163-167.

32. Hikita, H., K. Nakanishi, and T. Kataoka. 1959. Liquid phase mass transfer in wetted-wall columns. Chem. Eng. Tokyo 23: 459-466.

33. Hobler, T., and S. Kedzierski. 1967. Analysis of the equations of mass transfer in the liquid phase in the flow of liquid down a wall. International Chem. Eng. 7: 654-666.

34. Iyer, V. 1930. The temperature variation of the viscosity of liquids and its theoretical significance. Indian J. Phys. 5: 371-383.

35. Jameson, G. J., S. R. C. Burchell, and J. C. Gottfredi. 1970. Mass transfer with chemical reaction in a finite falling film. Chem. Eng. Sci. 13: 1629-1632.

36. Javdani, K. 1974. Mass transfer in wavy liquid films. Chem. Eng. Sci. 29: 61-69.

37. Jennis, J. H. 1973. Diffusion into a falling laminar film with heat transfer and interfacial shear. M.S. thesis. Iowa State University, Ames.

38. Jones, L. O., and S. Whitaker. 1966. An experimental study of falling liquid films. A. I. Ch. E. J. 12: 525-529.

39. Kamei, S., and J. Oishi. 1955. Mass and heat transfer in a falling liquid film of wetted wall tower. Mem. Fac. Kyoto Univ. 17: 277-289.

40. Kapitza, P. L. 1948. Wave flow of thin layers of a viscous fluid. English translation in Collected Papers of P. L. Kapitza. Macmillan, New York, 1964. pp. 662-709.

41. Kayihan, F., and O. C. Sandall. 1974. Gas absorption with first-order reaction in turbulent liquid films. A. I. Ch. E. J. 20: 402-404.

42. Keller, H. B. 1968. Numerical methods for two-point boundary-value problems. Blaisdell Publishing Co., Waltham, Mass.

43. King, C. J. 1966. Turbulent liquid phase mass transfer at a free gas-liquid interface. I&EC Fundamentals 5: 1-8.

44. Krantz, W. B., and S. L. Goren. 1971. Stability of thin liquid films flowing down a plane. I&EC Fundamentals 10: 91-101.

45. Lamourelle, A. P., and O. C. Sandall. 1972. Gas absorption into a turbulent liquid. Chem. Eng. Sci. 27: 1035-1043.

46. Lapidus, L. 1962. Digital computation for chemical engineers. McGraw-Hill, New York.

47. Lebedev, N. N. 1965. Special functions and their applications. Prentice-Hall, Inc., Englewood Cliffs, N.J.

48. Levich, V. G. 1962. Physicochemical hydrodynamics. Prentice-Hall, Englewood Cliffs, N.J.

49. Marschall, E., and C. Y. Lee. 1973. Stability of condensate flow down a vertical wall. Int. J. Heat Mass Transfer 16: 41-48.

50. Mashelkar, R. A., and M. A. Soylu. 1974. Diffusion in flowing films of dilute polymeric solutions. Chem. Eng. Sci. 29: 1089-1099.

51. Mashelkar, R. A., V. V. Chavan, and N. G. Karanth. 1973. Solution of the problem of gas absorption in falling films of non-Newtonian fluids by orthogonal collocation technique. Chem. Eng. J. 6: 75-77.

52. Massot, C., F. Irani, and E. N. Lightfoot. 1966. Modified description of wave motion in a falling film. A. I. Ch. E. J. 12: 445-455.

53. Mendez, F., and O. C. Sandall. 1975. Gas absorption accompanied by instantaneous bimolecular reaction in turbulent liquids. A. I. Ch. E. J. 21: 534-540.

54. Menez, G. D., and O. C. Sandall. 1974. Gas absorption accompanied by first-order chemical reaction in turbulent liquids. I&EC Fundamentals 13: 72-76.

55. Miles, J. W. 1957. On the generation of surface waves by shear flows. J. Fluid Mech. 3: 185-204.

56. Miles, J. W. 1962. On the generation of surface waves by shear flows. Part 4. J. Fluid Mech. 13: 433-448.

57. Mills, A. F., and D. K. Chung. 1973. Heat transfer across turbulent falling films. Int. J. Heat Mass Transfer 16: 694-696.

58. Mohr, C. M., Jr., and M. C. Williams. 1973. Diffusion of gas into a non-Newtonian falling film. A. I. Ch. E. J. 19: 1047-1049.

59. Olbrich, W. E., and J. D. Wild. 1969. Diffusion from the free surface into a liquid film in laminar flow over defined shapes. Chem. Eng. Sci. 24: 25-32.

60. Oliver, D. R., and T. E. Atherinos. 1968. Mass transfer to liquid films on an inclined plane. Chem. Eng. Sci. 23: 525-536.

61. Perez, J. F., and O. C. Sandall. 1973. Diffusivity measurements for gases in power law non-Newtonian liquids. A. I. Ch. E. J. 19: 1073-1075.

62. Portalski, S. 1963. Studies of falling liquid film flow: Film thickness on a smooth vertical plate. Chem. Eng. Sci. 18: 787-804.

63. Portalski, S. 1964. Eddy formation in film flow down a vertical plate. I&EC Fundamentals 3: 49-53.

64. Porter, K. E., and D. Roberts. 1969. Similarities between the effect of different flow patterns on diffusion with chemical reaction near an interface. Chem. Eng. Sci. 24: 695-704.

65. Potter, M. C., and E. Graber. 1972. Stability of plane Poiseuille flow with heat transfer. Phys. Fluids 15: 387-391.

66. Prasher, B. D., and A. L. Fricke. 1974. Mass transfer at a free gas-liquid interface in turbulent thin films. I&EC Process Des. Develop. 13: 336-340.

67. Ratcliff, G. A., and J. G. Holdcroft. 1961. Gas absorption with first-order chemical reaction in a spherical liquid film. Chem. Eng. Sci. 15: 100-110.

68. Rotem, Z., and J. E. Neilson. 1969. Exact solution for diffusion to flow down an incline. Can. J. Chem. Eng. 47: 341-346.

69. Ruckenstein, E., and C. Berbente. 1965. Mass transfer in wave flow. Chem. Eng. Sci. 20: 795-801.

70. Sandall, O. C. 1974. Gas absorption into turbulent liquids at intermediate contact times. Int. J. Heat Mass Transfer 17: 459-461.

71. Shah, Y. T. 1972. Gas-liquid interface temperature rise in the case of temperature-dependent physical, transport and reaction properties. Chem. Eng. Sci. 27: 1469-1474.

72. Shah, Y. T., and A. Z. Szeri. 1974. Marangoni instability in non-isothermal first order gas-liquid reactions--evaluations of Cl_2-toluene and CO_2-sodium hydroxide systems. Chem. Eng. Sci. 29: 2219-2228.

73. Shair, F. H. 1971. Dispersion in laminar flowing liquid films involving heat transfer and interfacial shear. A. I. Ch. E. J. 17: 920-926.

74. Shkadov, V. Ya. 1967. Wave flow regimes of a thin layer of viscous fluid subject to gravity. Izv. AN SSSR. Mekhanika Zhidkosti i Gaza 2: 43-51.

75. Smith, F. I. P. 1970. Stability of liquid film flow down an inclined plane with oblique airflow. Phys. Fluids 13: 1693-1700.

76. Stainthorp, F. P., and J. M. Allen. 1965. The development of ripples on the surface of a liquid film flowing inside a vertical tube. Trans. Instn. Chem. Engrs. 43: T85-T91.

77. Stepanek, J. B., and S. K. Achwal. 1975. Absorption with first order chemical reaction into turbulently flowing liquids. Can. J. Chem. Eng. 53: 517-520.

78. Stepanek, J. B., and S. K. Achwal. 1975. Turbulent absorption with instantaneous irreversible chemical reaction. Chem. Eng. J. 10: 49-56.

79. Stucheli, A., and M. N. Ozisik. 1976. Hydrodynamic entrance lengths of laminar falling films. Chem. Eng. Sci. 31: 369-372.

80. Tailby, S. R., and S. Portalski. 1962. The determination of the wavelength on a vertical film of liquid flowing down a hydrodynamically smooth plate. Trans. Instn. Chem. Engrs. 40: 114-122.

81. Tamir, A., and Y. Taitel. 1971. Diffusion to flow down an incline with surface resistance. Chem. Eng. Sci. 26: 799-808.

82. Vander Mey, J. E. 1967. Process for sulfonation of organic compounds. U.S. Patent 3,328,460.

83. Vivian, J. E., and D. W. Peaceman. 1956. Liquid-side resistance in gas absorption. A. I. Ch. E. J. 2: 437-443.

84. Wazzan, A. R., T. Okamura, and A. M. O. Smith. 1968. The stability of water flow over heated and cooled flat plates. J. Heat Transfer (Trans. ASME) 90: 109-114.

85. Whitaker, S. 1964. Effect of surface active agents on the stability of falling liquid films. I&EC Fundamentals 3: 132-142.

86. Wilkes, J. O., and R. M. Nedderman. 1962. The measurement of velocities in thin films of liquid. Chem. Eng. Sci. 17: 177-187.

87. Yih, C.-S. 1963. Stability of liquid flow down an inclined plane. Phys. Fluids 6: 321-334.

ACKNOWLEDGMENTS

I would like to express my sincere gratitude to Professor Richard C. Seagrave, my advisor, for his generous guidance and support during the course of this study. Without his stimulating initiations and encouraging directions, this thesis could never have been written. I also wish to thank the members of my thesis committee, Professors L. E. Burkhart, D. L. Ulrichson, D. F. Young and R. H. Homer, for their valuable comments.

This work was partially supported by the Engineering Research Institute of Iowa State University, the financial assistance of which is gratefully acknowledged.

To my beloved parents, who have already given me too much and have made so many things possible, this work is specially dedicated.

APPENDIX A: VARIATION OF PHYSICAL PROPERTIES AND KINETIC RATE CONSTANTS WITH TEMPERATURE IN THE LIQUID FILM

The following four models are employed to describe the variation of the physical properties and reaction rate constants as a function of temperature in a laminar liquid film:

1. An exponential dependence of viscosity on temperature,

$$\mu = A_a e^{E_a/T} \tag{A1}$$

2. The molecular diffusivity follows the Stokes-Einstein relationship,

$$\frac{D\mu}{T} = \text{constant} \tag{A2}$$

3. An exponential dependence of gas solubility on temperature,

$$C_s = B^* e^{H_s/R_g T} \tag{A3}$$

4. The reaction rate constants obey the Arrhenius relationship,

$$\hat{k} = A^* e^{-\hat{E}/R_g T} \tag{A4}$$

For a linear temperature profile in the liquid film in which

$$T = T_0 + (T_1 - T_0)\eta \tag{A5}$$

the four models above become respectively, provided $(T_1 - T_0)/T_0 \ll 1$,

$$\mu = \mu_0 e^{-E_a\left(\frac{1}{T_0} - \frac{1}{T}\right)} = \mu_0 e^{-E_a\left[\frac{(T_1-T_0)\eta/T_0}{T_0(1+(T_1-T_0)\eta/T_0)}\right]}$$

$$\doteq \mu_0 e^{-E_a[(T_1-T_0)\eta/T_0^2]} = \mu_0 e^{-\alpha\eta} \tag{A6}$$

$$D = \frac{D_0\mu_0}{T_0} \cdot \frac{T}{\mu} = \frac{D_0\mu_0}{T_0} \cdot \frac{T_0+(T_1-T_0)\eta}{\mu_0 e^{-\alpha\eta}}$$

$$= D_0 e^{\alpha\eta[1+(T_1-T_0)\eta/T_0]} \doteq D_0 e^{\alpha\eta} \qquad \text{(A7)}$$

$$C_s(T_1) = C_s(T_0)e^{-\frac{H_s}{R_g}(\frac{T_1-T_0}{T_0T_1})} \doteq C_s(T_0)e^{-\frac{H_s}{R_g}(\frac{T_1-T_0}{T_0^2})}$$

$$= C_s(T_0)e^{-\frac{H_s\alpha}{R_gE_a}} = C_s(T_0)e^{-h\alpha}$$

$$\doteq C_s(T_0)(1-h\alpha) \quad \text{for a small temperature range} \qquad \text{(A8)}$$

$$\hat{k} = \hat{k}_0 e^{\frac{\hat{E}}{R_g}[\frac{(T_1-T_0)\eta/T_0}{T_0(1+(T_1-T_0)\eta/T_0)}]} \doteq \hat{k}_0 e^{\frac{\hat{E}}{R_g}[(T_1-T_0)\eta/T_0^2]}$$

$$= \hat{k}_0 e^{\frac{\hat{E}\alpha\eta}{R_gE_a}} = \hat{k}_0 e^{p\alpha\eta} \qquad \text{(A9)}$$

APPENDIX B: COMPUTER PROGRAM LISTING

```
//STEP1  EXEC  WATFIV,REGION.GO=132K,TIME.GO=6
//GO.SYSIN  DD  *
$JOB      'PROGRAMMER',TIME=355,PAGES=30
C-----COMPUTER PROGRAM LISTING FOR THE QUASI-NUMERICAL SOLUTION
C-----THIS PROGRAM COMPUTES THE EIGENVALUES BY THE RUNGE-KUTTA-GILL-4
C-----METHOD AND THE EXPANSION COEFFICIENTS BY SIMPSON'S RULE
C-----OF INTEGRATION
       IMPLICIT REAL*8(A-H,O-Z)
      EXTERNAL EVAL
       COMMON DK1,V(101)
       DIMENSION YZR(4),A(401,5)
      EPS=1.0D-6
       ICOUNT=1
        DK1=0.0D+0
  41  READ,ALPHA,BETA,DLAM
      J=0
      IFREQ=20
      NEQ=4
      LL=400
      XZR=0.0
      XF=1.0
      DX=0.0025
      WRITE(6,100) ALPHA,BETA
 100  FORMAT(/10X,'ALPHA=',F7.2,5X,'BETA=',F9.2/)
      WRITE(6,701) DLAM
      NROW=LL+1
      NCOL=NEQ+1
      YZR(1)=1.
      YZR(2)=0.
      YZR(3)=0.
      YZR(4)=0.
```

```
  31   IF(J .GT. 15)  GO TO 40
       CALL JSRKB(NEQ,NROW,NCOL,NROW,A,DX,XZR,YZR,EVAL,ALPHA,BETA,DLAM)
       DLAM=DLAM-A(NROW,2)/A(NROW,4)
       WRITE(6,701) DLAM
  701  FORMAT(10X,'L=',D23.16)
       DELX=A(NROW,2)/A(NROW,4)
       IF(DABS(DELX) .LE. EPS)  GO TO 30
       J=J+1
       GO TO 31
  30   WRITE(6,701) DLAM
       DO 50  I=1,NROW,IFREQ
       WRITE(6,702) A(I,2)
  702  FORMAT(10X,D23.16)
  50   CONTINUE
C------------------
       DL2=DLAM**2
           DO 7  K=1,3
        IF(K .EQ. 1)  DK0=20.
        IF(K .EQ. 2)  DK0=30.
        IF(K .EQ. 3)  DK0=40.
       CALL SIMPS(NEQ,NROW,NCOL,A,ALPHA,BETA,DLAM,CC,Z2,Z3,ICOUNT,DK0)
       WRITE(6,704)  DL2,CC,A(NROW,2),A(NROW,3),A(NROW,4)
  704  FORMAT(10X,'L**2=',D23.16,10X,'CC=',D23.16/10X,3D23.16)
C------------------
       WRITE(7,81) (A(I,2), I=1,NROW,IFREQ)
 81    FORMAT(5(D16.9))
       WRITE(7,83) Z2,DL2,CC,A(NROW,3),Z3
   83  FORMAT(5(D16.9))
  7     CONTINUE
```

```
      ICCUNT=ICOUNT+1
        IF(ICOUNT .LE. 15)  GO TO 41
  40  STOP
      END
C--
      SUBROUTINE EVAL(NEQ,XA,YA,G,ALPHA,BETA,DLAM)
       IMPLICIT REAL*8(A-H,O-Z)
       COMMON DK1,V(101)
      DIMENSION YA(4),G(4)
      G(1)=YA(2)/(1.+BETA*(1.-XA)*(1.-XA))
      G(2)=-DLAM**2*YA(1)+DK1*YA(1)
      G(3)=YA(4)/(1.+BETA*(1.-XA)*(1.-XA))
      G(4)=-YA(3)*(DLAM**2)-2.*DLAM*YA(1)+DK1*YA(3)
      RETURN
      END
C--
      SUBROUTINE JSRK8(NEQ,NROW,NCOL,LL,A,DX,XZR,YZR,EVAL,ALPHA,BETA,
     1DLAM)
       IMPLICIT REAL*8(A-H,O-Z)
       COMMON DK1,V(101)
      DIMENSION YZR(4), A(NROW,NCOL)
      DIMENSION AK1(4), AK2(4), AK3(4), AK4(4), YM(4), YMP(4)
      S=0.2D+1
      P=DSQRT(S)
      NEQP=NEQ+1
      DO 80  L=1,LL
      DO 80  K=1,NEQP
      A(L,K)=0.0
   80  CONTINUE
      DXD=DX/2.0
```

```
      DXDD=DX/6.0
      A(1,1)=XZR
      DO 50  K=1,NEQ
      KD=K+1
      A(1,KD)=YZR(K)
   50 CONTINUE
      DO 100 L=2,LL
      LD=L-1
      XM=A(LD,1)
      DO 2  K=1,NEQ
      KD=K+1
      YM(K)=A(LD,KD)
    2 CONTINUE
      CALL EVAL(NEQ,XM,YM,AK1,ALPHA,BETA,DLAM)
      XMP=XM+DXD
      DO 4  K=1,NEQ
      YMP(K)=YM(K)+DXD*AK1(K)
    4 CONTINUE
      CALL EVAL(NEQ,XMP,YMP,AK2,ALPHA,BETA,DLAM)
      DO 6  K=1,NEQ
      YMP(K)=YM(K)+(-0.5+1./P)*AK1(K)*DX+(1.-1./P)*AK2(K)*DX
    6 CONTINUE
      CALL EVAL(NEQ,XMP,YMP,AK3,ALPHA,BETA,DLAM)
      XMP=XM+DX
      DO 8  K=1,NEQ
      YMP(K)=YM(K)+(-1./P)*AK2(K)*DX+(1.+1./P)*AK3(K)*DX
    8 CONTINUE
      CALL EVAL(NEQ,XMP,YMP,AK4,ALPHA,BETA,DLAM)
      A(L,1)=XMP
      DO 10  K=1,NEQ
```

```
      KD=K+1
      A(L,KD)=A(LD,KD)+DXDD*(AK1(K)+AK4(K))+1./3.*(1.-1./P)*AK2(K)*DX+1.
     1*(1.+1./P)*AK3(K)*CX/3.
   10 CONTINUE
  100 CONTINUE
      RETURN
      END
       SUBROUTINE SIMPS(NEQ,NROW,NCOL,A,ALPHA,BETA,DLAM,C,Z2,Z3,JJ,DK0)
      IMPLICIT REAL*8(A-H,O-Z)
       COMMON DK1,V(101)
       DIMENSION A(NROW,NCOL), H(2),W(2),W2(2)
      DIMENSION W3(2)
        BE=DSQRT(BETA)
      II=1
       U=1.
      Q=0.
      BB=1.
       H(1)=0.02
       H(2)=0.01
   14 CONTINUE
C      2N SUBINTERVALS ARE USED
        NN=25
      IF(II .EQ. 2)  GO TO 1
      GO TO 55
    1   NN=NN*2
   55 CONTINUE
C     INITIALIZE S1, S2
      S1=0.
      S2=0.
       S3=0.
```

```
      S4=0.
       S5=0.
      S6=0.
        NIN=401
        NU=51
      IEC=0
       IFR=8
      IFREQ=2
       IF(II .EQ. 2)   IFR=4
       IF(II .EQ. 2)   NU=101
      ETA=0.0
       J=0
      DO 137   I=1,NIN,IFR
       IEC=IEC+1
      K=I
        KK=J
       IF(II .EQ. 2)   GO TO 711
        KK=2*KK+1
       GO TO 712
  711  CONTINUE
         KK=KK+1
  712 CONTINUE
       UK=1.-DK0/BE*DATAN(BE*(1.-ETA))+DK0/2.*DLOG(1.+BETA*(1.-ETA)**2)
     1/BETA
       IF(UK .LE. 0.)  UK=0.
C-------------------
C      EVALUATE THE SUMS OF S1 AND S2
       IF(I .EQ. 1)  FA=A(K,2)*U*UK
       IF(JJ .NE. 1)  GO TO 320
       IF(I .EQ. 1)  FA1=U*UK
```

```
  320 CONTINUE
      IF(I .EQ. 1)  FA3=U*A(K,2)
      IF(I .EQ. NIN)  GO TO 141
        IF(IEC/IFREQ*IFREQ .EQ. IEC)  GO TO 139
       S1=S1+A(K,2)*U*UK
      IF(JJ .NE. 1)  GO TO 321
      S3=S3+U*UK
  321 CONTINUE
       S5=S5+A(K,2)*U
      GO TO 137
  139  S2=S2+A(K,2)*U*UK
      IF(JJ .NE. 1)  GO TO 322
       S4=S4+U*UK
  322 CONTINUE
        S6=S6+A(K,2)*U
       J=J+1
  137  ETA=ETA+1./(NU-1)
  141 FB=A(K,2)*U*UK
      IF(JJ .NE. 1)  GO TO 323
      FB1=U*UK
  323 CONTINUE
       FB3=U*A(K,2)
      S1=S1-FA
      IF(JJ .NE. 1)  GO TO 324
      S3=S3-FA1
  324 CONTINUE
       S5=S5-FA3
C     COMPUTE INTEGRAL USING SIMPSON'S RULE
      W(II)=H(II)/3.*(FA+2.*S1+4.*S2+FB)
      IF(JJ .NE. 1)  GO TO 325
      W2(II)=H(II)/3.*(FA1+2.*S3+4.*S4+FB1)
```

```
  325 CONTINUE
       W3(II)=H(II)/3.*(FA3+2.*S5+4.*S6+FB3)
       WRITE(6,30) H(II),Q,BB,W(II)
      WRITE(6,30) H(II),Q,BB,W2(II)
      WRITE(6,30) H(II),Q,BB,W3(II)
   30 FORMAT(1H0, 10X, 'NUMERICAL INTEGRATION USING SIMPSON''S RULE'
     1//5X,'FOR H=', F6.3,' THE VALUE OF THE INTEGRAL FROM A=', F3.0,
     22X,'TO B=', F3.0, 2X, 'IS', D16.9)
       II=II+1
      IF(II .GE. 3) GO TO 24
      GO TO 14
   24 CONTINUE
C     COMPUTE IMPROVED VALUE OF INTEGRAL
      ZZ=W(2)+1./15.*(W(2)-W(1))
      IF(JJ .NE. 1)  GO TO 326
      Z2=W2(2)+1./15.*(W2(2)-W2(1))
  326 CONTINUE
      Z3=W3(2)+1./15.*(W3(2)-W3(1))
      WRITE(6,31) ZZ
      WRITE(6,31) Z2
      WRITE(6,31) Z3
   31 FORMAT(//5X, 'IMPROVED VALUE OF INTEGRAL=', D16.9)
       DNN=1./2./DLAM*A(NROW,3)*A(NROW,4)
        C=-ZZ/DNN
      PRINT61,C
 61   FORMAT(' ',T4,'PRODUCT SOLUTION COEFFICIENT C=',D23.16)
       RETURN
      END
$ENTRY
```